UPCONVERTING NANOPARTICLES IN BIOAFFINITY ASSAYS:

New Insights and Perspectives

Satu Lahtinen

UNIVERSITY OF TURKU

UPCONVERTING NANOPARTICLES IN BIOAFFINITY ASSAYS:

New Insights and Perspectives

Satu Lahtinen

University of Turku

Faculty of Science and Engineering
Department of Biochemistry
Analytical Biotechnology
Doctoral Programme in Molecular Life Sciences, DPMLS

Supervised by

Professor Tero Soukka, PhD
Department of Biochemistry
Biotechnology
University of Turku
Turku, Finland

Johanna Pyylampi, PhD
Kaivogen Oy
Turku, Finland

Reviewed by

Timo Piironen, PhD, Docent,
SYRINX Bioanalytics Oy
Adjunct Professor at University of Turku
Turku, Finland

Senior Professor Hans Ågren, PhD
Department of Theoretical Chemistry
and Biology
Royal Institute of Technology
Stockholm, Sweden

Opponent

Assistant Professor Eva Hemmer, PhD
Department of Chemistry and
Biomolecular Science
University of Ottawa
Ottawa, Canada

"Even miracles take a little time"

- Fairy Godmother, Cinderella

CONTENTS

LIST OF ORIGINAL PUBLICATIONS

This thesis is based on the following original publications, referred to in the text by the Roman numerals (**I-IV**):

I   Satu Lahtinen, Qi Wang and Tero Soukka (2016). Long-lifetime luminescent europium(III) complex as an acceptor in an upconversion resonance energy transfer based homogeneous assay. *Analytical Chemistry* **88**: 654–658.

II   Satu Lahtinen, Annika Lyytikäinen, Henna Päkkilä, Emmy Hömppi, Niina Perälä, Mika Lastusaari and Tero Soukka (2017). Disintegration of Hexagonal NaYF$_4$:Yb^{3+},Er^{3+} upconverting nanoparticles in aqueous media: the role of fluoride in solubility equilibrium. *The Journal of Physical Chemistry C* **121**: 656–665.

III   Satu Lahtinen, Annika Lyytikäinen, Nina Sirkka, Henna Päkkilä and Tero Soukka (2018). Improving the sensitivity of immunoassays by reducing non-specific binding of poly(acrylic acid) coated upconverting nanoparticles by adding free poly(acrylic acid). *Microchimica Acta* **185**: 220.

IV   Satu Lahtinen, Stefan Krause, Riikka Arppe, Tero Soukka and Tom Vosch (2018). Upconversion cross-correlation spectroscopy of a sandwich immunoassay. *Chemistry – A European Journal* **24**: 9229–9233.

In addition, unpublished data is included.

The original publications have been reproduced with the permission of the copyright holders.

ABBREVIATIONS

AC	Autocorrelation
A_{CC}	Cross-correlation amplitude
CC	Cross-correlation
cTnI	Cardiac troponin I
CUC	Co-operative upconversion
EDTA	Ethylenediaminetetraacetic acid
ELISA	Enzyme-linked immunosorbent assay
EMU	Energy migration mediated upconversion
EphA2	Ephrin type-A receptor 2
ESA	Excited state absorption
ETU	Energy transfer upconversion
FRET	Förster resonance energy transfer
GSA	Ground state absorption
HR-TEM	High resolution transmission electron microscopy
ICP-MS	Inductively coupled plasma mass spectrometry
LF	Lateral flow
LOD	Limit of detection
OA	Oleic acid
PA	Photon avalanche
PAA	Poly(acrylic acid)
PEG	Polyethylene glycol
PSA	Prostate specific antigen
TEM	Transmission electron microscopy
TR	Time-resolved
TSH	Thyroid-stimulating hormone
UCCS	Upconversion cross-correlation spectroscopy
UCNP	Photon upconverting nanoparticle
UC-RET	Upconversion resonance energy transfer
UV	Ultraviolet

ABSTRACT

Photon upconverting nanoparticles (UCNPs) are promising reporters for supersensitive bioaffinity assays because they can be detected completely without autofluorescence background. This is enabled by anti-Stokes shifted luminescence where low-energy infrared radiation is converted to high-energy emission at visible wavelengths. Because the excitation and emission are at an optical window for biomaterials, UCNPs can be detected even in challenging sample materials such as whole blood. However, wider use of UCNPs in bioaffinity assays is limited due to certain challenges. Recently, there has been ongoing studies on UCNP structural integrity and luminescence in water and the effect of surface modification to biomolecule interactions, which should still be studied further in order to use the full potential of UCNPs in bioaffinity assays.

The aim of this thesis was to study the applicability of UCNP reporters in sensitive homogeneous and heterogeneous bioaffinity assays. The applicability of UCNPs to homogeneous assays was demonstrated by introducing Eu^{3+} chelate as an acceptor in an upconversion resonance energy transfer based assay. The Eu^{3+} chelate's intrinsic luminescence lifetime was longer than that of the UCNP donor and therefore the sensitized acceptor emission could be measured even after the donor's luminescence had decayed resulting in higher signal-to-background ratios. Additionally, the potential of UCNPs as reporters for cross-correlation spectroscopy was demonstrated with a homogeneous sandwich immunoassay. The assay was based on simultaneous detection of two differently emitting UCNPs brought together by binding of an analyte. UCNPs would be suitable reporters for cross-correlation spectroscopy applications where traditional fluorescence reporters suffer from autofluorescence.

One of the major factors limiting the immunoassay sensitivity is non-specific binding of UCNP conjugates. In this thesis, the non-specific binding of poly(acrylic acid) (PAA)-functionalized UCNP conjugates was reduced significantly in heterogeneous sandwich immunoassays by adding free PAA to the buffer during reporter incubation. The free PAA most likely blocked those areas in solid support where the UCNP conjugate might have bound non-specifically. The reduction in non-specific binding enabled detection of three and half times lower analyte concentration demonstrating that high sensitivity assays can be achieved with UCNP reporters.

In addition, the ion dissolution from fluoride-based UCNPs and its effect on luminescence and structural integrity of nanoparticles was studied in water-based solutions. The ions were found to dissolve until solubility equilibrium was achieved and the fluoride ions were observed to have major impact on the dissolution. The UCNPs disintegrated completely in highly diluted suspensions resulting in the disappearance of luminescence. The ion dissolution was prevented by adding free fluoride ions to the solution, which was an important observation in order to use diluted UCNP concentrations in bioaffinity assays. The study also demonstrated the requirement for surface capping that would protect the UCNPs from environmental effects.

TIIVISTELMÄ

Käänteisviritteiset nanopartikkelit soveltuvat leimoiksi erittäin herkkiin bioaffiniteettimäärityksiin, koska niiden fotoluminesenssi voidaan havaita täysin ilman mittausta häiritsevää autofluoresenssia. Tämä perustuu käänteisviritteisten partikkelien Stokesin siirtymän vastaiseen fotoluminesenssiin, jossa matalaenerginen infrapunasäteily muutetaan korkeanergiaiseksi emissioksi näkyvillä aallonpituusalueilla. Käänteisviritteisiä nanopartikkeleita voidaan erityisesti käyttää hankalissa näytemateriaaleissa kuten kokoveressä, koska niiden viritys ja emissio tapahtuvat biomateriaaleille optisesti läpinäkyvillä alueilla. Kuitenkin käänteisviritteisten nanopartikkelien ominaisuuksia vesiliuoksissa sekä niiden pintamodifikaation vaikutusta vuorovaikutukseen biomolekyylien kanssa tulisi tutkia lisää, jotta niitä voitaisiin käyttää laajemmin bioanalyyttisissä sovelluksissa.

Väitöskirjan tarkoituksena oli tutkia käänteisviritteisten nanopartikkelien soveltuvuutta leimoiksi herkkiin homogeenisiin ja heterogeenisiin bioaffiniteettimäärityksiin. Soveltuvuutta homogeenisiin määrityksiin tutkittiin resonanssienergiansiirtoon perustuvassa määrityksessä, jossa Eu^{3+}-kelaatti oli energian vastaanottaja. Eu^{3+}-kelaatin luontainen elinikä on pidempi kuin energian luovuttajana toimivan käänteisviritteisen nanopartikkelin, mikä mahdollisti vastaanottajan herkistetyn emission mittaamisen sen jälkeen, kun luovuttajan emissio oli sammunut. Lisäksi käänteisviritteisten nanopartikkelien soveltuvuus ristikorrelaatiospektroskopiaan osoitettiin kehittämällä kaksipuoleinen homogeeninen määritys, joka perustui kahdella eri aallonpituudella emittoivaan käänteisviritteiseen nanopartikkelin samanaikaiseen havainnointiin analyytin läsnä ollessa.

Erityisesti nanopartikkelikonjugaattien epäspesifinen sitoutuminen rajoittaa alhaisten analyyttipitoisuuksien havainnointia bioaffiniteettimäärityksissä. Väitöskirjassa polyakryylihapolla pinnoitettujen käänteisviritteisten nanopartikkelien epäspesifistä sitoutumista vähennettiin merkittävästi kaksipuoleisissa heterogeenisissä määrityksissä lisäämällä leimapuskuriin vapaata polyakryylihappoa. Tämä mahdollisti kolme ja puoli kertaa matalampien analyyttipitoisuuksien havaitsemisen, mikä on esimerkkinä käänteisviritteisten nanopartikkelien soveltuvuudesta leimoiksi erittäin herkkiin määrityksiin.

Lisäksi väitöskirjassa tutkittiin fluoripohjaisten käänteisviritteisten nanopartikkelien ionien liukenemista vesiliuoksissa ja sen vaikutusta nanopartikkelin rakenteen ehjyyteen ja luminesenssiin. Tutkimuksessa havaittiin, että ionien liukeneminen perustui liukoisuustuloon, mihin fluorilla oli erittäin suuri vaikutus. Erityisesti alhaisissa pitoisuuksissa käänteisviritteiset nanopartikkelit hajosivat melkein kokonaan, minkä vuoksi myös luminesenssia ei juuri enää havaittu. Ionien liukeneminen nanopartikkeleista voitiin kuitenkin estää lisäämällä liuokseen vapaata fluoria. Tämä havainto edistää käänteisviritteisten nanopartikkelien käyttämistä sovelluksissa, joissa tarvitaan alhaisia nanopartikkelin pitoisuuksia.

1 INTRODUCTION

Bioaffinity assays are used in life sciences research to detect and quantify molecules of interest, such as biomarkers, which are used in diagnosing diseases or monitoring a person's health. Bioaffinity assays are based on specific binding reactions between a biomarker, i.e. the analyte, and the recognition molecule, such as antibody, enzyme, or oligonucleotide. Presence of the bound analyte can then be detected with a reporter which binds to the analyte through a recognition molecule and produces a detectable signal. Bioaffinity assays are commonly classified as heterogeneous or homogeneous assays. Heterogeneous assays are based on immobilization of recognition molecules, i.e binders, to the solid support, which allows washing of unbound reporters. Homogeneous assays are referred to as separation free assays because the analyte recognition is detected by reporter signal modulation, and thus no washing of the unbound analytes or reporters is needed. Detection of the analyte binding in bioaffinity assays is most commonly measured with luminescent reporters due to the high sensitivity of the optical detection and fast response.[1, 2] However, conventional luminescent labels, such as organic fluorophores, suffer from autofluorescence interference originating from assay matrix or solid support materials causing high measurement background. Additionally, ultraviolet (UV) and visible light used for excitation of the labels is strongly absorbed by biological materials. These drawbacks limit the assay sensitivity.[3]

Photon upconverting nanoparticles (UCNPs) are under 50nm-sized unique nanoparticle reporters that can be measured in biological matrices completely without autofluorescence.[4, 5] This is enabled by the photon upconversion luminescence (i.e anti-Stokes photoluminescence), where low-energy infrared radiation is converted to high-energy emission at visible wavelengths[6, 7], and therefore the autofluorescence background occurring at infrared can be entirely separated spectrally from the detection window at visible wavelengths. Furthermore, infrared light used for UCNP excitation is not absorbed by biological materials. UCNPs contain lanthanide ions, and thus their luminescence has many beneficial characteristic shared with other lanthanide reporters, such as long emission lifetimes, narrow emission bands, and large (anti)-Stokes shift. In addition, UCNPs have a high photostability enabling long excitation times with high power intensities. Therefore, UCNPs are highly attractive reporters for bioaffinity assays requiring extremely sensitive detection.

The feasibility of UCNP reporters has been demonstrated in homogeneous[8-10] and heterogeneous[11-13] bioaffinity assays. At the moment, UCNP technology is of major interest in academic studies, but commercial applications are still lacking[14] although commercial instruments are already available. Sensitivities of UCNP-reporter-based bioaffinity assays have been comparable to commercial applications, but there is still major room for improvement. The transition from microsized to nanosized particles was a step forward in the utilization of upconversion in applications. However, the increased surface-to-volume ratio brought new challenges and the phenomena of luminescence

and the effect of surface modifications to biomolecule interactions should be studied further.[15]

2   REVIEW OF THE LITERATURE

2.1   Photon upconverting nanoparticles

2.1.1   Photon upconversion luminescence

Photon upconversion luminescence is a non-linear optical process where low-energy excitation is converted to high-energy emission. With UCNPs, excitation is usually at near infrared or infrared wavelengths and the emission can range from UV to visible wavelengths and even extend to infrared. In conventional fluorescence, the absorption of one high-energy photon results in the emission of a lower-energy photon according to the Stokes law, whereas in the anti-Stokes shifted photon upconversion luminescence, two or more low-energy photons are absorbed sequentially per single emitted higher-energy photon.[6, 7] The most efficient upconversion efficiency is observed with materials which have ladder-like metastable energy levels with long lifetimes to increase the probability of successive photon interactions.[16] Lanthanide ions incorporated in the UCNPs meet these criteria. The 4f orbitals of trivalent lanthanide ions are shielded by the filled $5s^2 5p^6$ subshells and the 4f orbitals have multiple metastable excited states with long lifetimes of microseconds to milliseconds due to the parity-forbidden but partially allowed 4f-4f optical transitions.[17-19] Figure 1 presents the two most common upconversion luminescence mechanisms in UCNPs, the excited state absorption (ESA) and the energy transfer upconversion (ETU),[6] in comparison to conventional fluorescence.
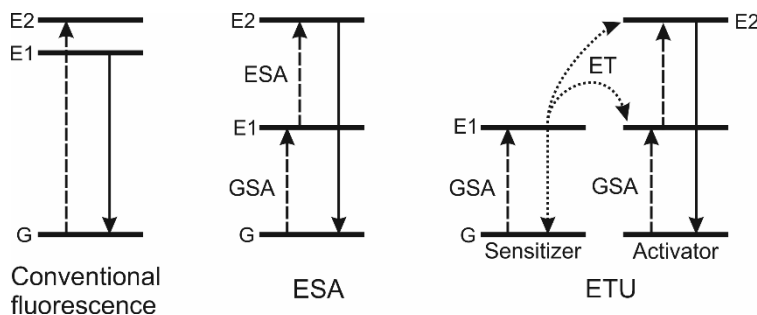
Figure 1. Energy diagrams of three different upconversion mechanism and conventional fluorescence for comparison. The dashed upward arrows represent the absorption and the solid-line downward arrows emission processes. The dotted arrows represent the energy transfer (ET) between the ions. GSA = ground-state absorption, ESA = excited state absorption, ETU = energy transfer upconversion, G = ground state, E1 and E2 = excited state. Adapted from Auzel[6] and Nadort et al.[16]

In the ESA mechanism, single ion with multiple energy levels absorbs two or more photons. The first absorbed photon excites the ion from the ground state (G) to the first metastable excited state (E1). Due to the long-lived metastable excited state, a second photon is absorbed exciting the ion from E1 to the second excited state (E2). The ion then emits one photon with higher energy than the energy of either absorbed photons. The first transition is referred to as ground-state absorption (GSA) and the second as ESA.[18]

ETU is based on the same transitions principles as ESA, but instead of one ion, ETU employs two adjacent ions. The ion referred to as sensitizer absorbs the sequential photons and transfers the energy non-radiatively to the activator ion. The activator ion is excited to E2 via two energy transfers from the sensitizer and emits the high-energy photon. The ions need to be close to one another and the energy difference of the G to E1 of the sensitizer needs to be in resonance with the E1 to E2 transition of the activator.[18] If there is a slight energy difference, the energy transfer needs to be phonon-assisted.[6]

Upconversion efficiency is dependent on the mechanism. Low absorption cross section of lanthanides limit the efficiency of ESA[20], and high excitation powers are needed to enable the ESA process. The ETU process utilizes sensitizers with larger absorption cross sections and is therefore around 100 times more efficient than ESA.[6] Due to the efficiency, ETU process with sensitizers and activators is by far most prominent mechanism used in UCNPs. As mentioned above, photon upconversion luminescence is also a non-linear optical process and thus the luminescence intensity is dependent on n^{th} power of the excitation intensity, n denoting the number of absorbed photons per one emitted photon.[21, 22]

In addition to the presented mechanisms, photon avalanche (PA), co-operative upconversion (CUC), and energy migration mediated upconversion (EMU) processes have also been recognized as upconversion luminescence mechanisms. PA is based on the cross-relaxation between two identical ions and looping of excitation and cross-relaxation.[23-25] PA is considered to produce the most efficient upconversion emission, but emission response is strongly delayed due to the looping process and only few nanomaterials have been reported to exhibit PA upconversion.[26] CUC is based on virtual and non-real intermediate states, and therefore the upconversion process is not efficient.[6, 27, 28] The EMU process is more complex exploiting four types of luminescent centers in different layers.[29, 30]

2.1.2   Composition and optical properties

UCNPs are composed of inorganic crystalline host lattice doped with lanthanide ions as the luminescent centers. As the ETU mechanism is considered to be most efficient in upconverting nanoparticles, the host lattice is usually doped with two different lanthanide ions acting as the excitation energy absorbing sensitizers and the emitting activators. Yb^{3+} is the most commonly used sensitizer because it has the highest absorption cross-section from all the lanthanide ions, which is needed for the efficient upconversion emission. The energy level diagram of Yb^{3+} is simple, and the ion is usually excited with 976 nm from $^2F_{7/2}$ ground state to $^2F_{5/2}$ excited state. In addition, the excited state energy of Yb^{3+} matches with the lanthanide ions used most commonly as activators.[31] Excitation wavelength of Yb^{3+} around 980 nm is absorbed by water, and therefore Nd^{3+} has been used as a sensitizer in some cases to shift the excitation to lower wavelengths around 800 nm to diminish the heating of the water solutions.[32] However, in order to achieve efficient upconversion, Nd^{3+} is mostly used in co-operation with the Yb^{3+} and requires additional shell structure around the nanoparticle core to prevent

cross-relaxations with the activators.[33-35] Recently, Er^{3+} ions have also been used as sensitizers in UCNPs with excitation around 1535 nm.[36-38] In addition to lanthanides, organic chromophores have been used as sensitizers to shift the excitation to lower wavelengths.[39-41] Sensitization through organic chromophore has also been claimed to enhance upconversion emission.[42] By using organic chromophores as sensitizers, UCNPs lose their advantage of photostability, since organic chromophores can photobleach during long-term excitation with high-power densities.[43]

Most of the lanthanide ions can act as activators in upconversion emission. In order to gain efficient upconversion, the activators should have ladder-like excited energy states with long luminescent lifetimes. However, if the energy states are too close to each other, the probability of non-radiative relaxations decrease diminishing the upconversion efficiency.[31] The most efficient upconversion and therefore the most common activators in UCNPs are Er^{3+}, Tm^{3+} and Ho^{3+} due to their energy level composition with multiple long lifetime excited states and proper gaps between certain energy levels.[44, 45] In figure 2, the emission spectra of the most commonly used activators of Er^{3+} and Tm^{3+} are presented. The emission spectrum of Ho^{3+} activator resembles the Er^{3+} spectrum, but the upconversion efficiency of Ho^{3+} is lower than that of Er^{3+}, and therefore Ho^{3+} is not used as widely.
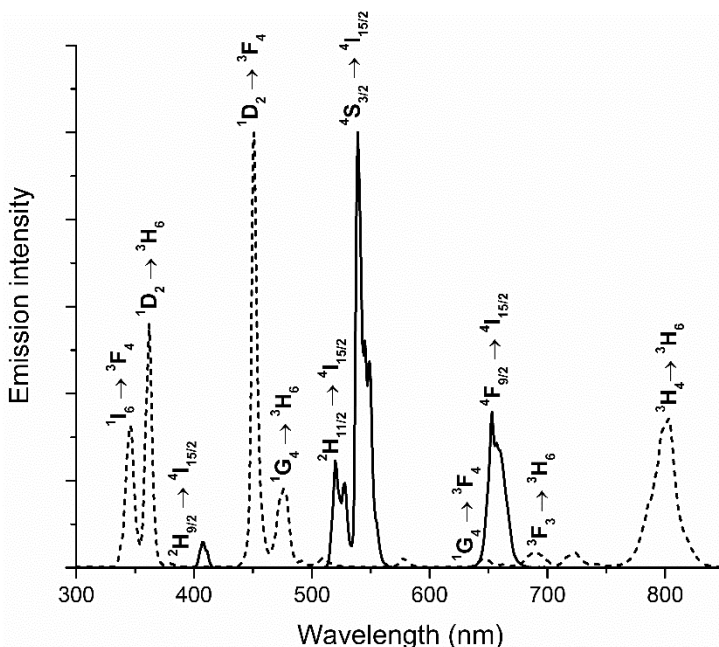
Figure 2. Upconversion emission and the radiative transitions of $NaYF_4$:Yb^{3+},Er^{3+} (solid-line) and $NaYbF_4$:Tm^{3+} (dashed-line) nanoparticles upon 980 nm excitation. Adapted from Vuojola et al.[46] and Kale et al.[47] The emission intensities have been normalized to the 450 nm and 546 nm wavelengths in Tm^{3+} and Er^{3+} doped particles, respectively.

The host matrix's composition has high impact on the upconversion luminescence efficiency and emission peak ratios because it defines the distance between the lanthanide ions, their spatial position, their coordination numbers, and the crystal fields around them.[7] The most important quality of the host matrix is that the host lattice needs to be transparent to the excitation and emission light. The host lattice also needs to have low phonon energy to prevent non-radiative multiphonon relaxations that can lower the upconversion efficiency. Additionally, chemical and thermal stabilities are very important qualities of the host lattice in order to use UCNPs in applications.[31]

Heavy halides, such as chloride, bromide and iodide-based materials, have phonon energies lower than 300 cm^{-1}. However, the host lattice should be chemically stable, and as heavy halides are hygroscopic, they cannot be widely used in applications.[45] Oxide-based materials have been considered to have a high chemical stability, but the phonon energies are over 500 cm^{-1}.[48] Fluoride-based host lattices have low phonon energies of around 350 cm^{-1} [49] and they are the most common UCNP host materials. Fluoride materials have been considered to be chemically stable, but recent studies have presented conflicting results, which are discussed in the section 2.1.4 Upconversion efficiency and environmental sensitivity. Host lattice cations should have ionic radius close to the lanthanide ions doped in the UCNPs in order to avoid crystal defects and lattice stress. Rare earth ions such as Y^{3+}, Lu^{3+}, and La^{3+}, alkali metals and earth metals such as Na^+, K^+, Ca^{2+} and transitions metals such as Mn^{2+} have been studied in UCNP host lattices.[45]

The crystal structure of the host lattice also has a significant effect on upconversion efficiency as it determines the crystal field and site symmetry of the lanthanide ions in the host lattice. Upconversion efficiency of hexagonal $NaYF_4$:Yb^{3+},Er^{3+} (also known as β-$NaYF_4$:Yb^{3+},Er^{3+}) emission is stronger than the emission of cubic $NaYF_4$:Yb^{3+},Er^{3+} (also known as α-$NaYF_4$:Yb^{3+},Er^{3+}).[50] Hexagonal crystal structure has lower symmetry having crystal fields with more uneven components around the lanthanides, and therefore the probability of 4f-4f transitions is increased.[26] So far, $NaYF_4$ host lattice with hexagonal crystal structure has been considered to have the most efficient upconversion luminescence.[50-53]

Upconversion efficiency is also dependent on the dopant concentrations in the host lattice. Upconversion emission intensity is higher with higher amounts of absorbing and emitting ions to certain extent. Furthermore, in ETU upconversion mechanism, the resonant energy transfer efficiency is dependent on the distance between the sensitizer and the activator ions in the particle lattice, and the distance between the ions usually shortens as the doping concentration increases in the nanoparticles. However, the high doping concentrations can lead to concentration quenching, which decreases the upconversion emission efficiency. There can be three different mechanisms for concentration quenching: energy migration, cross-relaxation, and energy back transfer (Figure 3). The concentration quenching of Yb^{3+} sensitizer ions originates from energy migration from Yb^{3+} ions to the surface defects. The activator ions usually have more complex energy levels and thus the concentration quenching is thought to originate from cross-relaxations between two adjacent ions.[26] Johnson et al. claimed, however, that the

quenching in high activator concentration originates from the energy migration as the growth of a shielding $NaLuF_4$ shell around 100 mol% Er^{3+} doped $NaF_4:Er^{3+}$ particles reduced the quenching signifantly.[54] Concentration quenching can also be caused by energy back transfer from the activator to the sensitizer ion. The doping levels in $NaYF_4$ host matrix are therefore usually low. The doping concentration of Yb^{3+} does not usually exceed 20 mol% [55] and the concentrations of Er^{3+} and Tm^{3+} activators are lower than 3 and 0.5 mol% [56, 57], respectively. It should be noted that the optimal doping concentrations are dependent on the host matrix.[58]
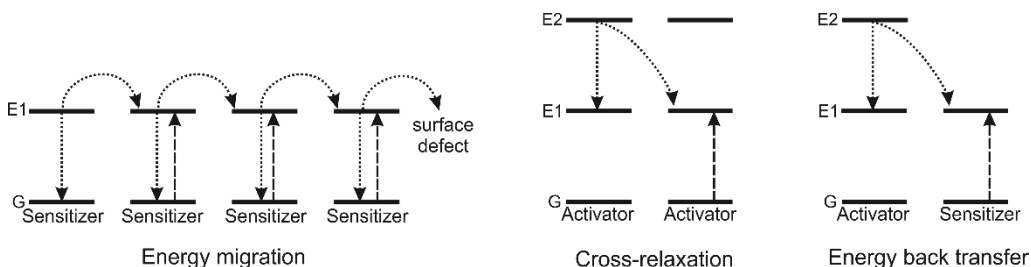
Figure 3. The concentration quenching mechanisms in lanthanide ion doped upconverting nanoparticles. The dashed upward arrows represent the absorption and the dotted arrows the energy transfer between the lanthanide ions. G = ground state, E1 and E2 = excited state.

UCNPs are usually excited with low excitation powers (<100 W cm^{-2}) due to the efficient upconversion mechanism, and low-power laser diodes are also inexpensive excitation sources. However, the concentration quenching can be circumvented by using high-power excitation. Jin et al. demonstrated that, by using high excitation densities of 2.5×10^6 W cm^{-2}, bright Yb^{3+}-Tm^{3+} doped UCNPs with up to 8 mol% Tm^{3+} concentration can be achieved.[59] Similar observation was done by Drees et al. with Yb^{3+}-Er^{3+} doped UNCPs.[60] Bright UCNPs were achieved with the excitation power density of 1.8×10^4 W cm^{-2} when Er^{3+} concentration was increased up to 20 mol%.[60] These bright UCNPs excited with high-power densities enable single nanoparticle detection, for example, in imaging applications. Nevertheless, the high excitation power is not always possible to achieve and is not suitable for every application, for example, due to the heating of the water-based solution caused by the infrared absorption of water.[61, 62] As mentioned above, an inert shell around the UCNPs has also been proven to alleviate concentration quenching due to prevention of energy migration to surface defects.[54, 63]

Lanthanide ion doping concentrations can also affect the emission peak ratios in Yb^{3+}-Er^{3+} and Yb^{3+}-Tm^{3+} doped UCNPs. For example, a higher Yb^{3+} doping concentration has been reported to enhance red emission while decreasing green emission in Yb^{3+}-Er^{3+} doped UCNPs in different host matrices.[64-68] In addition, increase in the activator concentration increases red emission[69]. The increased red emissions were attributed to the increased cross-relaxation between two Er^{3+} ions or to the energy back transfer from the Er^{3+} to Yb^{3+}. The red emission of Yb^{3+}-Er^{3+} doped UCNPs is affected by multiple conditions and is more thoroughly discussed in the section 2.1.4 Upconversion efficiency and environmental sensitivity. In Yb^{3+}-Tm^{3+} doped

nanoparticles, higher Tm^{3+} concentrations have been observed to favor two (800 nm) or three photon emissions (644, and 475 nm)[56, 68], whereas the higher Yb^{3+} concentrations favor the four and five photon emission (450 , 362, and 342 nm)[47, 70]. The enhanced NIR emission was attributed to Tm^{3+}-Tm^{3+} cross-relaxations and the higher blue and UV emissions to the more efficient absorption and energy transfer from Yb^{3+} to Tm^{3+}.

In addition, composition and local structure of host lattice components affect the emission peak intensities and ratios. The red emission of Yb^{3+}-Er^{3+} doped UCNPs was higher in oxide lattice than fluoride lattice because the higher phonon energy of the oxide lattice increased the phonon assisted energy transfer to the red emitting state.[71] Increasing the Na/rare earth ion ratio in cubic Na_xYF_x:Yb^{3+},Er^{3+} UCNPs increased the red to green ratio significantly, changing the local structure around lanthanide luminescent centers[72]. The effect was hypothesized to result from Er^{3+}-Er^{3+} cross relaxation or from the Er^{3+}-Yb^{3+} back energy transfer. Mn^{2+} doping in the particle host lattice has also been demonstrated to result in only red upconverted emission.[73-75]

2.1.3   Synthesis and biomodification

Synthesis

The most common synthesis methods are thermal decomposition, solvo/hydrothermal synthesis, and high temperature co-precipitation.[76, 77] In the thermal decomposition method, lanthanide trifluoriacetates are usually used as organometallic precursors in high boiling solvents. The solvo/hydrothermal method uses an autoclave, where temperature and pressure above the solvents critical points is applied. Temperatures used in solvo/hydrothermal method are lower than in thermal decomposition. The high temperature co-precipitation does not need as stringent initial synthesis conditions as the thermal decomposition, but usually an additional annealing step is required to improve the crystallinity of the nanoparticles. The method is based on lanthanide precursors in solvents with a high boiling point, such as 1-octadecene.

Synthesis determines the size, shape, monodispersity, and crystal structure of UCNPs, which are important parameters of the nanoparticles used in bioaffinity assays. Synthesized particles should possess narrow size distribution, have pure crystal structure, and the synthesis should have high batch-to-batch reproducibility. Therefore, synthesis parameters, such as temperature, heating time, ligand-to-solvent ratios, ligand type, and doping ions, need to be carefully controlled. The crystal structure is important as the hexagonal UCNPs have higher upconversion intensity than the cubic UCNPs.[50] Hexagonal nanoparticles are suggested to originate from cubic nanoparticles that are first formed in the synthesis. The hexagonal particles grow at the expense of dissolving cubic particles[78-81] yielding particles with narrow size distribution[82]. Nevertheless, hexagonal $NaYF_4$ particles are more difficult to synthesize in nanoscale than the cubic ones because the high surface tension of smaller particles thermodynamically favors the cubic phase.[83] Thus, higher reaction temperatures and longer heating times have been used to overcome the high energy barrier between the transformation from cubic to hexagonal nanocrystals.[84-86] Lanthanide ion doping also

affects the crystal structure and size of the particles, especially if smaller nanoparticles are pursued. Gd^{3+} doping has been observed to favor small hexagonal particles[87] whereas high Yb^{3+} doping can lead to larger cubic particles[88].

Polar head groups containing capping ligands coordinate with reactants/ions, therefore controlling the particle growth by preventing lattice expansion. The choice and concentration of capping ligand in the synthesis affects the crystal morphology, size and shape of the nanoparticles. According to Sui et al., oleic acid (OA) capping ligand coordinates especially with Y^{3+} ions, and thus facilitates the orderly arrangement of the ions, which promotes the phase transition from cubic to hexagonal[89]. However, other studies suggest that hexagonal particles are difficult to achieve only with the OA ligand, and mixtures of oleylamine/OA or tri-*n*-octylphosphine/OA are needed to yield hexagonal particles.[85, 90, 91] OA to the 1-octadecence solvent ratio has also been observed to affect particle size and shape. Increasing the OA amount led to smaller particles[92, 93], but with high OA amounts the particle shape changed from sphere to rod as OA prefers to adsorb to the (010) crystal plane promoting growth mainly from the (001) plane.[92] In addition to the control of reagents composition, concentration, reaction time, and temperatures, controlling other parameters, such as argon flow, cooling times, and stirring rates affect the nanoparticle size, morphology and luminescence.[94] The local crystal structure can be modified also by controlling the sodium/rare earth or fluoride/rare earth ratios[72]. The results for optimal synthesis method and parameters vary between publications and research groups. According to Resch-Genger and Gorris, differences in the synthesis methods and variation in optical characterization of UCNP luminescence partly explain the differences in the results obtained by different groups.[95]

In most cases, particle constituting ions have been assumed to be homogeneously distributed in single nanoparticles. However, heterogeneous distribution was observed when the ion composition of single nanoparticles was studied.[96-98] In $NaGdF_4$:Y^{3+},Tb^{3+} nanoparticles, Gd^{3+} ions were more concentrated in the core and Y^{3+} ions on the surface of the nanoparticles.[96] In $NaYF_4$:Yb^{3+},Er^{3+} UCNPs, a concentration gradient of Yb^{3+} was observed, Yb^{3+} ions being more concentrated in the nanoparticle core.[97] The concentration gradient was independent of the particle size and Yb^{3+} doping concentration. The heterogeneous doping was attributed to different reactivity of rare earth ions during nanoparticle nucleation and growth.[98] Heterogeneous ion distribution can affect the upconversion efficiency of the UCNPs. If there is a higher local concentration of the sensitizer ions, they are locally more prone to concentration quenching. In addition, if activator ions are homogeneously distributed compared to heterogeneous distribution of sensitizers, local ion-ion distances between the sensitizer and activator are too long for efficient energy transfer.[98] More homogeneous doping was achieved with synthesizing successive monolayers with layer-by-layer synthesis methods, which was observed to enhance upconversion efficiency.[98]

Inorganic shells can be added around the core particles to shield UCNPs from surface related quenching[99, 100] or to isolate the optically active ions in distinct layers in the nanoparticle to control the ion interactions with each other and the environment[101]. The

inorganic shell is commonly the same or similar material as the core host matrix. A shell can be formed with different synthesis strategies. The most popular method is a seed mediated epitaxial growth where core nanoparticles serve as nuclei for the shell layer growth. The shell precursors are added either straight to the growing solution of core particles or the core particles are washed and the shell is grown on a separate step.[99, 102] Johnson et al. used a seed-mediated Ostwald ripening method for shell growth.[103] They injected small α-NaYF$_4$ nanoparticles into the hot solution of core particles. The sacrificial α-NaYF$_4$ particles acted as precursor shell materials by dissolving and depositing on the core particles. The cation exchange method has been used for subnanometer shell formation.[104] Multishell layers can be formed by using multiple steps of epitaxial growth or Ostwald ripening[99, 103], although multishell formation can be time consuming and laborious. Interfaces between the core and the shell or multiple shells might not be sharp, and an intermixing of core and shell materials, especially cations, has been observed.[105-107] Additionally, as with the core particles, gradient ion distribution has been observed in the shell.[106]

Biomodification

UCNPs need to be water dispersible if they are employed in bioanalytical applications. Synthesis can yield water dispersible UNCPs if hydrophilic capping ligands, such as citrate[65], ethylenediaminetetraacetic acid (EDTA)[108], poly(acrylic acid) (PAA)[109], or polyethylenimine[110], are used. However, OA is the most commonly used capping ligand (Figure 4a) yielding hydrophobic UNCPs, and subsequent surface modification steps are therefore needed to render water dispersible UCNPs. In addition, the as-synthesized UCNPs do not have functional groups, such as COOH, NH$_2$, sulfonate, thiol, or maleimide, needed for biomolecule conjugation. The surface modification should yield UCNPs that are water dispersible, colloidally stable, monodisperse, and contain functional groups for biomolecule conjugation. Sedlmeier and Gorris have extensively reviewed the different strategies for surface modification of UCNPs[111]. Commonly, surface modification is done by silanization, ligand exchange, layer-by-layer method, or ligand interaction method (Figure 4). Ligand oxidation is based on the oxidization of OA's carbon double bond yielding carboxylic acid functional group[112, 113]. Ligand oxidation is a rarely used strategy for surface modification and therefore not presented in figure 4.

Encapsulating the UCNPs in silica shell has been one of the most common surface modification methods. Hydrophobic UNCPs with OA on the surface can be rendered water dispersible by using a reverse microemulsion method, where tetraalkyl ortholilicate is hydrolyzed in the presence of ammonia and detergents which form micelles in nonpolar solvent. Functional groups are obtained by adding organosilanes during the silica shell formation or in additional silanization step (Figure 4b).[111] In the layer-by-layer method, positively and negatively charged polymers are deposited sequentially on the particle surface allowing control of surface thickness by regulating the amount of layers (Figure 4c).[114, 115] In the ligand exchange method, the hydrophobic OA is changed to hydrophilic ligands that coordinate with lanthanide ions via -SH, -NH$_2$, -COOH or -PO$_3$H groups. Multidentate ligands are usually more stable than bi- or monodentate ligands (Figure 4d

and f). Ligand exchange can be done directly by adding high excess of the hydrophilic ligands in elevated temperatures[116], or by first removing the OA with acidic treatment creating bare UCNPs and then adding the new ligand[117, 118]. Ligand exchange can also be done with nitrosonium tetrafluoroborate, which first replaces the original ligand and can then be replaced with the desired ligand.[119, 120] Ligand interaction method uses amphiphilic molecules that intercalate with the OA ligand through hydrophobic van der Waals interactions (Figure 4e).[121-123] The cross-linking of the amphiphilic polymer can lead to improved colloidal stability in aqueous solutions.[121]
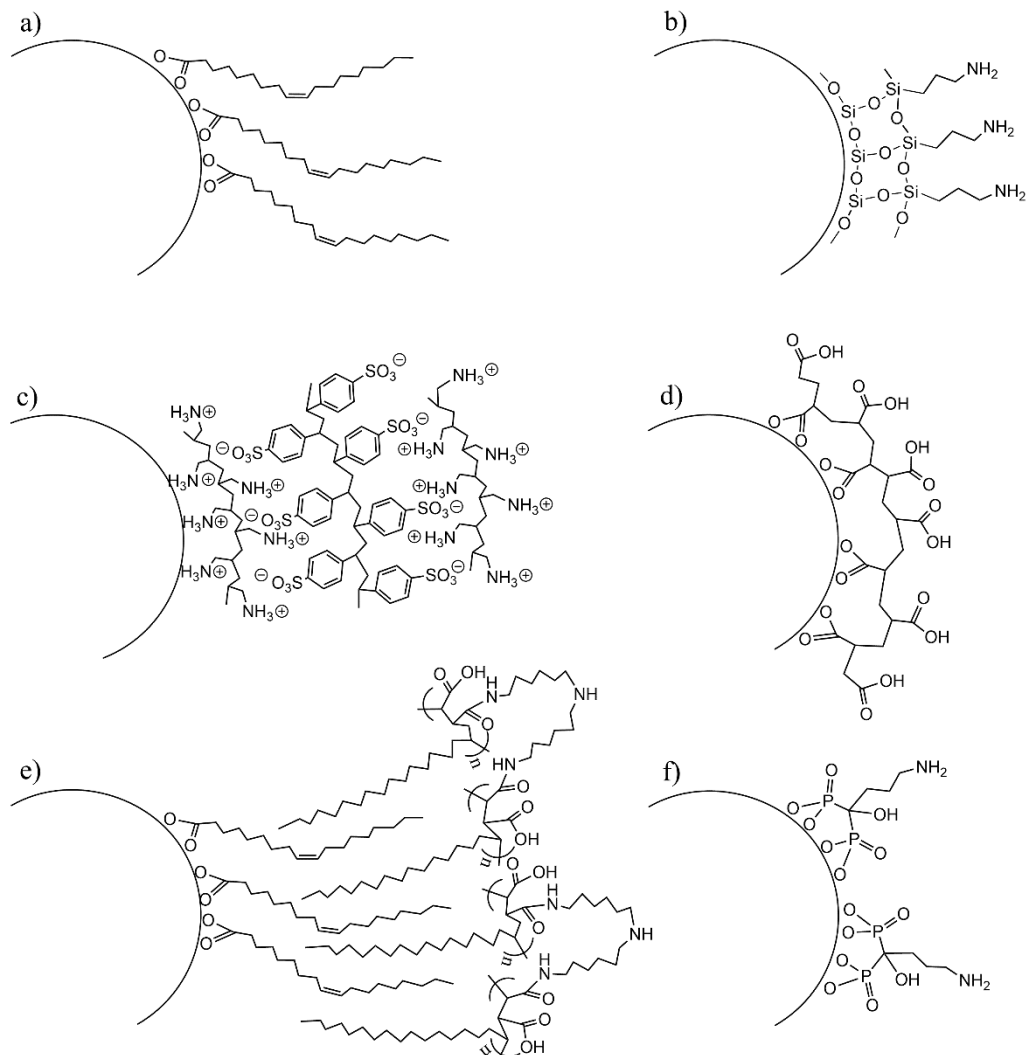
Figure 4. Surface chemistry of upconverting nanoparticles. a) Oleic acid surface after synthesis, b) silica shell with amino groups, c) layer-by-layer coating with alternating layers of positive poly(allylamine) polymer and negative poly(sodium 4-styrenesulfonate) polymer (modified from Wang et al.[114]), d) poly(acrylic acid) polymer multidentate ligand, e) amphiphilic coating with poly(maleic anhydride-alt-1-octadecene) cross-linked with bis(hexamethylene)triamine[121], f) alendronic acid ligand[124]. Figure not in scale.

All the presented methods can yield water dispersible UCNPs with functional groups for biomodification. The conjugation of biomolecules is usually done with well-known coupling chemistries, such as carbodiimide[125] or click chemistry[126]. Surface modification should be carefully chosen because it affects the stability of UCNPs in different biologically important media, such as serum or plasma, and their non-specific binding in bioaffinity assays. UCNPs are also susceptible to environmental effects decreasing their luminescence efficiency. Therefore, the surface modification should also shield the UCNPs from the environment. The effect of surface modification on the protection of UCNPs from the environment and on non-specific binding and stability are discussed in the sections 2.1.4 Upconversion efficiency and environmental sensitivity and 2.2.2 Heterogeneous assays, respectively.

2.1.4   Upconversion efficiency and environmental sensitivity

The upconversion emission intensity and efficiency are strongly dependent on the particle size. Initially, submicrometer particles were studied and utilized in bioanalytical applications and they were considered to be unaffected by their environment.[125, 127] Nanosized particles have become prevalent in the last decade because they are colloidally stable and do not suffer from sterical hindrances in bioapplications. Upconversion luminescence intensity and efficiency are, however, significantly lower in nanosized than in submicrometer particles or bulk material. Nanosized particles have lower amounts of active ions taking part in the upconversion process. More importantly, quantum yield has also been found to be size dependent, and quantum yields of nanoparticles are extremely low when compared to bulk material, commonly less than 1 %.[128, 129] It should be noted, however, that the quantum yield is dependent on the excitation power density since upconversion is a non-linear optical process.[130] Excitation power density should always be determined in the sample when measuring quantum yields and preferably measured with a range of excitation power densities.[130, 131] The lower quantum yield of nanoparticles can be explained by the high surface-to-volume ratio, which exposes higher proportions of the nanoparticle to surface defects and environmental quenchers resulting in decreased quantum yields as well as luminescence lifetimes.[100, 128, 129, 132, 133] Upconversion efficiency does not decrease linearly with the particle size because surface quenching can affect several nanometers of depth from the particle surface due to the energy migration and can therefore quench almost an entire nanoparticle under 20 nm in size.[133-136] Kraft et al. calculated that surface quenching effect can be ignored with UCNPs over 115 nm.[137]

Solvents are the main environmental quenchers of upconversion luminescence and upconversion efficiency, and emission peak ratios are strongly dependent on the solution that the UCNPs are dispersed in.[138] Significantly decreased luminescent intensities, quantum yields, and luminescent lifetimes have been observed especially in water when compared to organic solvents or heavy water.[120, 139, 140] The lower luminescence efficiency in water has been attributed to the energy vibrational modes of OH-groups at 3,300−3,700 cm^{-1}.[141] The OH-groups of water enable multiphonon relaxations of $^4I_{11/2}$ to $^4I_{13/2}$ and $^2H_{11/2}$/$^4S_{3/2}$ to $^4F_{9/2}$ transitions of Er^{3+} ions in Er^{3+}-doped

UCNPs (Figure 5).[118, 140] However, the main quenching mechanism of upconversion emission is most likely caused by multiphonon deactivation of the Yb^{3+} sensitizer due to the overtone OH vibrations of water molecules[142, 143], which explains the significant decrease in luminescence efficiency with both Tm^{3+} and Er^{3+} doped UCNPs. The non-radiative relaxation of Yb^{3+} excited state by water can cause the quenching of almost entire volume of nanosized particles due to the Yb^{3+}-Yb^{3+} energy migration. The quenching of Er^{3+} activator near-infrared excited states has also been proposed as the major contributor to the low upconversion efficiency in different solvents.[144] There has been discussion whether the Yb^{3+} or Er^{3+} infrared excited state quenching is the main reason for low efficiencies.[136, 143-145] The quenching effect was studied in different solvents in different studies and therefore final conclusions cannot be drawn yet. Although the water quenching is detrimental to UCNP luminescence, it can exploited in sensing of minor amounts of water in organic solvents.[146]
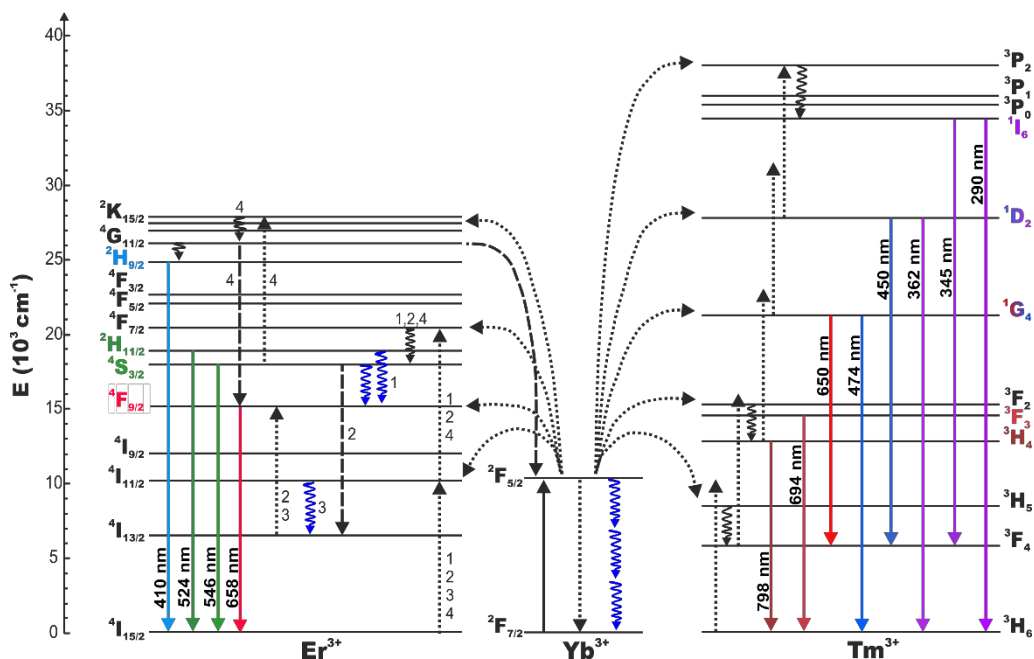
Figure 5. Energy level diagram of Er^{3+} or Tm^{3+} doped upconverting nanoparticles. Solid-line, dotted and dashed arrows represent photon absorption or emission, energy transfer, and energy back transfer, respectively. Wavy black arrows represent the relaxation processes and wavy blue arrows the multiphonon relaxations caused by OH vibrations. Adapted from Arppe et al.[142], Hyppänen et al.[147] and Berry et al.[148]

Mechanism of red emission in Yb^{3+} and Er^{3+} doped $NaYF_4$ materials has created discussion over the years, especially whether the red emission is a two-photon or a three-photon process. Four of the most commonly proposed excitation paths for red emission are presented in figure 5. Traditionally, red emission has been considered to originate from two-photon excitation paths. Two different two-photon excitation paths have been proposed. Firstly, the green emitting states of $^2H_{11/2}$ and $^4S_{3/2}$ are populated by the ETU

mechanism from Yb^{3+} to Er^{3+}, after which the red emitting state $^4F_{9/2}$ is populated by multiphonon relaxation (path 1, Figure 5). Secondly, energy transfer from Yb^{3+} to Er^{3+} populates the $^4I_{11/2}$ state, after which the multiphonon relaxation populates the $^4I_{13/2}$ state and the red emitting state is then populated by the ETU mechanism (path 3, Figure 5). According to group of Lee, path 3 is the dominant excitation path.[149, 150] Traditionally proposed three-photon excitation path includes first the population of the green emitting states followed by the Er^{3+}-Er^{3+} cross-relaxation populating the $^4I_{13/2}$ state (path 2, Figure 5). The red emitting state is then populated through the ETU mechanism. However, Anderson et al. presented an alternative three-photon excitation path for the red emission, where the red emission originates from the $^4G/^2K$ manifold states and is excited from the green emitting states via the ETU mechanism (path 4, Figure 5).[151] The red emitting state is then populated by back energy transfer to Yb^{3+}. Berry et al. studied the four hypothesized paths and claimed that the population of $^4I_{13/2}$ state does not lead to red emission and therefore path 2 and 3 would not be active.[152] In their study, path 4 was proposed as the predominant mechanism for red emission as suggested by Anderson et al.

The conflicting observations on the red emission excitation paths can be explained by the differences on the nanoparticle environment. The red-to-green ratio of Er^{3+} doped UCNPs has been observed to vary depending on the nanoparticle environment.[120, 138, 140] Both Hyppänen et al. and Würth et al. demonstrated that in aqueous media the red emission originates from a two-photon path and in organic solvents or other solvents without OH vibrations the red emission is dominated by the three-photon process.[147, 153] Würth et al. also demonstrated that the red emission mechanism is dependent on the power density of the excitation and, in high power densities, the population of the red emitting state is similar in water and organic solvents.[153] In aqueous environments, OH vibrations cause multiphonon relaxation of the $^2H_{11/2}/^4S_{3/2}$ and $^4I_{11/2}$ states preventing the excitation to higher energy levels, where the three-photon process occurs. Due to the OH vibrations, red emission is most prominent in water, whereas green emission is favored in organic solvents in low excitation power densities.[147, 153] Thus, sample solution should be taken into account when using UCNPs in different applications. Furthermore, Würth et al. raised a question that which dopant concentrations in $NaYF_4$ host materials are optimal for water solutions.[153] Most of the luminescent characterizations are made after synthesis in organic solvents. Optimal dopant concentrations have not been studied in water solutions although luminescent properties differ between organic solvents and water, and thus the dopant concentrations should be assessed in water. These studies were conducted with $NaYF_4$ host matrix and different mechanism may therefore be applied to other matrices.

Water-based solutions do not only quench the excited states of the lanthanides doped in the UCNPs but also affect the structural integrity of the particle. The dissolution of nanoparticle constituting ions in water solutions has been observed in fluoride-based host matrices.[154-156] The dissolution rate was dependent on the crystal structure as hexagonal UCNPs were more stable in water solutions than cubic UCNPs.[155] Composition of the water solution was also found to have a significant effect on the

dissolution rate, which was most extensive in the phosphate buffer and lower in the phthatale buffer.[156, 157] According to Lisjak et al., dissolution in the phosphate buffer happens due to the formation of lanthanide phosphate compounds, and in the water and phthatale buffer due to the hydrolysis of the UNCP surface resulting in the release of fluoride ions.[157] The dissolution of ions can lead to changes in particle morphology and poor structural integrity[158, 159] leading to decreased upconversion luminescence intensities and lifetimes.[156, 158] According to the study of single nanoparticle dissolution by Dukhno et al., the dissolution of ions from the nanoparticles is not uniform between nanoparticles and can lead to heterogenic luminescent properties and unrepeatable measurements.[159] Dissolution has been studied with fluoride-based materials and there are no studies yet regarding the dissolution of other host matrix materials such as oxide-based UCNPs.

In order to retain the high luminescence efficiency and particle integrity in water solutions, UCNPs should be protected from the environment. Environmental luminescence quenching is considered to be non-radiative Förster resonance energy transfer (FRET) by dipole-dipole coupling between electronic transitions of UCNP lanthanides and solvent or ligand molecule vibrations, and it is therefore distance dependent.[144] UCNPs have been protected from surface-related luminescence quenching with inorganic shells.[100, 144, 160] Different shell thicknesses from 3 to 10 nm has been presented for the sufficient prevention of quenching[134, 161, 162]. A quantum yield of 9 % was achieved with UCNPs of 45 nm in size including a 11 nm-thick shell, which is close to the quantum yield of bulk material.[163] Nevertheless, it should be underlined that in most of the studies the luminescence properties of the core/shell materials have been characterized in organic solvents or dried powders. Wang et al. studied luminescence intensity of 20 nm core/shell UCNPs (5 nm shell) in 20 % water and, although the intensity was higher with core/shell particles when compared to bare particles, the overall intensity had decreased 35 % in 20 % water when compared to solution with no water.[100] In addition, because the inorganic shell is a similar fluoride structure as the core, it can be assumed that shell dissolves similarly as the core. Quenching of the luminescence can be also caused by the incorporation of ions with OH vibrations to the crystal lattice during the synthesis, which can be avoided by decreasing water content in the synthesis.[163]

Surface-related quenching and ion dissolution in water solutions has also been prevented with polymer surface modifications. A silica shell of 7-10 nm has been observed to diminish the luminescent quenching in water, but the decrease in luminescence was still significant.[142] Amphiphilic coating with poly(maleic anhydride-alt-1-octadecene)-bis(hexamethylene)triamine[164], layer-by-layer method by alternating PAA and Nd^{3+} ions[165] or crosslinked PAA and poly(allylamine hydrochloride) layers[166], and polysulfonate capping[167] were reported to effectively shield UCNPs from the ion dissolution in water solutions. However, new efficient methods to protect the nanoparticles from luminescence quenching and ion dissolution should still be studied and tested in bioanalytical applications. There are some studies observing that the OH and CH vibrations of surface ligands can quench the upconversion luminescence[129, 132]

but other studies have found that the quenching of ligands have minor or negligible effects[120, 153].

Upconversion luminescence is also dependent on the temperature due to the thermal quenching, which leads to more efficient nonradiative relaxations of the excited states. Especially, the ratio of green emission intensities at 525 and 545 nm has been observed to change with the temperature.[168] The ratio of these emission bands has been used for thermal sensing in biological systems.[169-171] The host matrix composition has been observed to affect the thermal sensing range and sensitivity of UCNPs. Hexagonal $NaYF_4$ host matrix has the brightest upconversion intensity, but its temperature sensing range is lower compared to other materials, such as Al_3O and Gd_2O^3, due to lower thermal stability.[171-173] The temperature sensing range of $NaYF_4$ host matrix nanoparticles was increased both by inactive shell[170] and by Yb^{3+} and Nd^{3+} co-doped shell[174]. When comparing the host matrix compositions of Y_2O_3, YVO_4, and YPO_4, it was observed that the YPO_4 matrix with the highest phonon frequency maxima had the lowest temperature sensitivity.[175] Hyppänen et al. also demonstrated that the environment has an effect on the intensity ratios of 525 and 545 nm due to the local warming of water under 980 nm laser excitation, which does not occur in heavy water or organic solvents.[176] This observation should be considered when designing UCNP-based thermal sensors.

In addition, heavy metals quench the upconversion luminescence, of which Hg^{2+} has the highest effect.[177] However, the concentration of heavy metals needs to be high (mM range) to observe an effect in the intensity, and thus, in practice, UCNPs are not suitable for heavy metal sensing without chromophore that binds ions, for example.[178]

2.2 Upconverting nanoparticles in bioaffinity assays

2.2.1 Homogeneous FRET-based assays

Homogeneous bioaffinity assays are separation- and wash-free assays that are fast and simple to perform because they contain only mix and measure steps. Analyte detection in homogeneous assays is commonly based on FRET, which is based on non-radiative energy transfer from excited donor fluorophore to an emissive or non-emissive acceptor via dipole-dipole interactions. In FRET systems, the emission intensity and lifetime of the donor should decrease and the emission of the emissive acceptor should appear. If long-lifetime luminescence donors are paired with intrinsically short-lived fluorescence lifetime acceptors, apparent fluorescence lifetime of the acceptor increases upon FRET.[179, 180] Energy transfer efficiency is dependent on two critical aspects. First, the emission spectrum of the donor and the excitation spectrum of the acceptor have to overlap. Second, energy transfer is strongly distance-dependent, the FRET efficiency being inversely proportional to the sixth power of the distance between the donor and acceptor.[181, 182] FRET is deemed as the main mechanism of energy transfer in distances below 10 nm. Therefore, FRET is an excellent tool for detecting nanometer-scale biomolecule interactions in homogeneous assays.[183-185] Additionally, transition dipole

orientations between the donor and acceptor and the quantum yield of the donor affect the FRET efficiency and the Förster distance.[186]

In bioaffinity assays, the donor and acceptor are brought in close proximity to each other usually by a biomolecule binding reaction to enable FRET between them. Three assay formats are usually applied: non-competitive, i.e. sandwich, competitive, and enzyme activity assay (Figure 6). In sandwich assay, both the donor and acceptor are conjugated to different analyte-specific capture molecules. Binding of the analyte brings donor and acceptor together resulting in change of the FRET emission. In competitive assays, the analyte competes with the analyte analogue conjugated to the acceptor for binding to the capture molecule conjugated to the donor. The FRET emission is inversely proportional to the analyte amount. The third format is common especially in enzyme activity assays. The donor and acceptor are brought together in close proximity via linkage, such as peptide or oligonucleotide. Decrease in the FRET emission is detected when the linkage is cleaved by an analyte, such as protease or nuclease enzyme. From these formats, sandwich assays can have large distance between the donor and the acceptor and therefore they are not always favored in FRET based assays.
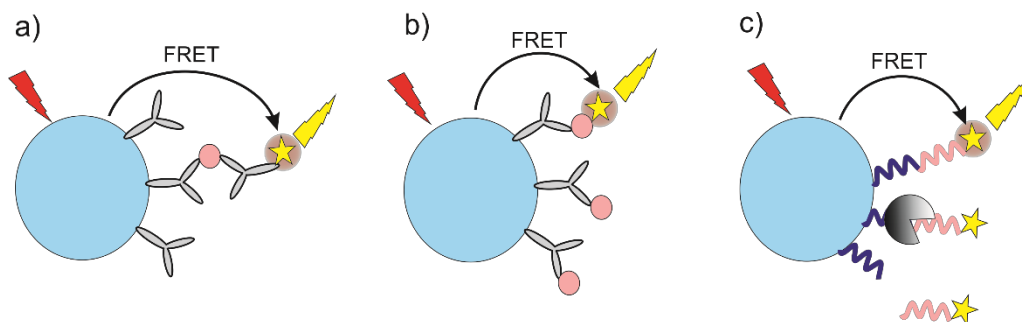
Figure 6. Principles of homogeneous assays based on Förster resonance energy transfer (FRET). a) Sandwich assay, where the donor and acceptor are brought close by the binding of the analyte, b) Competitive assay, where the analyte competes for binding to the capture molecule conjugated to the donor with the analyte analogue conjugated acceptor, c) Enzyme activity assay, where the cleavage of the linker molecule by an enzyme leads to the detachment of the acceptor from the vicinity of the donor.

Organic dyes or proteins have been used commonly as FRET donors, but they have drawbacks, such as high fluorescent background, photobleaching, spectral crosstalk with the acceptor, and short fluorescence lifetimes.[186, 187] Lanthanide-based complexes or down-shifting nanoparticles with long luminescent lifetimes have been used as donors, which enables time-gated detection of sensitized acceptor emission in order to avoid short-lived autofluorescence background.[188-190] They also have large Stokes shifts and narrow emission peaks, which diminishes the spectral crosstalk. However, these lanthanide-based donors require UV-excitation, which is strongly absorbed by biological materials and can be damaging to cells and tissue. UCNPs lack all of these drawbacks since they are photostable, they do not have autofluorescence background in biological matrices, have large anti-Stokes shift with sharp emission bands minimizing

spectral crosstalk, and the luminescence lifetimes are in microsecond range. In addition, UCNPs are excited at infrared and have emission peaks located at over 660 nm wavelengths, and they can therefore be used for detection of analytes in optically challenging materials, such as whole blood or urine, which have strong light absorptions under 600 nm wavelengths.[191] For example, UCNPs were successfully used as donors and Alexa Fluor 680 as acceptor in a homogeneous assay for whole blood folate without separation steps and the performance correlated well with a more laborious heterogeneous assay.[8] Lanthanide-based FRET is also referred to as luminescent or lanthanide resonance energy transfer, and the term is sometimes extended to UCNP-based energy transfer. In this thesis, however, UCNP-based FRET is referred to as upconversion resonance energy transfer (UC-RET).

In all FRET applications organic dyes are the most common acceptors. Organic dyes and fluorescent proteins have also been used in homogeneous UC-RET based bioaffinity assays.[8, 9, 112] For example, $NaYF_4$:Yb^{3+},Tm^{3+} UCNP donors and an intercalating dye SYBR Green acceptor were used to detect DNA with a 3.2 nM limit of detection (LOD).[9] Feasibility of quantum dots as acceptors in UC-RET applications has been studied extensively.[148, 192-195] Mattsson et al. were, however, one of the first to demonstrate their use in a homogeneous biotin replacement assay, which reached a LOD of 5 nM.[196] Additionally, due to the multiple narrow emission peaks of UCNPs, multiplex assays with single excitation wavelength can be developed. Multiplexed assays enable detection of multiple different analytes in one assay, which saves time, reagents and costs. For example, Doughan et al. used three quantum dots emitting at different wavelengths as acceptors in a DNA hybridization-based assay to detect three different gene fragments simultaneously.[197]

Non-emissive nanoparticles can be used as acceptors that quench the donor luminescence. Gold nanoparticles can be used as quenchers for Er^{3+} and Tm^{3+} doped UCNPs as they have wide absorbance spectra at visible wavelenghts.[10, 198-201] Quenching mechanism of gold nanoparticles is not based on dipole-dipole interactions between the donor and acceptor, but on dipole-surface effects-induced collective resonant oscillation. Down to 5 nM of HIV-1 viral DNA was detected with $NaYF_4$:Yb^{3+},Er^{3+} donors and gold nanoparticle acceptors.[10] The gold nanoparticle acceptor enabled even single particle counting in a homogeneous sandwich-type digital immunoassay when paired with $NaYF_4$:Yb^{3+},Er^{3+} UCNP donors.[201] As low as 2.3 pM of prostate specific antigen (PSA) was detected with the digital immunoassay. As gold nanoparticles, carbon nanoparticles and graphene oxides have also been used for efficient quenching of UCNP emission.[202-206] Carbon and graphene have similar electronic structures and they have wide absorption spectra at UV and visible wavelengths.[206, 207] The strong emission quenching is based on sp^2 orbital hybridization leading to electron transfer from the donor to the π-rich electronic structures of the carbon atoms. Other efficient UCNP emission quenchers are silver nanoplates[208] or nanodisks[209] and palladium nanoparticles[210] used with Tm^{3+} doped UCNP donors.

Energy transfer between UCNP donors and acceptors is more complicated than in traditional FRET between two organic dyes. UCNPs themselves contain multiple energy transfer steps between the sensitizers and activators inside the nanocrystals before the energy transfer to the acceptor. These steps also compete with the non-radiative deactivation of the excited states caused by surface defects and environment-related quenching. Thus, activator ions, which donate the energy to the acceptors, have low intrinsic quantum yields,[128, 131] which decreases the FRET efficiency. Nanocrystals also contain multiple activator ions that can act as donors per one acceptor molecule. Assuming that the activator ions are evenly distributed in the nanocrystals, there are several possible donor ions at different distances to the acceptor (Figure 7). Depending on the donor ion's location in the nanocrystal, it has different local environments that affect the intrinsic quantum yield of the donor ion.[211] Only one ion at a time can act as a donor, and the quantum yield of that ion can be difficult to determine.[211] Donor ions on UCNP surface can be quenched due to environmental effects and the energy transfer to the acceptor competes with the energy transfer to the surface ligands or solvent molecules causing non-radiative deactivation. On the other hand, ions in the nanoparticle center do not participate in the resonant energy transfer especially in larger particles because the distance to the acceptor is too high. Thus, the center ions produce background luminescence to the measurements. Therefore, only activator ions at a certain distance of the surface are efficient donors in UCNPs. Melle et al. calculated the FRET efficiency between each possible donor ion in UCNP nanocrystal and the acceptor, and the most efficient FRET was determined to originate from the donor ions near the surface, i.e. where the FRET distance was the shortest.[212] The measurements were not done in water and therefore the water related quenching was negligible.
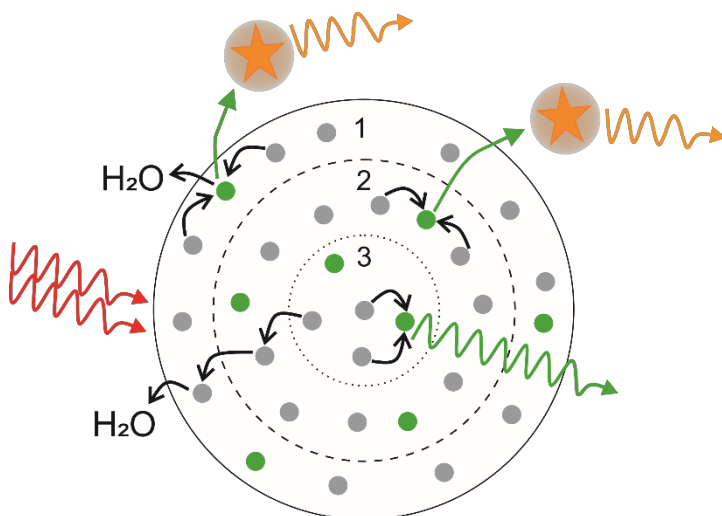
Figure 7. Simplified presentation of the lanthanide ion distribution in the UCNP nanocrystal donor. In the first region (1), the Yb^{3+} (grey circles) and Er^{3+} (green circles) ions are located near surface and energy transfer to the acceptor competes with the energy transfer to surface quenchers. In the second region (2), the donor ions are more shielded from the environment and transfer the energy to the acceptor. In the third region (3), the donor ions are not at the efficient FRET distance causing background luminescence.

Because FRET is distance-dependent, the UCNP size affects the energy transfer efficiency. When different nanoparticle sizes have been compared, smaller nanoparticles are found to have higher energy transfer efficiency because more ions are at the FRET distance. According to Marin et al., FRET efficiency was doubled with smaller UCNPs.[213] High FRET efficiencies have been observed for nanoparticles around 10 to 20 nm,[9, 214, 215] but in a study by Muhr et al., 10 nm UCNPs had lower FRET efficiency than 20 nm UCNPs because higher surface-to-volume ratio leads to higher quenching.[214] Thus, when designing UC-RET-based applications, the UCNP size should be taken into consideration. Additionally, dye quantity on the nanoparticle surface affect the FRET efficiency and sensitized acceptor emission intensity. According to Dukhno et al., a higher quantity of Rhodamine B acceptor increased RET efficiency and emission intensity because there is a higher concentration of acceptors on the surface of one donor particle.[215] Nevertheless, too high a concentration of especially organic dye acceptors with narrow Stokes shift can lead to self-quenching due to the homo-FRET caused by short distances between the dyes.[216]

As mentioned before, the quantum yield of the donor ions and the distance between the ions and the acceptor limit the FRET efficiency. Thus, different core/shell nanostructures have been applied to yield better UCNP donors (Figure 8). By applying an inert shell around the active core, the quantum yield of the donor increases because surface-related quenching is decreased, which could increase the FRET efficiency (Figure 8a). However, the inactive shell increases the distance between donor ions in the active core and the acceptor.[217] According to Wang et al., FRET efficiency was highest with core-only particles, but the FRET emission intensity was highest with an around 6 nm shell.[217] Thicker than 6 nm shells increased the donor−acceptor distances leading to lower intensities. To minimize the donor ion−acceptor distance, inactive core/active shell particles were synthesized where the luminescent lanthanides Yb^{3+} and Er^{3+} were doped to the active shell (Figure 8b).[211] The inactive core/active shell particles had higher RET efficiency than active core/inactive shell particles, but the sensitized emission intensity was vice versa. Donor ions were close to the acceptor in inactive core/active shell composition, but the surface-related quenching decreased the emission intensity. Active core/inactive shell composition shields the donor ions from quenching, but the distance to the acceptor increases while decreasing the FRET efficiency.[211] The results of the inactive core/active shell should be interpreted with caution, because it was observed that the lanthanide ions in an active shell were non-statistically distributed and were located quite close to the core/shell interface.

More complex core/shell structures have also been developed by doping the lanthanide ions in distinct layers to increase the FRET efficiency. Doping donor activator ions to the shell and the sensitizer Yb^{3+} to both core and shell led to doubled FRET efficiency when compared to core-only UCNPs (Figure 8c).[213] In these UCNP core/shell structures, Yb^{3+} ions were situated near the surface and the particles were therefore prone to high quenching, as non-radiative deactivation of Yb^{3+} has been deemed as the main quenching pathway. Huang et al. circumvented this problem by designing core/shell donor particles with Yb^{3+} sensitizers in the core and Er^{3+} activators in the shell

(Figure 8d).[218] This way the Yb^{3+} ions are protected from the environment and higher doping concentrations can be used because energy migration to the surface is minimized. Er^{3+} ions acting as donors are close to the surface, which decreases the distance to the acceptor and increases the FRET efficiency. In addition, higher Er^{3+} concentrations can be used because Er^{3+} to Yb^{3+} energy back transfer is minor in this structure. With optimized core/shell particle structure, Huang et al. obtained six times more efficient energy transfer.[218] The "sandwich" structure UCNPs with inactive core/active shell/inactive shell have also been proven to increase the FRET efficiency when the lanthanide ions are near the surface, but have a shell protecting them from the quenching (Figure 8e).[219] FRET was also increased by a higher Er^{3+} activator ion doping (20 %) coupled with a higher excitation power density (20 kW cm^{-1}).[60]
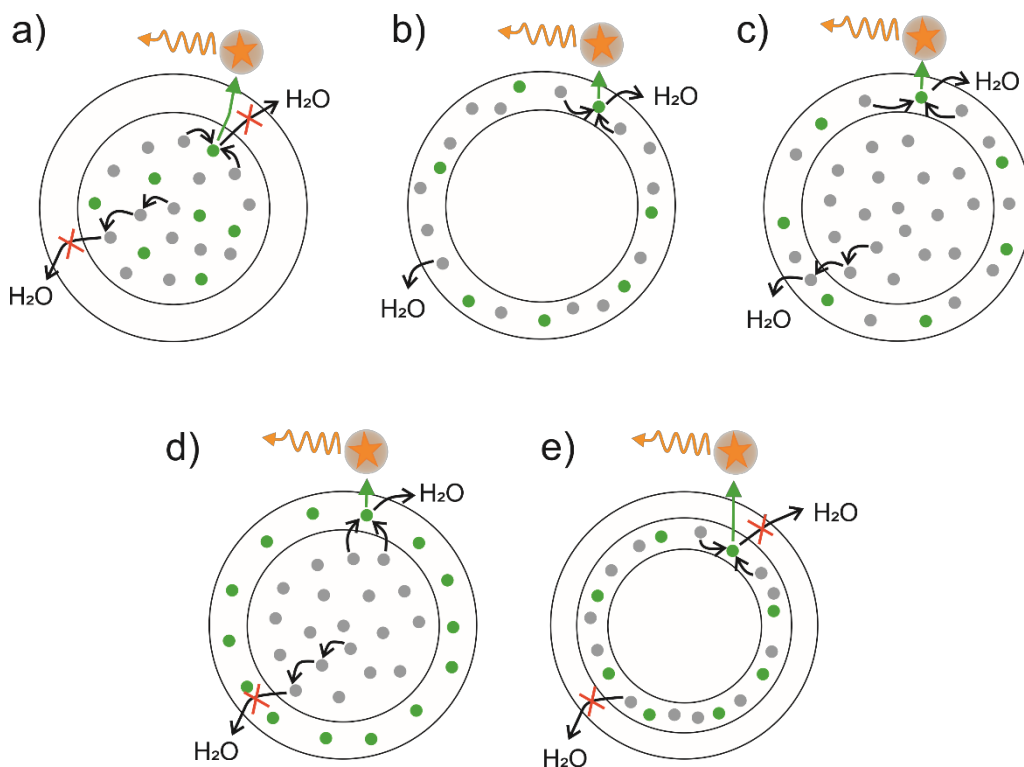
Figure 8. Simplified presentation of the different core-shell compositions and the effect on energy transfer. a) Active core/inactive shell where both sensitizer (grey circles) and activator (green circles) ions are in the core, b) inactive core/active shell where both sensitizers and activators are in the shell, c) activators doped only in the shell and sensitizer both in the core and shell, d) activators only in the shell and sensitizers only in the core, and e) inactive core/active shell/inactive shell, where both sensitizers and activators are in first shell.

In some publications with UCNPs as donors, acceptor emission is often claimed as occurring due to FRET, although no appropriate studies, such as steady-state and decay measurements of the donor-acceptor pair, have been presented.[46, 220, 221] Proper FRET

mechanism studies should be carried out especially with larger nanoparticles because several studies indicate that often part of the energy transfer from UCNPs to the acceptor is also radiative.[196, 217, 222, 223] According to the study by Ding et al., the larger the distance between donor ions in the UCNPs and the acceptor, the higher the proportion of the energy transfer is radiative.[223] However, FRET studies can be difficult to conduct since there are several donor ions at different distances and environments as described above, and changes in the lifetime and emission intensity of the donor ions are therefore difficult to distinguish from the ions that produce background.[196, 211, 222] This problem has been circumvented by determining FRET efficiencies from the lifetime of the sensitized acceptor emission. A significant lifetime change of the intrinsically short luminescence lifetime acceptor has been used as a proof of FRET and for calculations on FRET efficiency.[196, 211, 215] Nevertheless, these calculations should be regarded with caution because, although the activator ion Er^{3+} or Tm^{3+} acts as the donor in the UCNPs, the sensitizer ion Yb^{3+} has a significant effect on the lifetime of the activator ion and also on the sensitized acceptor lifetime. Sensitizer Yb^{3+} ions can affect the sensitized lifetime of the acceptor not only from the surface, but also Yb^{3+} ions in the center of the particles can affect it through energy migration.[224] Additionally, the Yb^{3+} ions might not be homogeneously distributed in the nanoparticles[97], which can complicate the energy transfer studies even more.

In UC-RET applications, red emission in Er^{3+} activator doped UCNPs has been used as reference wavelength because it has been deemed as unaffected by UC-RET when the acceptor absorption spectrum overlaps with the green emission of the UCNP donor.[196, 225, 226] However, in studies by Dukhno et al. and Huang et al., the red emitting state was also quenched in addition to the green emitting state.[215, 218] This can be explained by the observation that in certain environments, such as water-based solutions, the red emitting state is partially populated through the green emitting state, or on the other hand, the green emitting state is depopulated faster in UC-RET and therefore the red emission is not populated through the green emitting state as efficiently.[215] Therefore, red emission should be used as reference with consideration.

UCNP surface modification has significant effect on FRET efficiency as FRET is distance dependent. UCNPs need to be surface-modified to render them water dispersible and also to enable biomolecule conjugation for assay applications. The surface modification should be thin, preferably a monolayer, to enable efficient FRET. Melle et al. demonstrated that with a 33 nm sized UCNP the FRET efficiency was 10 % with a 3 nm-thick silica layer, but the efficiency decreased with the increase of the silica layer thickness and, with a 12 nm layer, the efficiency was nonexistent.[212] Biomolecule conjugation to the nanoparticle surface increases the FRET distance further since the dimensions of large proteins, such as antibodies, can be several nanometers.[196, 222] Therefore, the used surface modification and biomolecule should be taken into consideration in addition to the particle size and composition when designing UC-RET-based assays.

2.2.2　Heterogeneous assays

Heterogeneous assays contain washing or separation steps before the emission of the bound reporter on the solid support is detected. During the separation steps, unbound reagents are removed, which results in higher detection sensitivities than in homogeneous assays. Heterogeneous assays can be divided into non-competitive assays, i.e. sandwich assays, or competitive assays. The assay formats are the same as described in homogeneous assays, but instead of a binding reaction in the solution the binder molecule is attached to the solid support to enable washing of the unbound reagents.

UCNPs are highly attractive reporters in heterogeneous assays because they can potentially enable supersensitive detection of analytes. Because autofluorescence background is not produced from any biological materials or from the solid support materials due to the anti-Stokes shifted emission, extremely low concentrations of UCNPs can be detected. UCNPs are also photostable, which enables multiple measurements of the assays, and high excitation power densities can be used to enhance the detectability of the reporter. Since the reporters are detected commonly from dried solid support, solvent quenching or heating of the water-based solvent are not factors in the measurements.

Hlavacek et al. developed a competitive heterogeneous immunoassay for detecting diclofenac anti-inflammatory drug from water by using UCNPs as reporters, and compared the results to a conventional enzyme-linked immunosorbent assay (ELISA).[12] LOD for diclofenac was 0.05 ng mL^{-1} (170 pM) with the UCNP reporters and 0.01 ng mL^{-1} (34 pM) with ELISA. Although LOD was five times higher with UCNPs than with the ELISA reporter technology, UCNPs enable simpler detection technology because no enzymatic amplification of the signal is needed. Sensitivities comparable to commercial high-sensitivity assays were achieved with the UCNP reporters in heterogeneous sandwich immunoassay for cardiac troponin I (cTnI).[11] LOD was 3.14 ng L^{-1}, which corresponded to the 100 fM cTnI concentration in the sample. Two sandwich assays for detecting miRNA were developed based on the covalent attachment of the UCNP reporter and capture probe brought close together by the target. The covalent attachments were done by click chemistry[227] or with UV light promoted photochemical ligation[13] and LODs of 100 and 10 fM were obtained, respectively. Photochemical ligation was also demonstrated by using Tm^{3+} doped UCNPs as the UV light source.[13] Distinct patterns could be created on the solid support surface upon NIR radiation.

Due to their excellent detectability, UCNPs enable digital assays based on the counting of single analyte molecules. One of the first UCNP-based digital heterogeneous sandwich immunoassay was developed by Farka et al.[228] The assay for PSA was based on counting the amounts of bound UCNP reporter conjugates under a 980 nm laser-modified, wide-field epifluorescence microscope (Figure 9). LOD for PSA was 1.2 pg mL^{-1} (42 fM) in the digital assay, which corresponded to 4.8 pg mL^{-1} (168 fM)

in the serum sample. Digital detection was 17 times more sensitive than analog detection, where the intensity of the bound reporter was determined by scanning the microtiter well bottom with an under one mm spot size laser. The obtained LOD was also approximately two times more sensitive than some of the most sensitive commercial analog ELISA assays, such as Abcam's Human PSA ELISA kit or Thermo Fisher's PSA human ELISA kit with LODs of 8 pg mL^{-1}. The sensitivity of the digital UCNP-based immunoassay is not yet, however, comparable to the digital ELISA, where LOD for PSA was 6 fg mL^{-1} (200 aM) determined from the serum sample.[229]
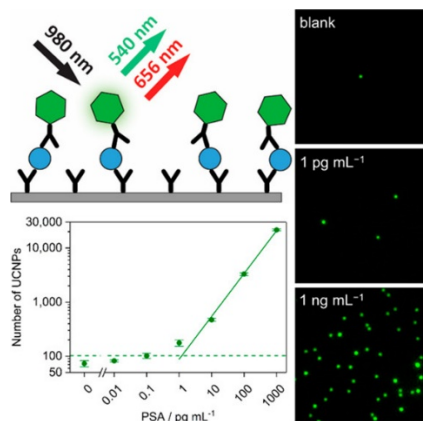
Figure 9. Principle of digital UCNP-based immunoassay for prostate specific antigen. Individual UCNPs bound on the solid surface were calculated from the images taken with wide-field epifluorescence microscopy modified with a 980 nm laser. Based on the number of UCNPs in different analyte concentration, a calibration curve was formed. Reprinted with permission from Farka et al.[228] Copyright (2017) American Chemical Society.

Multiplexed heterogeneous assays are commonly based on spatial detection using microarrays, where different analytes are recognized based on their coordinates on the solid support surface. Rijke et al. developed one of the first UCNP-based microarrays where they detected complementary DNA.[230] In a UCNP-based microarray, four times lower DNA concentrations were detected compared to the microarray with Cyanin 5 as a reporter. Ylihärsilä et al. developed a nucleic acid microarray that was able to discriminate different Adenovirus genotypes based on spot patterns on the microwell surface.[231] The same group also developed a multiplexed microarray for serum IgG antibodies against human Adenovirus and Parvovirus.[232] The results correlated excellently with the enzyme immunoassays used as references. Previous examples were qualitative assays recognizing the presence or the absence of an analyte. Microarrays are suitable also for quantitative detection by measuring the emission intensity from the individual spots. The quantitative detection of protein biomarkers PSA, thyroid-stimulating hormone (TSH), and luteinizing hormone in plasma with one assay was successfully demonstrated using the UCNP reporters.[233] Multiplexing did not affect the assay performance when compared to the single analyte assays, but LOD of TSH was not clinically relevant because of non-specific binding around the TSH spot.

Due to the multiple emissions in the visible wavelengths, the UCNP reporters can be used in microarrays that combine spatial and color based detection. For example, green emitting $NaYF_4:Yb^{3+},Er^{3+}$ and blue emitting $NaYF_4:Yb^{3+},Tm^{3+}$ UCNPs were conjugated to anti-human IgG or anti-human IgM, respectively, in order to detect serum IgG and IgM antibodies against influenza A and human adenoviruses in a single assay (Figure 10).[234] Antigen specificity was determined by the position of the spot in the solid support and the antibody class was determined by the emitted color of the spot. No spectral cross-talk was observed between the emission channels, and both of the UCNPs were excited with the same wavelength enabling the use of only one excitation source.
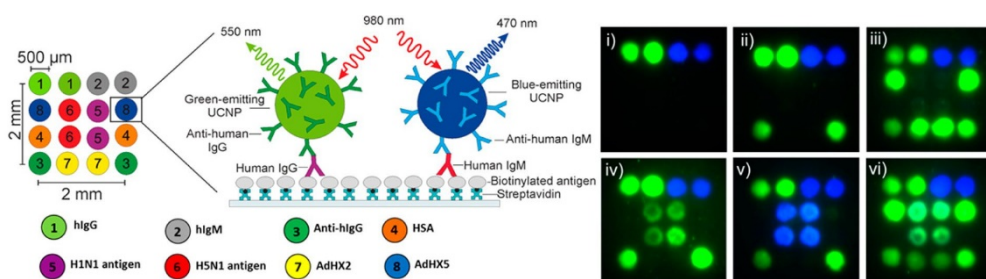
Figure 10. Principle of the dual color microarray for serum IgG and IgM against influenza A and human adenoviruses. Biotinylated antigens were added as spots to a streptavidin coated microplate well to certain positions to capture human IgG and IgM in the serum sample. Bound IgG and IgM were detected with green-emitting and blue emitting upconverting nanoparticles (UCNP) upon 980 nm excitation. Assays containing i) no sample, ii) negative sample, iii) adenovirus positive sample, iv) anti-influenza IgG positive sample, (v) anti-influenza IgM positive sample, and (vi) IgG positive sample for both adenovirus and influenza. Reprinted with permission from Kale et al.[234] Copyright (2016) American Chemical Society.

Lateral flow (LF) tests are immunochromatographic assays developed for point-of-care settings. LF test strips are comprised of multiple consecutive porous matrices and the added solutions flow through the strip due to the capillary forces. Binder molecules are immobilized to specific regions on the matrices and unbound solution components flow through these regions. Conventional LF tests commonly use gold nanoparticle reporters and the qualitative results are generally detected visually. UCNP reporters have enabled over 10- to 100-fold improved LODs in LF tests when compared to gold nanoparticle reporters.[235, 236] LF tests based on UCNP reporters are mostly quantitative, and require therefore readers to detect the amount of bound reporter. The reader should preferably be suitable for point-of-care settings, i.e. be small, portable and battery-operated. Readers have been developed for UCNP-based LF strips[237, 238] and few of the readers are small and portable smartphone-based devices.[239, 240] For example, He et, al. developed an LF test for PSA and ephrin type-A receptor 2 (EphA2) using highly doped UCNPs and high power lasers for high brightness, and the emission was detected with a mobile phone.[240] LODs for PSA and EphA2 were 89 and 400 pg mL^{-1}, respectively. Juntunen et al. compared LODs in LF tests with Eu^{3+} nanoparticles and UCNPs reporters.[241] In an LF test for cTnI, LODs were around six times lower with UCNPs than with Eu^{3+} nanoparticles. However, in the LF test for PSA, LODs were two to three times lower with Eu^{3+} nanoparticles. The lowest LOD was achieved with UCNP-based LF test

for cTnI in a serum sample (41 ng L^{-1}).[241] For comparison, a gold-nanoparticle-based LF test was able to detect a 10 ng L^{-1} concentration of serum cTnI.[242] LF tests can also enable multiplexed assays based on spatial and spectral recognition by adding multiple specific analyte binding regions on the test strips.[239, 243]

When the performance of UCNP-based assays are compared to other reporter technologies in this thesis or in the review by Mendez-Gonzalez et al., LODs obtained with UCNP reporters are comparable to other reporters.[244] Despite the recent active research in the upconversion nanoparticle field[245], commercial assay applications are lacking because manufacturers are not prepared to change their current technologies without obvious benefits. UCNPs have the potential to enable supersensitive assays outweighing other reporters because minor concentrations of UCNPs can be detected due to their brightness and lack of autofluorescence. However, the sensitivity of the assays is limited by the non-specific binding of UCNP conjugate to the solid support, and the aggregation of the particles.[11, 233, 246] Most likely, the non-specific binding of UCNP conjugates is no higher than with other reporters, but due to their high brightness, even small amounts of the non-specifically bound reporters can be detected.

Surface modification of UCNPs render them water dispersible and enable bioconjugation, but it also has a high impact on colloidal stability, aggregation rate, and non-specific binding of the nanoparticles. Monodispersity and colloidal stability of the UCNPs are very important in bioaffinity assays because nanoparticles are more reactive, and there are less steric hindrances preventing binding. Surface modification can prevent aggregation of the nanoparticles by providing steric and electrostatic repulsions.[247, 248] However, aggregation of the nanoparticles can occur already in the surface modification process.[249] For example, during the silica shell formation in the microemulsion method, more than one nanoparticle can end up inside the silica shell.[250, 251] Encapsulation of multiple nanoparticles in one silica shell can be controlled with the amount of detergent in the reaction as the detergents control the size and shape of the micelles. Higher detergent amounts form smaller micelles that can capture only single nanoparticles.[111, 252] Multidentate ligands, such as PAA, can also form bridges between the nanoparticles during the coating process resulting in aggregation.[253] Hlaváček et al. purified biomolecule conjugated silica and PAA-coated UCNPs with agarose gel electrophoresis to separate aggregates from single UCNPs.[254] Monodispersity of nanoparticles is very important especially in digital assays, and Hlaváček et al. demonstrated that gel-electrophoresis-purified single nanoparticles are highly suitable for bioassays with a digital readout. In addition, purified bioconjugated UCNPs had better reactivity in the bioassay than unpurified bioconjugates.[254]

Surface modified UCNPs usually have a high colloidal stability in water. However, colloidal stability in buffers or biological media can be limited depending on the surface modification. Colloidal stability is especially poor in phosphate buffer with UCNPs coated with coordinated ligands[140, 255-257], which are typically produced with the ligand exchange method. The instability in buffers has been attributed to buffer salts that have an affinity to lanthanide ions on the UCNP surface and can therefore replace the ligands

from the UCNP surface.[258] Phosphate buffer has the largest effect on the colloidal stability as phosphate groups have a high affinity towards lanthanides, which can also cause the dissolution of the nanoparticle ions as mentioned above.[156] Stability and detachment of the ligand is also affected by the buffer pH. PAA polymer coated UCNPs showed aggregation in phosphate buffer pH 7.4, but in a pH 9.3 borate buffer, no aggregation was observed due to the full ionization of the PAA polymer.[255] Polyethylene glycol (PEG) phosphate ligand was observed to detach from the UCNP surface at above pH 8, which was attributed to the replacement of the ligand with the OH groups in the solution.[140] In some cases, crosslinking the ligands has been proven to prevent aggregation in the buffers.[121] Additionally, the coordinating group of the ligand affects the stability. Because the phosphate groups have the highest adsorption strength to lanthanides, phosphate containing ligands are not easily detached from UCNPs' surface even in phosphate buffer when compared to carboxylic or sulphonic acid groups.[257]

Silica forms a shell around the nanoparticle and it therefore does not detach from the nanoparticle surface rendering the coating fairly stable. However, silica-coated nanoparticles have a negative charge, and thus the pH, salt concentration, and buffer ion need to be carefully optimized to keep the silica coated UCNPs colloidally stable.[259, 260] Thin silica shell formed with a water-in-oil microemulsion method has been shown to lead to aggregation when the silica coated particles are washed after the coating reaction.[261] Aggregation has been attributed to surface ligands, such as OA, which is not completely removed from the particle surface during silica coating, and therefore leads to aggregation.[258] This problem can be solved by first removing the hydrophobic ligand and replacing it with a hydrophilic ligand in a ligand exchange reaction before the silica coating.[248, 262]

Nanoparticles can also aggregate in biological media and the sample matrices have different effects on the aggregation rate. Juntunen et al. observed that the anticoagulant in venipuncture tubes had a significant effect on the nanoparticle mobility in LF tests, which affected also the LOD.[241] EDTA anticoagulant was observed to cause aggregation and the UCNP mobility was therefore limited in the matrix. The aggregation of nanoparticle conjugates can be also caused by non-specific adsorption of biomolecules to the nanoparticle surface. This non-specific adsorption of proteins is called as the formation of protein corona and all the nanoparticles can most likely adsorb some protein corona even if they are not designed to do so.[263] Most of the surface modification methods produce nanoparticles with surface charges, which promotes their colloidal stability but leads to electrostatic interactions with biomolecules of the sample material in the assay. The instability of PAA coated UCNPs in serum and aggregation of amine-modified silica nanoparticles were hypothesized to result from non-specific protein adsorption on the nanoparticle surface.[253, 264] In heterogeneous bioaffinity assays, non-specific binding of conjugated nanoparticles to the solid support without the specific biomolecule recognition is most likely caused by this non-specific protein adsorption to the nanoparticle surface. The nanoparticles can adsorb proteins attached to the solid support or the interactions can occur through the biomolecules in the sample matrix.

By preventing the non-specific interactions of the nanoparticle conjugates with each other and with the solid support, the sensitivity of the bioaffinity assays could be vastly improved because emission based only on biomolecule recognition would be detected. Non-specific binding can be affected with surface modification. Combining other surface ligands with PEG has been proven to reduce surface adsorption of proteins and also non-specific binding.[247, 253, 265, 266] Nsubuga et al. demonstrated that PEG-phosphate, alendronic acid, and photocrosslinked polydiacetylenes had almost a neutral surface charge at physiological pH and prevented the formation of protein corona even in high serum concentrations.[124, 267] By using these surface modifications, UCNPs would be great candidates for bioaffinity assays with low, non-specific binding of the reporter. However, reports on their use in bioaffinity assays have not yet been reported.

3 AIMS OF THE STUDY

The overall objective of the thesis was to study UCNPs as reporters in bioaffinity assays and to demonstrate their potential to assays that require high sensitivity detection. In the thesis, drawbacks that limit the use of UNCPs in bioaffinity assays were studied in order to find solutions for them. In addition, the aim was to demonstrate the potential of UCNPs for new bioaffinity assay applications.

More specifically, the aims were:

I   To introduce a **new donor acceptor pair in UC-RET-based bioaffinity assay** where the acceptor has intrinsically longer luminescent lifetime than the donor. UNCPs were used as donors and intrinsically luminescent lanthanide chelate as an acceptor in homogeneous back titration assay for biotin.

II   To study the **dissolution of particle constituting ions of hexagonal fluoride-based host matrix UCNPs** in water suspensions and characterize the impact of ion dissolution to nanoparticle structural integrity and upconversion luminescence. The dissolution was studied with different UCNP concentrations and different surface modifications.

III   To reduce **non-specific binding of antibody conjugated UCNPs** to solid support to improve the sensitivity of heterogeneous sandwich immunoassays employing UCNP reporters. Heterogeneous assays with two model analytes, cTnI and TSH, were used to demonstrate that the method to decrease non-specific binding is generic.

IV   To demonstrate the applicability of **UCNPs to upconversion cross-correlation spectroscopy (UCCS)** and to develop a homogeneous sandwich immunoassay by using two UCNPs emitting at different wavelengths. TSH was used as model analyte and the measurement was based on simultaneous detection of green- and blue-emitting UNCPs.

4 SUMMARY OF MATERIALS AND METHODS

A brief summary of materials and methods employed in this study is presented here. More detailed information can be found in the original publications (**I–IV**).

4.1 Synthesis and surface modification of UCNPs

OA-capped crystalline UCNPs used in the original publications **I–IV** were synthesized by high-temperature co-precipitation in organic oils.[94, 268, 269] The compositions of UCNPs used in the original publications are presented in table 1. In the original publication **I**, part of the Na^+ was replaced with K^+ in order to enhance the blue emission.[269] The size of the synthesized UCNPs was characterized with transmission electron microscopy (TEM, JEM-1400 Plus TEM, 80 kV, JEOL, Massachusetts, USA) by measuring the diameters of 60–100 nanoparticles from the TEM images with ImageJ software (http://rsb.info.nih.gov/ij/).

After the synthesis, UCNPs were insoluble to water and did not contain functional groups for biomolecule conjugation. In order to render the UCNPs water dispersible, they were coated with PAA of Mw 2000[11], a thin silica shell according to modified protocol by Zhang et al.[270] or a thick silica shell according to Wilhelm et al.[271] Silica shell formations were based on reverse microemulsion method using tetraethylorthosilicate and (N-(3-trimethoxysilyl)-propyl)ethylene diamine to introduce primary NH_2 groups, which were subsequently converted to carboxylic acid groups with glutaric anhydride.[272] The carboxylic acid groups on the UCNP surface were conjugated to biomolecules using standard carbodiimide chemistry.[125] The surface modifications and possible biomolecule conjugated to the UCNPs are presented in Table 1. UCNP concentrations were determined after every biomodification step by comparing the luminescence of the coated UCNPs to the luminescence of the as-synthesized UCNPs.

Table 1. Nanoparticle composition and surface modifications in the original publications (**I–IV**)

Nanoparticle composition		Surface mofication	Conjugated to	Publication
$Na_{0.8}K_{0.2}YF_4$:Yb^{3+},Tm^{3+}	X_{Yb} 0.2, X_{Tm} 0.005	Thin silica shell	Streptavidin	**I**
$NaYF_4$:Yb^{3+},Tm^{3+}	"	Poly(acrylic acid)	Mab-5404*	**IV**
$NaYF_4$:Yb^{3+}, Er^{3+}	X_{Yb} 0.17, X_{Er} 0.03	Thin silica shell	-	**II**
$NaYF_4$:Yb^{3+}, Er^{3+}	"	Thick silica shell	-	**II**
$NaYF_4$:Yb^{3+}, Er^{3+}	"	Poly(acrylic acid)	Nothing (**II**) or Mab-625** (**III**)	**II–III**
$NaYF_4$:Yb^{3+}, Er^{3+}	"	Poly(acrylic acid)	Mab-5409*	**III-IV**

*Monoclonal antibodies specific to human thyroid-stimulating hormone
**Monoclonal antibody specific to cardiac troponin I

4.2 Luminescence measurements

4.2.1 Luminescence intensity

The steady-state upconversion luminescence of the UCNPs in the original publications **I–III** and the sensitized emission of the acceptors in the publication **I** were measured with Plate Chameleon fluorometer (Hidex Oy, Finland) equipped with a 980 nm laser.[5] In the original publication **I**, the steady-state measurement of the sensitized acceptor emission was collected for 2 s under continuous excitation at 980 nm. The time-resolved (TR) sensitized acceptor emission intensity was measured using 2900 cycles with 10 ms cycle time, 3 ms wide-pulsed excitation at 980 nm, 1 ms delay after the excitation pulse, and 2 ms measurement window. Both steady-state and TR sensitized acceptor emission of the Eu^{3+} chelate were measured from solution by using a 615 nm bandpass filter with a half width of 15 nm. In the original publication **II**, the green emission of UCNPs was measured from the solution by using a 535 nm bandpass filter with a half width of 40 nm, and 2 s readout was used under 980 nm continues excitation. In the original publication **III**, the emission was measured with the same bandpass filter, but the emission intensity from each well was measured from the bottom of the microtiter well surface with a nine-point raster and a 2 s readout for each point.

4.2.2 Luminescence decays

In the original publication **I**, decays of the UCNP donor and sensitized Eu^{3+} chelate acceptor were recorded with lifetime measurement mode of the 980 nm laser modified Plate Chameleon fluorometer. Lifetimes of the $Na_{0.8}K_{0.2}YF_4:Yb^{3+},Tm^{3+}$ UCNPs and the sensitized Eu^{3+} chelate were obtained by exposing the samples repeatedly to a 3 ms wide, 980 nm excitation pulse and measuring the decays at 365 nm (365 nm bandpass filter with 20 nm half width) and 615 nm (615 nm bandpass filter with 15 nm half width), respectively, and fitting the obtained data with the single-order exponential decay function of Origin8 (OriginLab, Northampton, MA).

4.2.3 Luminescence spectra

In the original publication **I**, the spectra of the UCNP and acceptors were measured with the Cary Eclipse fluorescence spectrophotometer (Agilent Technologies, Santa Clara, CA). For the measurement of the UCNP emission spectrum, the device was equipped with a 980 laser diode. The emission spectrum of the UCNP was measured with the bio/chemiluminescent mode. The standard excitation source of the device was utilized for the measurements of emission and excitation spectra of the acceptors. The spectra of the Eu^{3+} chelates were measured with the phosphorescence mode.

4.2.4 Upconversion cross-correlation spectroscopy

In the original publication **IV**, the binding of the differently emitting UCNPs together was measured with UCCS using home-build confocal microscopy to acquire the time

traces.[273] The setup contained a continuous wave Ti-sapphire laser (3900S Spectra Physics, Santa Clara, CA) tuned to 977 nm emission wavelength. The laser was reflected by a 30:70 beam splitter (XF122 Omega Optical, Battleboro, VT) into an oil immersion objective (UPlanSApo 100x NA = 1.4, Olympus, Japan), which focused the laser on a spot with a $1/e2$ beam radius of about 840 nm. For the detection of Er^{3+} and Tm^{3+}-doped UCNPs, the upconversion emission was separated into two spectral channels with a 488 nm dichroic mirror. The emissions were detected with avalanche photodiodes (CD3226, PerkinElmer, Waltham, MA) connected to a single photon counting module (SPC-830, Becker & Hickl, Germany). A more detailed description and an illustration of the setup can be found in the original publication **IV**.

4.3   **Characterization of UCNP disintegration**

In the original publication **II**, disintegration of the differently coated UCNPs in water solutions was studied by measuring the amounts of ions dissolved from the UCNP nanocrystal, visually characterizing the structural integrity of the nanoparticles, and measuring the upconversion emission intensity over time. The prevention of the nanoparticle disintegration was also studied by adding free fluoride ions into the UCNP suspensions.

The dissolved fluoride ion concentration was determined from the water suspensions of the PAA-functionalized UCNPs in three concentrations. The UCNPs were incubated for 0, 24 or 96 hours in water, after which TISAB III concentrate (Mettler Toledo, Switzerland) was added to adjust ionic strength of the suspensions, and the fluoride ion concentration was measured with fluoride electrode (perfectION, Mettler Toledo) according to manufacturer's instructions. The dissolved concentrations of Y^{3+}, Yb^{3+} and Er^{3+} were determined with an inductively coupled plasma mass spectrometer (ICP-MS, PerkinElmer Elan 6100 DRC Plus, MDS, SCIEX, Concord, ON, Canada) after incubating the PAA-functionalized UCNPs in water or KF solution for 24 h. Before the analysis, possible nanoparticle remnants were removed by centrifugation and the supernatant was diluted to deionized water for the measurements. The structural integrity of the PAA-functionalized UCNPs in water suspensions was characterized with TEM using an 80 kV electron beam. The UCNPs were incubated in water or KF solution for 0 or 24 h, after which the UCNPs were concentrated with Nanosep 30K omega centrifugal devices (PALL Life Sciences, NY, U.S.A) and the concentrated solutions were pipetted onto silicon monoxide copper grids and were left to dry.

Time-course measurements of upconversion emission intensity were performed by diluting the thin and thick silica and PAA-functionalized UCNPs to water or KF solution. Water or 1 mM KF in water in a volume of 97 µL was added to the clear Greiner polypropylene microtiter plate (Sigma-Aldrich, Missouri, U.S.A). The differently functionalized UCNPs were added to the wells in the volume of 3 µL to final concentrations from 0.5 to 200 µg mL^{-1} in four replicates, and the wells were incubated in slow shaking. Upconversion emission intensity was measured over time between 0 and 24 h.

4.4 Bioaffinity assays

4.4.1 Homogeneous assay using Eu³⁺ chelate as an acceptor

In the original publication **I**, a donor-acceptor pair was introduced in UC-RET system where biotinylated intrinsically luminescent nonadentate Eu^{3+} chelate (bio-Eu^{3+}) was used as an acceptor and streptavidin (SA) coated Tm^{3+}-doped UCNPs (UCNP-SA) were used as donors. The donor-acceptor pair was used in a homogeneous back-titration assay for biotin in order to demonstrate its functionality. The principle of the assay is depicted in Figure 11. The energy transfer mechanism between the donor and the acceptor and the lifetimes of the donor emission and sensitized acceptor emission were also studied.
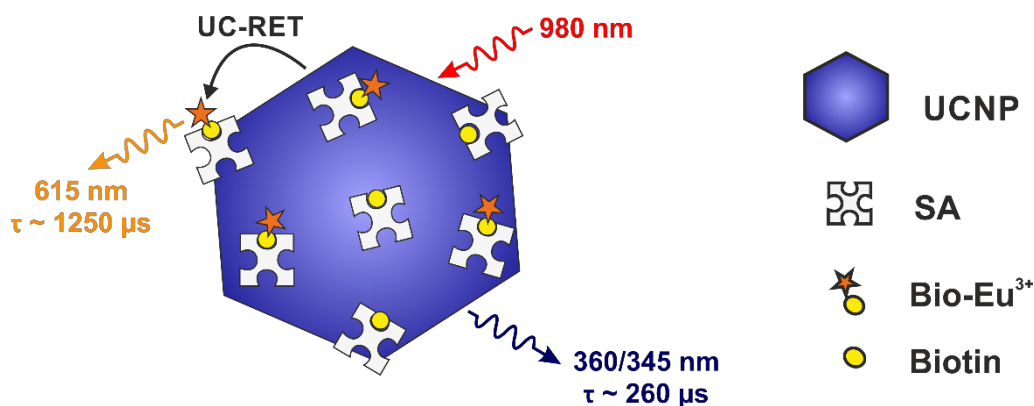
Figure 11. Principle of the homogeneous back-titration assay for biotin based on upconversion resonance energy transfer (UC-RET) between streptavidin (SA) conjugated Tm^{3+}-doped upconverting nanoparticle (UCNP) donors and biotinylated Eu^{3+} chelate (Bio-Eu^{3+}) acceptor. Biotin acting as an analyte competes with the bio-Eu^{3+} in binding to the SA on the surface of the UCNPs. When bio-Eu^{3+} is bound to the SA onto UCNP surface, the energy is transferred from the UCNP to the Eu^{3+} chelate upon 980 nm excitation and the sensitized acceptor emission can be measured at 615 nm with the steady-state or time-resolved mode.

The emission spectrum of the UCNP and the emission and excitation spectra of the Eu^{3+} chelate were measured with Cary Eclipse Varian fluorescence spectrophotometer. The UCNPs were diluted in dimethylsulfoxide to a concentration of 1 mg mL^{-1} and the Eu^{3+} chelate was diluted in TSA (50 mM Tris-HCl, pH 7.75, 150 mM NaCl, 0.5 g L^{-1} NaN₃) to a 1 μM concentration.

For the luminescence decay measurements of the UCNP-SA-bio-Eu^{3+} complex, the UCNP-SA was diluted in assay buffer (Kaivogen, Finland) to a 15 μg mL^{-1} concentration and bath sonicated (Finnsonic, Finland) for 3 minutes. Next, bio-Eu^{3+} was added to a final concentration of 50 nM and the solution was incubated for 15 min in order to allow the complex to form. The decays of the UCNP emission and sensitized acceptor emission were measured at 365 nm and 615, respectively, as described in

section 4.2.2. In addition, the decay of UCNP-SA at 365 nm was measured without the bio-Eu^{3+} bound to the UCNP surface.

The homogeneous back-titration assay was performed in black, half area 96-well microtiter plate (Corning, NY). The total reaction volume in a well was 80 µL, which contained 32 µL of biotin at final concentrations from 0 to 10,000 nM, 24 µL of UCNP-SA at a final concentration of 7.5 µg mL^{-1}, and 24 µL of bio-Eu^{3+} at a final concentration of 34 nM. The 0 concentration was studied in eight replicates and the other concentrations in four replicates. In the assay, first the biotin in different concentrations and UCNP-SA were mixed together and incubated for 15 min in slow shaking. Then, the bio-Eu^{3+} was added and the solutions were incubated again for 15 minutes in order to the bio-Eu^{3+} to bind those sites were the free biotin was not bound. The sensitized emission of the bio-Eu^{3+} was measured with the steady-state and TR modes as described in section 4.2.1.

4.4.2 Improving the sensitivity of UCNP-based immunoassays

In the original publication **III**, the background emission originating from non-specific binging of the antibody-conjugated UCNPs was reduced in heterogeneous sandwich immunoassays for cTnI and TSH in order to improve their sensitivity. The non-specific binding of the PAA-functionalized and antibody-conjugated UCNPs was reduced by mixing free PAA with the antibody UCNP conjugate before adding them into the microtiter wells.

The cTnI immunoassay was performed in Nunc C8 Lockwell LUMI White Maxisorp microtiter plates (Thermo Fisher, Waltham, MA), which were coated with SA[274] (Biospa, Italy). First, 150 ng of biotinylated monoclonal antibody 19C7 (Hytest, Finland) and 50 ng of biotinylated recombinant antigen binding fraction 9709 (cloned from Medix Biochemica, Finland, hybridoma cell line) were added to the prewashed wells in 50 µL volume of assay buffer and incubated for 30 min in RT and slow shaking. The wells were washed once with wash solution (Kaivogen), and then 10 µL of cTnI calibrators (human cardiac troponin I, T and C complex from Hytest) in Tris-buffered saline supplemented with bovine serum albumin (TSA-BSA, 50 mM Tris, pH 7.5, 150 mM NaCl, 0.5 g L^{-1} NaN$_3$, 75 g L^{-1} BSA) was diluted to 40 µL of sample buffer (37.5 mM Tris, pH 8.6, 500 mM NaCl, 0.4 g L^{-1} NaN$_3$, 0.6 g L^{-1} bovine gamma-globuline, 25 g L^{-1} BSA, 50 g L^{-1} D-trehalose, 0.8 g L^{-1} native mouse IgG, 0.05 g L^{-1} denatured mouse IgG, 2 g L^{-1} casein and 37.5 IU mL^{-1} heparin) and added to the wells. The calibrators were incubated for 30 min in RT and slow shaking, after which the wells were washed once with wash solution. The monoclonal antibody 625 conjugated UCNPs (Mab-625-UCNP) were diluted in modified assay buffer (assay buffer supplemented with 0.2 wt% milk powder, 0.8 g L^{-1} native mouse IgG, 0.05 g L^{-1} denatured mouse IgG) and 200 ng of UCNPs were added in 50 µL volume to the wells. Mab-625-UCNPs were incubated for 15 min before the wells were washed four times and left to dry before the measurement.

TSH-immunoassay was performed with small modifications to the cTnI immunoassay protocol. The immunoassay was performed in white streptavidin coated microtiter plates (Kaivogen). The plates were prewashed and 100 ng of biotinylated monoclonal antibody 5404 (the Mab was purchased from Medix Biochemica) was added to the wells in 50 µL volume. After 30 min incubation, the wells were washed once and 10 µL of TSH calibrators (Scripp Laboratories, San Diego, CA) in TSA-BSA was diluted with 40 µL of assay buffer and added to the wells. The calibrators were incubated for 30 min and the wells were washed once. The monocloal antibody 5409 conjugated UCNPs (Mab-5409-UCNPs) were diluted in assay buffer and 800 ng of UCNPs were added to the wells in 50 µL volume. The Mab-5409-UCNPs were incubated in wells for 30 min before washing the wells four times and left to dry.

In both assays, free PAA was mixed with the Mab-UCNP conjugates before adding them to the wells. In the cTnI immunoassay, 0.05 wt% of 1200 Mw PAA was used and, in THS immunoassay, 0.5 wt% of 2000 Mw PAA.

4.4.3   Upconversion cross-correlation spectroscopy of an immunoassay

In the original publication **IV**, the binding of the TSH analyte was detected with UCCS in a homogeneous sandwich immunoassay. The $NaYF_4$:Yb^{3+},Er^{3+} (green emission) and $NaYF_4$:Yb^{3+},Tm^{3+} (blue emission) UCNPs were conjugated to antibodies recognizing different epitopes of the TSH, thus forming a sandwich-complex. The binding of the analyte was detected by the simultaneous emission of blue and green light upon 977 nm laser excitation when the sandwich-complex diffused through the laser focal volume (Figure 12).
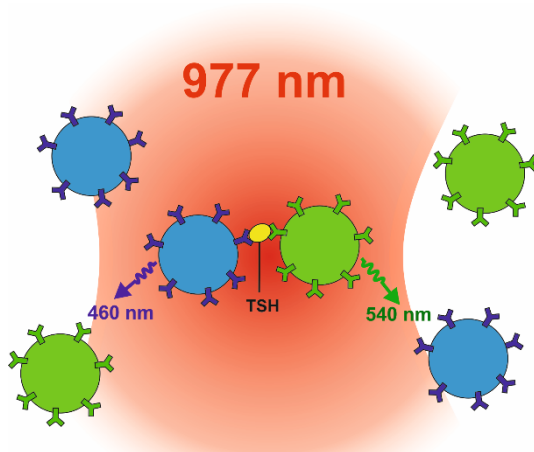

Figure 12. Principle of the upconversion cross-correlation spectroscopy sandwich immunoassay for thyroid-stimulating hormone (TSH). The bound TSH is detected by the coincident emission of $NaYF_4$:Yb^{3+},Tm^{3+} (blue) and $NaYF_4$:Yb^{3+},Er^{3+} (green) nanoparticles when the sandwich-complex diffused through the 977 nm laser focal volume.

The TSH immunoassay contained a 17.8 µL combined volume of Mab-5409 conjugated NaYF$_4$:Yb^{3+},Er^{3+} UCNPs and Mab-5404 conjugated NaYF$_4$:Yb^{3+},Tm^{3+} UCNPs and 10 µL of TSH in TSA-BSA. The final concentration of both UCNPs was 0.39 mg mL^{-1} and the TSH range tested was 0–2880 mIU L^{-1}. The total volume was adjusted to 30 µL with assay buffer. The reaction was incubated for 30 min and then a 33-fold dilution was made to assay buffer/D$_2$O (1/10) for the UCCS measurement resulting in 0.012 mg mL^{-1} UCNP concentration in the measurement. The dilution contained assay buffer to prevent aggregation of UCNPs in the dilution. D$_2$O was used to enhance UCNP emission intensity and to prevent heating of the sample by absorption of the laser.

5 SUMMARY OF RESULTS AND DISCUSSION

5.1 Characterization of upconverting nanoparticles

The UCNPs used in the original publications **I-IV** were spherical or rod-like in shape and between 20 to 50 nm in size according to the TEM images (Figure 13, Table 2). The UCNPs in the original publication **I** were larger and had more deviation in size than the UCNPs in the other publications. In the synthesis, a part of the Na^+ was replaced by K^+ in order to increase the upconversion emission at UV and blue wavelengths as in the previous study.[269] According to the study, K^+ did not actually enter the lattice, but affected the crystal lattice by controlling the $Na/Yb^{3+},Tm^{3+}$ ratio and thus the Yb^{3+}-Yb^{3+} and Yb^{3+}-Tm^{3+} distances. However, the K^+ addition to the synthesis resulted in a slightly higher nanoparticle size. The enhanced UV emission was important for energy transfer between the UCNPs and Eu^{3+} chelate, although smaller nanoparticle size would be more beneficial in UC-RET applications to prevent radiative background from the donor. All UCNPs used in the original publications were hexagonal in crystal structure (data not shown).
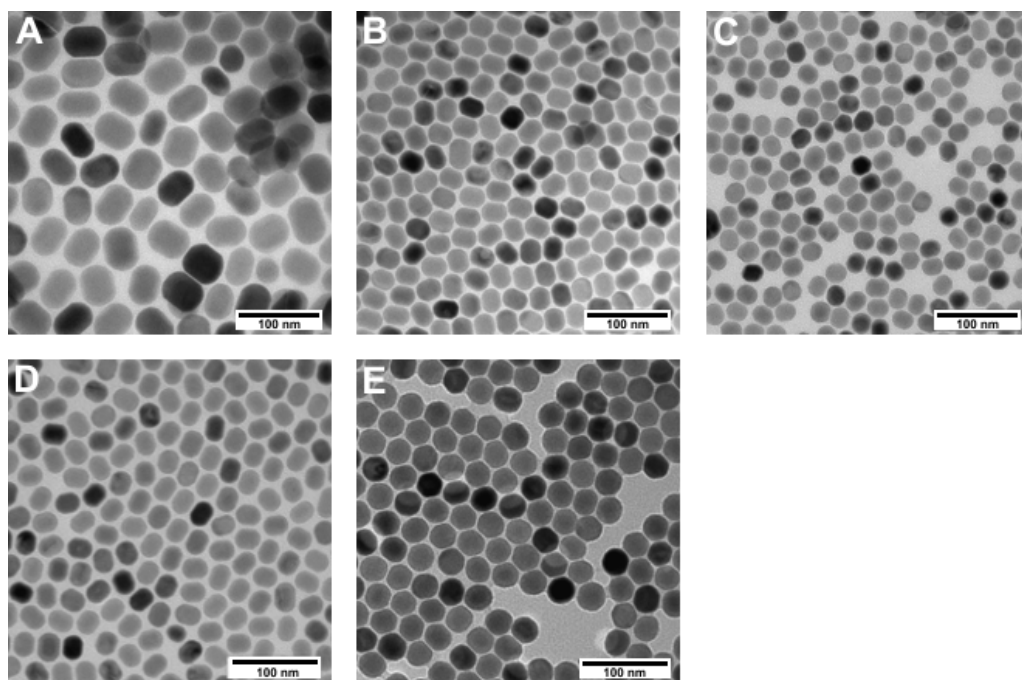
Figure 13. Transmission electron microscopy images of the $Na_{0.8}K_{0.2}YF_4$:Yb^{3+},Tm^{3+} nanoparticles used in the original publication **I** (A), $NaYF_4$:Yb^{3+}, Er^{3+} nanoparticles used in the original publications **II** (B), **III** (C) and **IV** (D), and $NaYF_4$:Yb^{3+},Tm^{3+} nanoparticles used also in the original publication **IV** (E). UCNPs were imaged with JEM-1400 Plus TEM using a 80 kV electron beam.

Table 2. Average diameters of the upconverting nanoparticles used in the original publications determined from transmission electron microscopy images by measuring the sizes of 60−100 nanoparticles with ImageJ.

	Nanoparticle	Width (nm)	Height (nm)	Publication
A	$Na_{0.8}K_{0.2}YF_4:Yb^{3+},Tm^{3+}$	43 ± 5	54 ± 5	I
B	$NaYF_4:Yb^{3+}, Er^{3+}$	25 ± 3	31 ± 3	II
C	$NaYF_4:Yb^{3+}, Er^{3+}$	21 ± 2	25 ± 2	III
D	$NaYF_4:Yb^{3+}, Er^{3+}$	24 ± 1	29 ± 1	IV
E	$NaYF_4:Yb^{3+},Tm^{3+}$	29 ± 1	31 ± 1	IV

In the original publication **I**, the UCNPs were coated with a thin silica shell in order to keep the energy transfer distance between the emitting ions in the UCNP donor and the acceptor as short as possible. The silica layer is so thin that it cannot be observed with ordinary TEM. The thin silica shell should be visualized with High resolution TEM (HR-TEM). The silica-functionalized UCNPs in the original publication **I** were not imaged with HR-TEM, but the thin silica shell acquired with the same protocol has been previously characterized and, according to the HR-TEM images, the silica shell was under 2 nm (data not shown).

In the original publication **II,** the UCNPs were functionalized with PAA, thin and thick silica shells in order to study the effect of the surface coating on the disintegration of the nanoparticles. As with the thin silica coating, the PAA surface on nanoparticles is so thin that it cannot be detected with TEM. The PAA surface is estimated to be under 2 nm thick, but further studies with e.g. HR-TEM are needed to confirm the hypothesis. However, the thick silica shell performed according to the protocol by Wilhelm[271] was detected with TEM (Figure 14). The silica shell thickness was on average 5.8 ± 0.55 nm measured with imageJ. The shell thickness varies slightly in the nanoparticle and between the nanoparticles. The shell thickness can be modified by alternating the amount of silane used in silanization.[250, 275, 276] The UCNPs were coated with silica with two different protocols, as UCNPs aggregated strongly when the amount of silane was reduced in protocol by Wilhelm et al. in order to achieve a thinner silica layer (data not shown). Therefore, the thin silica shell was formed according to modified protocol by Zhang et al.[270]
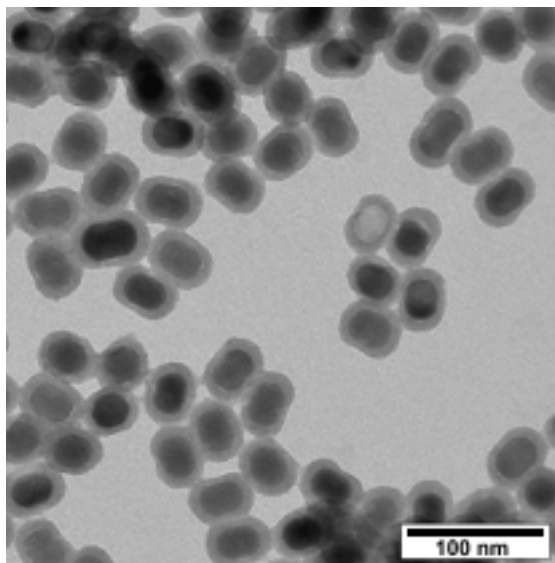
Figure 14. Transmission electron microscopy image of the thick silica-functionalized upconverting nanoparticles in the original publication **II**.

In the original publications **III** and **IV**, the nanoparticles were functionalized with PAA in order to obtain highly monodisperse and colloidally stable particles with carboxylic acid groups for bioconjugation. As stated above, the silica shell forms a stable covalently-coupled shell around the nanoparticles, but more than one nanoparticle can end up inside the silica shell[250, 251], and a silica shell formed with the microemulsion method can be prone to aggregation[261]. The PAA-functionalized UCNPs have been proven to be colloidally stable because of the high negative surface charge due to the multiple carboxylic acid groups.[253, 277, 278] The carboxylic acid groups provide electrostatic and steric repulsion preventing aggregation between the nanoparticles.[279, 280] Nevertheless, PAA is chemically adsorbed onto the UCNP surface and can detach in certain conditions, such as in highly acidic environments.

5.2   Disintegration of UCNPs

The disintegration of UCNPs' structural integrity in water and its effect on upconversion luminescence was studied in the original publication **II**. Fluoride ions dissolved from the PAA-coated UCNPs were determined with fluoride ion electrode by incubating the PAA-coated UCNPs in water at different concentrations for different lengths of time (Table 3). Dissolved fluoride ion concentration in the solution increased significantly until 24 h of incubation and, after that, it remained constant at 0.08 mM in all UCNP concentrations. Shorter incubation times than 24 h were not studied, but the dissolution is most likely faster as indicated by the time-course upconversion luminescent studies (figure 15). More importantly, the maximum dissolved fluoride ion concentration in the solution was constant and independent of the UCNP concentration. The dissolved fluoride mole fractions, i.e the amount of dissolved fluoride ions compared the total

fluoride ions in the nanoparticles at certain concentrations, were dependent on the UCNP concentration: the smaller the UCNP concentration, the higher the dissolved fluoride mole fraction. This implies that, after reaching a certain concentration of fluoride ions in the solution, a solubility equilibrium is achieved in the solvent and the dissolution stops. Therefore, in low UCNP concentrations, most of the nanoparticle fluoride ions need to be dissolved before the solubility equilibrium is achieved.

Table 3. Dissolved fluoride ion concentrations at different time points in water suspensions with different UCNP concentrations

|	UCNP concentration (µg/ml)		
	5	15	50
time	**[fluoride] (mM)**		
0 h	0.004	0.008	0.015
24 h	0.07	0.08	0.08
96 h	0.07	0.08	0.08
	dissolved fluoride (mol %)		
96 h	66.4	24.2	7.3

In addition to fluoride, the dissolution of the rare earth ions (Y^{3+}, Yb^{3+} and Er^{3+}) was determined with ICP-MS after the incubation of the PAA-coated UCNPs in water for 24 h. According to the ICP-MS analysis, rare earth ions also dissolved into to the solution (Table 4). The mole ratios of the dissolved ions differentiate from the mole ratios of the as-prepared UCNPs (Y^{3+} 80%, Yb^{3+} 17%, Er^{3+} 3 %), which might be due to the uneven distribution of ions in the nanoparticles.[96, 97] The Y^{3+}, ions might be concentrated on the surface of the nanoparticles and therefore they dissolved excessively when compared to Yb^{3+} which are more concentrated in the nanoparticle center and dissolved to a lesser extent.

Table 4. Molar amounts of dissolved rare earth ions, the percentage of dissolved ions when compared to the total amount of that ion in the nanoparticles, and the molar ratios of the dissolved ions determined with ICP-MS after incubating 5 µg/mL of PAA coated UNCPs in water for 24 h.

R^{3+} ion	dissolved R^{3+} (mol)	dissolved R^{3+} (mol %)	dissolved R^{3+}/ dissolved total R (%)
total Y^{3+}, Yb^{3+}, Er^{3+} (x 10^{-6} M)	4.18	53.3	100
Y^{3+} (x 10^{-6} M)	3.76	60.0	90.1
Yb^{3+} (x 10^{-6} M)	0.323	24.3	7.74
Er^{3+} (x 10^{-6} M)	0.0914	38.8	2.19

R^{3+} = rare earth ion

The dissolution of the ions can be described with the equilibrium equation (eq1), with the assumption that the ions would dissolve stoichiometrically. The R^{3+} denotes the rare earth ions Y^{3+}, Yb^{3+} and Er^{3+}.

$$NaRF_4 \text{ (s)} \overset{H_2O}{\longleftrightarrow} Na^+ \text{ (aq)} + R^{3+}\text{(aq)} + 4F^- \text{ (aq)} \quad \text{(Eq. 1)}$$
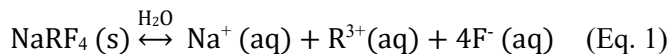
Based on equation 1, a solubility product K_{sp} can be formed (eq2).

$$K_{sp} = [Na^+][R^{3+}][F^-]^4 \quad\quad\quad\quad \text{(Eq. 2)}$$

From equation 2, it can be concluded that the fluoride ion has the highest impact on the solubility product, and therefore fluoride ions have also a major impact on the disintegration of the UCNPs.

The ion dissolution from the UCNPs most likely affects the upconversion luminescence, which was studied by measuring the emission intensity at different time points after diluting the PAA-coated UCNPs in water (Figure 15a). Upconversion luminescence decreased over time, which is presumably due to the loss of lanthanide ions that act as luminescent centers in the UCNPs. More importantly, the luminescence decrease was highly dependent on the UCNP concentration. This observation supports the hypothesis that the ions dissolve until an equilibrium is achieved. With low UCNP concentrations, the nanoparticles are disintegrated almost completely until the equilibrium is achieved in the solvent and most of the luminescence is lost. High concentrations of UCNPs contain high amounts of ions, and therefore only a minor disintegration is needed before equilibrium is achieved. The ion dissolution from the nanoparticles and its negative effect on the upconversion luminescence have also been observed in studies by Lisjak et al.[155-157] They studied the dissolution of ions in higher UCNP concentrations, and therefore they observed changes that were not as significant as in this thesis.
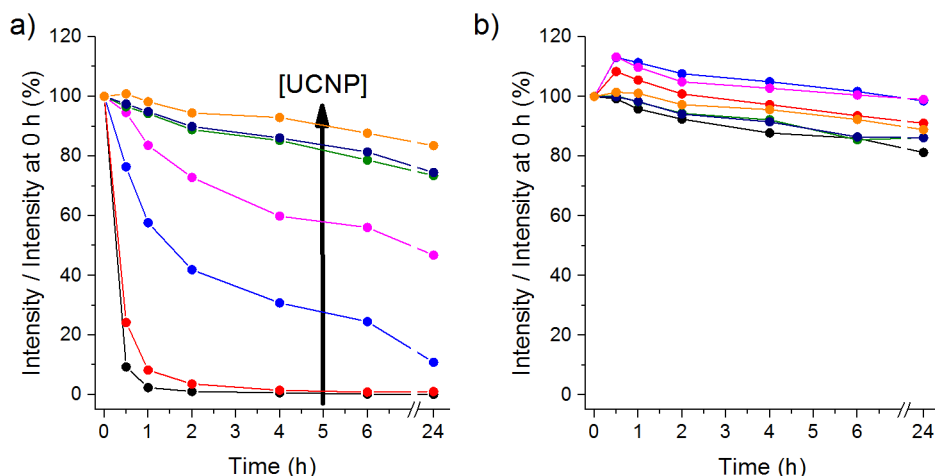

Figure 15. Time course upconversion with poly(acrylic acid) coated NaYF$_4$:Yb^{3+},Er^{3+} upconverting nanoparticles (UCNP) suspended a) in water (right) or b) in 1 mM KF in water. The nanoparticle concentrations were 0.5 (black), 1 (red), 5 (blue), 10 (magenta), 50 (green), 100 (dark blue), and 200 µg/mL (orange).

In addition, the different UCNP coatings were tested in order to study whether the coating can prevent the dissolution of ions. The upconversion luminescence decreased over time with the PAA, thin and thick silica coatings, but with the thick silica shell the decrease was slower than with the other coatings (detailed information in publication **II**). The thick silica shell protected the particle from the environment more effectively but could not completely prevent the dissolution of ions. Because the silica shell is amorphous, the solvent can access the nanoparticle surface. Also, as observed in figure 14, the silica shell thickness around the nanoparticles can vary rendering part of the surface more vulnerable. After the first publications on UCNP disintegration, different methods for surface modifications of UCNPs to prevent ion dissolution have been studied.[164-167]

If the ions dissolve until equilibrium is achieved, the disintegration of UCNPs could be prevented by adding free ions to the UCNP solution. As the fluoride ions have the highest impact on the solubility product, KF was added to the solution to prevent the disintegration of the UCNPs. The smallest amount of KF to prevent the disintegration was determined to be 0.1 mM, which corresponds to the dissolved fluoride ion concentration determined with a fluoride ion electrode (detailed information in the original publication **II**). However, a ten times higher concentration was chosen for the study of the UCNP concentration effect on the upconversion luminescence. At 1 mM KF concentration, the upconversion luminescence did not decrease significantly with any of the UCNP concentrations (Figure 15b). Therefore, the free fluoride ion in the solution prevented the disintegration of the nanoparticles. These results were later confirmed also by Dukhno et al.[159]

The disintegration of the UCNPs was visually studied with TEM. The disintegration was clearly observed in the TEM images after incubating the PAA coated UCNPs in water for 24 h (Figure 16). According to the TEM images, the disintegration was anisotropic creating distinctive holes in the middle of the nanoparticle. The dissolution of ions seems to proceed from the (001) crystal plane of the hexagonal lattice, leaving the (100) and (010) crystal planes intact. This might be due to the stabilization of the (010) crystal plane by the PAA ligand. According to the studies on anisotropic synthesis of UCNPs, OA stabilizes the (101) plane.[92] In this study, the PAA ligand stabilized the (010) crystal plane, and therefore the dissolution of ions from the (001) plane is favored. For comparison, at the zero-time point, the TEM samples were prepared immediately after dilution of UCNPs to water, and therefore no disintegration was observed in the images. More importantly, no disintegration was observed at the UCNPs which were incubated in 1 mM KF in water for 24 h verifying the conclusion that the free fluoride ion in the solution prevents UCNP disintegration.
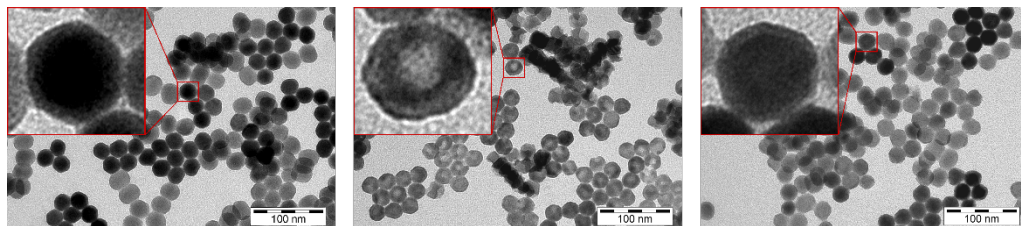
Figure 16. Visual detection of poly(acrylic acid coated) $NaYF_4:Yb^{3+},Er^{3+}$ upconverting nanoparticle disintegration based on TEM. The nanoparticles were incubated for 0 (left) or 24 h (middle) in water and 24 h in KF in water (right). A 5.5 times magnification of one nanoparticle is presented at the inset.

5.3   Bioaffinity assays

### 5.3.1   Homogeneous assay using Eu^{3+} chelate as an acceptor

In the original publication **I**, the suitability of an Eu^{3+} chelate acceptor for UC-RET-based applications was demonstrated. In the study, an intrinsically fluorescent nonadentate Eu^{3+} chelate with strong absorption centered at 330 nm and extending to 360 nm was used as an acceptor (Figure 17a). The Eu^{3+} chelate had sharp emission band at 613 nm corresponding to $^5D_0 \rightarrow {}^7F_2$ transition. The $Na_{0.8}Y_{0.2}KF_4:Yb^{3+},Tm^{3+}$ UCNP used as a donor had emission bands of Tm^{3+} at 345 and 362 nm, which overlap with the excitation spectrum of the Eu^{3+} chelate. In addition, the UCNPs had local emission minimum at 615 nm, where the emission of the Eu^{3+} chelate was measured. The emission of the Eu^{3+} chelate is easy to separate from the emission of the UCNP donor due to the large Stokes shift, which is not possible with traditional fluorescent dye acceptors.

Lifetime of the donor upconversion luminescence and sensitized acceptor emission were determined from the UCNP-SA alone or from the donor-acceptor complex in order to demonstrate that the decay of the sensitized Eu^{3+} chelate emission is longer than the emission decay of the donor. The photoluminescence lifetimes were determined to be 261 ± 1 and 258 ± 1 µs for UCNP-SA alone and UCNP-SA-bio-Eu^{3+} complex at 365 nm, respectively (Figure 17b). The lifetime of the sensitized Eu^{3+}-chelate emission at 615 nm was 1250 ± 7 µs, which was approximately five times longer than the lifetime of the donor. In traditional TR-FRET with lanthanide chelates as donors and fluorescent dyes as acceptors, the apparent luminescence lifetime of the acceptor is dependent on the luminescence lifetime of the donor. However, when using Eu^{3+} chelates as acceptors in the UC-RET application, the intrinsic luminescent lifetime of the acceptor is longer than the lifetime of the donor. Therefore, the lifetime of the sensitized Eu^{3+} chelate emission is not dependent on the donor lifetime and the energy-transfer efficiency.
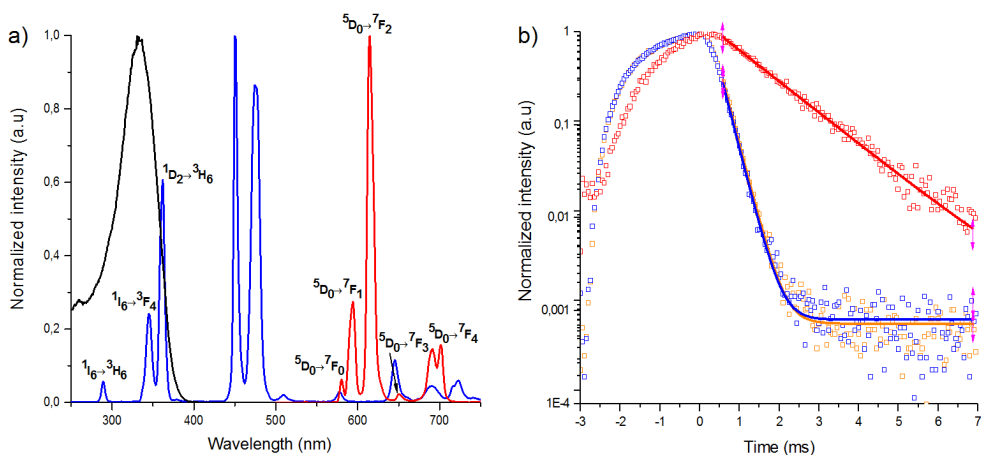
Figure 17. a) The spectral principle of the upconversion resonance energy transfer between UCNPs and Eu^{3+} chelate. The UCNP luminescence emission spectrum (blue), excitation (black) and emission (red) spectra of the intrinsically luminescent nonandentate Eu^{3+} chelate. b) Luminescence decay curves for UCNP-SA alone at 365 nm (orange), UCNP-SA-bio-Eu^{3+} at 365 nm (blue), and sensitized Eu^{3+} chelate emission at 615 nm (red). a.u. = arbitrary units

The feasibility of the introduced UC-RET donor-acceptor pair to bioaffinity assays was demonstrated with back-titration assay for biotin. The sensitized Eu^{3+} chelate emission was measured with the steady-state and TR mode (Figure 18). The data was analyzed by using sigmoidal fitting of Origin8. The LOD, calculated by subtracting three times the standard deviation from the mean of zero calibrator, were 3 nM with both measurement modes. The LODs did not differ between the steady-state and TR measurements, but there was a clear difference in the signal-to-background ratios, which were calculated by dividing the mean of the zero calibrator with the mean of the 10 000 nM calibrator. The ratios were 37 and 63 for the steady-state and TR, respectively. The higher signal-to-background ratios occur most likely due to the lower background originating from donor crosstalk. The donor has shorter luminescence lifetime than the acceptor, and thus the donor's luminescence has already decayed when the sensitized emission of the acceptor is measured.
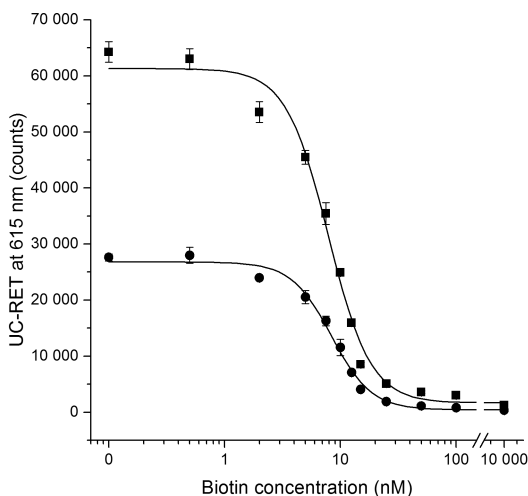
Figure 18. Back titration assay for biotin based on upconversion energy transfer (UC-RET) using upconverting nanoparticles as donors and intrinsically luminescent nonadentate Eu^{3+} chelates as acceptors. The sensitized Eu^{3+} chelate emission was measured at 615 nm with the steady-state (squares) and time-resolved (circles) mode when excited with 980 nm. The error bars represent the standard deviation of four replicates, except at 0 calibrator eight replicates.

The proposed energy transfer mechanism is illustrated in Figure 19. The hypothesis is that the energy is transferred from the Tm^{3+} ion of the UCNP to the Eu^{3+} ion via the antenna of the Eu^{3+} chelate. The hypothesis is supported by the observation that Eu^{3+} chelates with antennas of low or nonexistent absorption at 360 nm have low sensitized acceptor emission. More detailed information of UC-RET with other Eu^{3+} chelates can be found in original publication **I**. Therefore, after excitation with 980 nm, there are multiple energy transfer steps before the emission of Eu^{3+} chelate at 613 nm. Marin et al. also demonstrated the use of UCNPs as donors with lanthanide (Tb^{3+} and Eu^{3+}) complexes.[281] They demonstrated their energy transfer system in a casted film, not in bioaffinity assay in solution, and therefore the energy transfer was suggested to be radiative because no decrease in donor luminescence lifetime was detected.
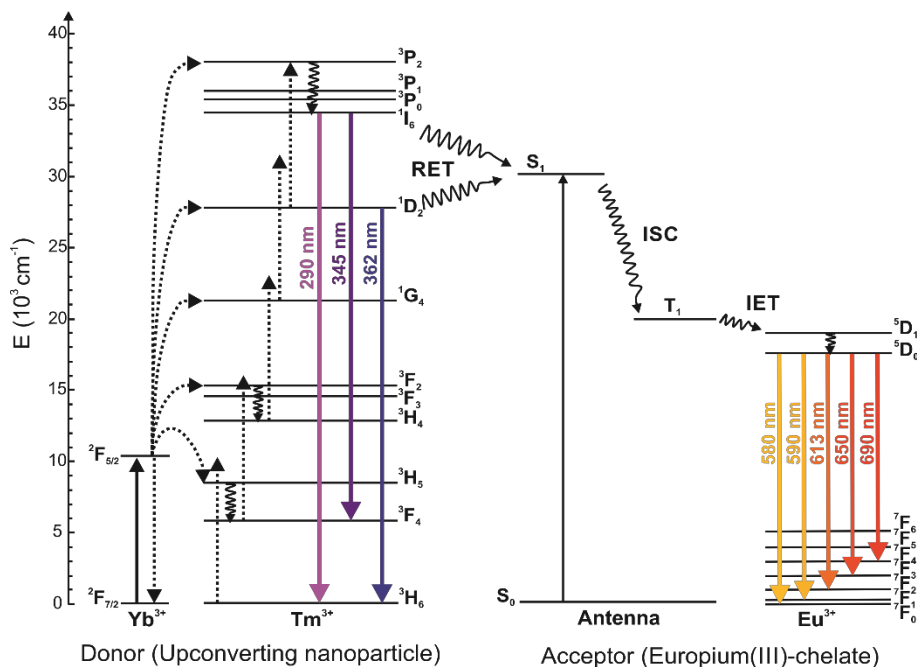
Figure 19. Energy level diagram of the energy transfer mechanism when the donor-acceptor pair is excited with 980 nm. The solid-line arrows are radiative transitions and the dotted arrows represent non-radiative energy transfer. The small curled arrows represent multiphonon relaxations. The energies of Yb^{3+} and Tm^{3+} are taken from the literature.[20] The antenna's energy level S1 is the measured absorption maxima of the antenna. The antenna's energy level T1 is an estimate. RET = resonance energy transfer, ISC = intersystem crossing, IET = intramolecular energy transfer.

5.3.2   Improving the sensitivity of UCNP-based immunoassays

In the original publication **III**, the non-specific binding of PAA-functionalized $NaYF_4$:Yb^{3+},Er^{3+} UCNP antibody conjugates was reduced in heterogeneous sandwich immunoassays by mixing free PAA to the buffer, in which the UCNPs were added to the wells. The effect of the free PAA in the buffer was tested in two different immunoassays. The free PAA added to the reporter buffer lowered the background signal caused by the non-specific binding at least threefold in both cTnI and TSH heterogeneous immunoassays (Figure 20). Five-parameter logistic regression was used for the fitting of the standard curves. The decrease in non-specific binding enabled the detection of three and a half times lower analyte concentrations in both assays. Because the background caused by the non-specific binding was reduced in both assays, the effect of free PAA is not analyte-specific and can therefore be used in all assays that utilize PAA-coated UCNPs. However, the concentration of PAA was analyte specific as ten times higher PAA concentration was needed to lower the non-specific binding in the TSH assay and therefore the PAA concentration needs to be optimized for immunoassays with different analytes.
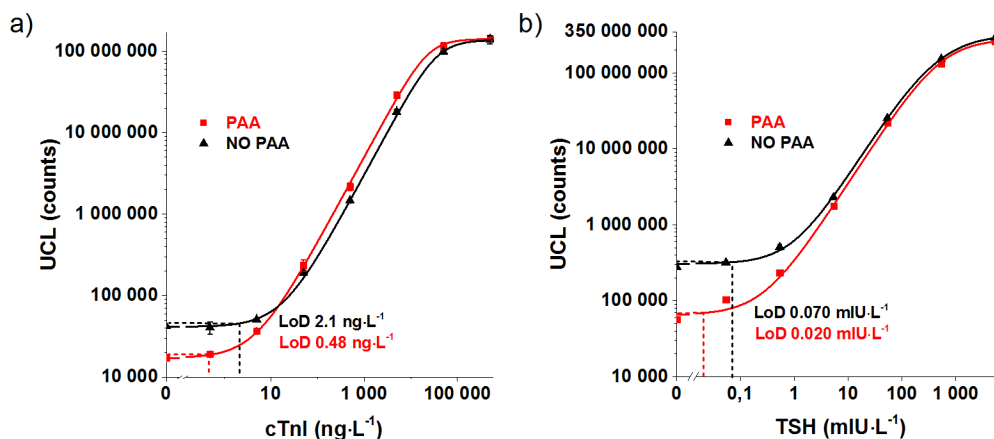
Figure 20. Standard curves for a) cardiac troponin I (cTnI) and b) thyroid-stimulating hormone (TSH) in heterogeneous immunoassays using poly(acrylic acid) (PAA)-coated $NaYF_4:Yb^{3+},Er^{3+}$ upconversion nanoparticles as reporters. The assays were performed with (red squares) or without (black triangle) free PAA mixed with the upconverting nanoparticles before they were added to the wells. The upconversion luminescence (UCL) was measured at 540 nm during 980 nm excitation. The error bars represent the standard deviation of three replicate calibrators, except the 0 calibrator six replicates.

Presumably, the free PAA reduces background by blocking the surface areas of the wells where the PAA coated UCNPs would bind non-specifically (Figure 21). The PAA-coated nanoparticles have proven to be monodisperse and colloidally stable in water because PAA molecules have strong negative charges. However, the highly negative PAA surface is most likely partly exposed to the environment even though the UCNPs are conjugated to antibodies. Therefore, the negatively charged surface of the PAA-coated UCNPs can bind to the positively net-charged proteins on the solid surface. The added free PAA in the buffer reduces the non-specific binding by binding to the areas where the PAA-coated UCNPs might bind non-specifically. Another explanation for the reduction of the non-specific binding by the free PAA is that there are gaps in the PAA coating on the surface of UCNPs leading to UCNP aggregation. Therefore, the addition of free PAA fills in the gaps preventing aggregation. This hypothesis is supported by a study where PEG-phospate ligands were stable in phosphate buffer as long as there was some excess PEG-phosphate ligands present in the buffer.[140]
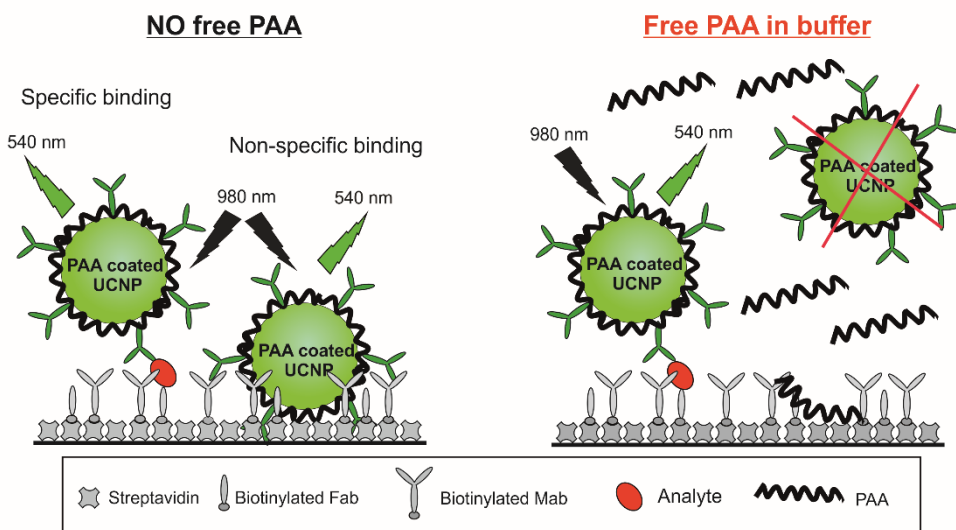
Figure 21. Effect of free poly(acrylic acid) (PAA) added to the buffer with antibody (Mab)-coated upconverting nanoparticles (UCNPs) in heterogeneous sandwich immunoassay. The assay principles are the same for thyroid-stimulating hormone and cardiac troponin I, except in the cardiac troponin I assay, a recombinant antigen binding fragment (Fab) is used for the capture of the analyte in addition to the Mab. The unbound UCNPs are washed away before the detection.

Although the non-specific binding was significantly reduced, the background caused by the non-specific binding is still limiting the assay sensitivity. The PAA-coated UNCPs can aggregate because of the crosslinking of two UCNPs by one PAA molecule or by pseudoaggregation of UCNPs due to hydrogen bonding of PAA molecules.[253, 279] By reducing the aggregation of the nanoparticles, the non-specific binding can be reduced even further, which can also improve the sensitivity. Most likely, the same approach for reducing the non-specific binding can be applied to UCNPs that are coated with other polymers than PAA.

5.3.3   Upconversion cross-correlation spectroscopy

In the original publication **IV**, the applicability of UCNPs to cross-correlation spectroscopy was demonstrated in homogeneous sandwich immunoassay for TSH using blue ($NaYF_4$:Yb^{3+},Tm^{3+}) and green ($NaYF_4$:Yb^{3+},Er^{3+}) emitting UCNPs. In order to form the auto- and cross-correlation (AC and CC) curves from the UCCS measurement, the photon macro times (elapsed time since the start of the measurement) were measured to construct time traces. The detected photons were binned to 2 ms time intervals. The binding between the two nanoparticles by the TSH analyte was analyzed by determining the cross-correlation amplitudes (A_{CC}) by fitting the stretched exponential with the correlation time τs and the stretching exponent β of the equation 3 to the data.

$$A(\tau) = A_{CC} \cdot \exp(-\tau/\tau_S)^{\beta} + 1 \qquad \text{(Eq. 3)}$$

Examples of the time traces with 0 and 2880 mIU·L^{-1} TSH concentration and the AC and CC curves formed on the basis of the time traces are illustrated in Figure 22. Without the TSH present, the UCNPs are barely bound together and there are no simultaneous fluorescence bursts resulting in low A_{CC} value. However, with TSH present in the binding reaction, simultaneous fluorescence bursts were detected, which resulted in an increase in the A_{CC} value. The increase in the number of simultaneous bursts and in the A_{CC} value in the presence of TSH is due to the binding of blue and green emitting UCNPs together via TSH, and the complex then diffuses trough the laser focus emitting green and blue photons simultaneously. It should be noted that the photon emission might not be exactly simultaneous since the two UCNPs have differences in their excitation energy migration dynamics and long apparent luminescence lifetimes of few hundred microseconds.[282] The simultaneous emission could be improved by using UCNPs with high Yb^{3+} doping, which decreases apparent luminescence lifetimes.[283] This could improve the probability of simultaneous photon emission in addition to enabling brighter emission under high power excitation.[284] However, in this application, the UCNP diffusion time through the laser focus is longer than the luminescence decay time, and possible differences in the photon emission could therefore be neglected.
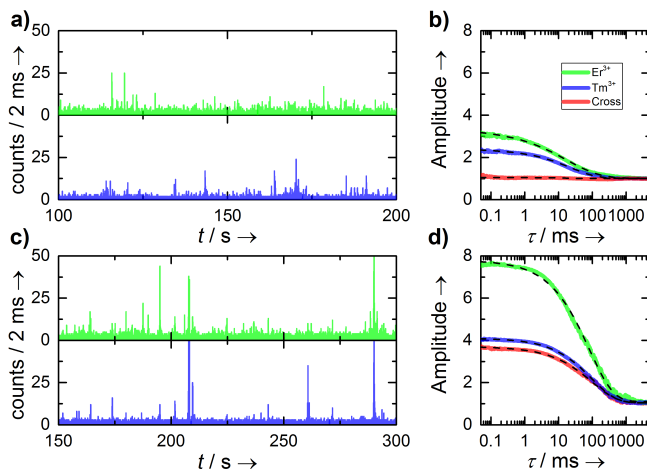
Figure 22. Time trace examples of upconversion cross-correlation measurements from the mixture of NaYF4:Yb^{3+},Er^{3+} (green) and NaYF4:Yb^{3+},Tm^{3+} (blue) antibody-conjugated UCNPs a) without thyroid-stimulating hormone and c) with 2880 mIU·L^{-1} thyroid-stimulating hormone. The traces were binned to 2 ms. b) The autocorrelation and cross-correlation curves formed form the data in a) and d) auto and cross-correlation formed from the data in c).

The greatest problem in the UCCS measurement was the formation of large UCNP aggregates leading to high fluorescent bursts. This problem was circumvented by removing large bursts above 100 counts per 2 ms from the data before calculating the AC and CC functions. The aggregates can form due to non-specific binding between the UCNP particles or due to TSH-induced bridging of multiple UCNPs together.

A standard curve for the homogeneous sandwich immunoassay was formed on the basis of A_{CC} values (Figure 23). There is a clear dependency between the A_{CC} and TSH concentration indicating increased binding of blue and green emitting UCNPs together with the increase of TSH concentration. The standard curve was fitted with a four-parameter logistic function. The LOD, calculated by adding three times the standard deviation to the zero-analyte concentration, was 15 mIU L[-1]. The LOD of the developed assay is too high to detect TSH concentration in normal serum, which is in the range of 0.3–5.0 mIU L[-1].[285] However, the assay was a proof-of-principle homogeneous assay, and thus it cannot be compared to highly sensitive heterogeneous assays with LODs as low as $60 \cdot 10^{-6}$ mIU L[-1].[286, 287]
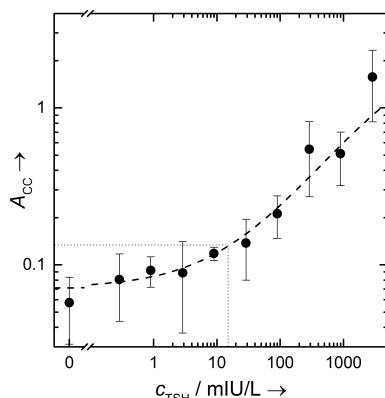
Figure 23. Standard curve of homogeneous sandwich immunoassay for thyroid-stimulating hormone (TSH). The dashed line represents the limit of detection of the curve and the error bars represent the standard deviation of at least five replicate measurements with a length of 300 s each.

UCNP aggregation is the major limiting factor of the assay sensitivity. The high luminescence bursts of the aggregates can cause strong variation in the CC curve even after the high bursts are removed from the data.[288, 289] The UCNP aggregation can be removed by optimizing the surface modification or optimizing the buffer combinations used in the assay. The sensitivity can also be lowered by optimizing the concentrations of UCNPs in the binding reaction. In the assay, the molar amount of individual UNCPs was adjusted to two times higher than the highest TSH concentration tested in order to reduce the bridging of the multiple UNCPs together. The sensitivity could be improved by optimizing the UCNP concentration for lower TSH values. Moreover, the sensitivity could be improved by increasing the measurement time, which would improve statistics.

6 CONCLUSIONS

Interest towards UCNPs and their use in bioaffinity assays has increased over the years due to their excellent luminescent properties and suitability for detection in biological matrices. The synthesis of nanosized UCNPs opened new possibilities for the reporter technology enabling higher specific activity, and the UCNP properties, such as luminescence, size, shape, and surface modification are still being developed. Despite the advancements in the field, UCNPs have drawbacks that have prevented their wider adaptation, especially in commercial applications. Additionally, the properties of luminescence, host matrix, and surface modification of nanosized particles have not been completely understood yet.

In this thesis, the properties of UCNPs were studied further and UCNPs were used as reporters in homogeneous and heterogeneous bioaffinity assays. The disintegration mechanism of the fluoride-based UCNP host matrix was studied and a method to prevent ion dissolution from the particle matrix was presented. Two homogenous bioaffinity assays were developed, which either introduced a new donor-acceptor pair in a UC-RET-based assay or demonstrated the applicability of UCNPs in cross-correlation spectroscopy measurements. Moreover, a method to reduce the non-specific binding of UCNP conjugates was presented.

The main conclusions based on the original publications are:

I   Intrinsically luminescent Eu^{3+} chelate was a highly suitable acceptor for UC-RET-based bioaffinity assay. The antenna of the Eu^{3+} chelate had significant absorption at 360 nm, which overlapped with the transitions of the UCNP used in the study. Since the intrinsic luminescence lifetime was longer than that of the UCNP, the sensitized acceptor emission could be measured even after the UCNP donor luminesce had decayed resulting in higher signal-to-background ratio. Furthermore, Eu^{3+} chelates have a large Stokes shift, and thus they did not self-quench in high concentration, and the donor crosstalk was minimal. The presented donor-acceptor pair has a great potential also for sensing and imaging applications because the sensitized acceptor lifetime is independent from donor lifetime and could therefore be used for modulation.

II   UCNPs disintegrated in aqueous solutions due to the dissolution of particle constituting ions. The ions dissolved until a solubility equilibrium was achieved, in which the fluoride ion had a major impact. Thus, in diluted UCNP suspensions, most of the nanoparticles are disintegrated before the equilibrium is achieved, which could be observed also as an almost complete disappearance of luminescence. Nevertheless, the disintegration could be prevented by adding free fluoride ions to the solution creating the equilibrium in the solvent without the dissolution of the nanoparticle ions. This observation is critical for the use and measurement of diluted UCNP concentration in bioaffinity assays.

III The non-specific binding of PAA-coated UCNP conjugates was significantly reduced by adding free PAA to the buffer during reporter incubation. By reducing the non-specific binding to the solid support, highly sensitive immunoassays were achieved. The method for lowering the non-specific binding was simple and easy to perform and did not require time consuming optimization of surface modification.

IV UCNPs have great potential as reporters in UCCS, which was demonstrated with a proof-of-concept homogeneous sandwich immunoassay. The presence of the analyte was detected by simultaneous emission of two differently emitting UCNPs. The detectability of TSH with UCCS was limited by the aggregation of UCNPs, and thus, by preventing the aggregation, the performance of the assay would enhance significantly. UCCS is not restricted to only *in vitro* -assays, but could be highly suitable for *in vivo* -applications, where conventional cross-correlation spectroscopy is limited due to the autofluorescence background.

In conclusion, new insights and improvements of UCNPs were provided in this thesis for the use of UCNPs in bioaffinity applications. Despite the solutions presented for the certain drawbacks of UCNPs, aggregation, non-specific interactions, low upconversion efficiency, and protection of the host lattice from the environment remain as challenges for the use of UCNPs in bioaffinity applications. By solving these issues, UCNPs would enable extremely sensitive assays and would facilitate the transition from academic studies to commercial applications.

ACKNOWLEDGEMENTS

Turku, September 2019

Satu Lahtinen

REFERENCES

1. Hemmilä, I., Fluoroimmunoassays and immunofluorometric assays. *Clinical Chemistry*. **31**(3): p. 359-370 (1985).

2. Pei, X., Zhang, B., Tang, J., Liu, B., Lai, W., and Tang, D., Sandwich-type immunosensors and immunoassays exploiting nanostructure labels: A review. *Analytica Chimica Acta*. **758**: p. 1-18 (2013).

3. Rantanen, T., Järvenpää, M.-L., Vuojola, J., Kuningas, K., and Soukka, T., Fluorescence-Quenching-Based Enzyme-Activity Assay by Using Photon Upconversion. *Angewandte Chemie International Edition*. **47**(20): p. 3811-3813 (2008).

4. Xu, C.T., Svensson, N., Axelsson, J., Svenmarker, P., Somesfalean, G., Chen, G., Liang, H., Liu, H., Zhang, Z., and Andersson-Engels, S., Autofluorescence insensitive imaging using upconverting nanocrystals in scattering media. *Applied Physics Letters*. **93**(17): p. 171103 (2008).

5. Soukka, T., Kuningas, K., Rantanen, T., Haaslahti, V., and Lövgren, T., Photochemical characterization of up-converting inorganic lanthanide phosphors as potential labels. *Journal of fluorescence*. **15**(4): p. 513-528 (2005).

6. Auzel, F., Upconversion and Anti-Stokes Processes with f and d Ions in Solids. *Chemical Reviews*. **104**(1): p. 139-174 (2004).

7. Haase, M. and Schäfer, H., Upconverting Nanoparticles. *Angewandte Chemie International Edition*. **50**(26): p. 5808-5829 (2011).

8. Arppe, R., Mattsson, L., Korpi, K., Blom, S., Wang, Q., Riuttamäki, T., and Soukka, T., Homogeneous Assay for Whole Blood Folate Using Photon Upconversion. *Analytical Chemistry*. **87**(3): p. 1782-1788 (2015).

9. Wu, B., Cao, Z., Zhang, Q., and Wang, G., NIR-responsive DNA hybridization detection by high efficient FRET from 10-nm upconversion nanoparticles to SYBR green I. *Sensors and Actuators B: Chemical*. **255**: p. 2853-2860 (2018).

10. Zhou, Y., Chen, Y., He, H., Liao, J., Duong, H.T.T., Parviz, M., and Jin, D., A homogeneous DNA assay by recovering inhibited emission of rare earth ions-doped upconversion nanoparticles. *Journal of Rare Earths*. **37**(1): p. 11-18 (2019).

11. Sirkka, N., Lyytikäinen, A., Savukoski, T., and Soukka, T., Upconverting nanophosphors as reporters in a highly sensitive heterogeneous immunoassay for cardiac troponin I. *Analytica chimica acta*. **925**: p. 82-87 (2016).

12. Hlaváček, A., Farka, Z., Hübner, M., Horňáková, V., Němeček, D., Niessner, R., Skládal, P., Knopp, D., and Gorris, H.H., Competitive Upconversion-Linked Immunosorbent Assay for the Sensitive Detection of Diclofenac. *Analytical Chemistry*. **88**(11): p. 6011-6017 (2016).

13. Mendez-Gonzalez, D., Lahtinen, S., Laurenti, M., López-Cabarcos, E., Rubio-Retama, J., and Soukka, T., Photochemical Ligation to Ultrasensitive DNA Detection with Upconverting Nanoparticles. *Analytical Chemistry*. **90**(22): p. 13385-13392 (2018).

14. Wilhelm, S., Perspectives for Upconverting Nanoparticles. *ACS Nano*. **11**(11): p. 10644-10653 (2017).

15. Mandl, G.A., Cooper, D.R., Hirsch, T., Seuntjens, J., and Capobianco, J.A., Perspective: lanthanide-doped upconverting nanoparticles. *Methods and Applications in Fluorescence*. **7**(1): p. 012004 (2019).

16. Nadort, A., Zhao, J., and Goldys, E.M., Lanthanide upconversion luminescence at the nanoscale: fundamentals and optical properties. *Nanoscale*. **8**(27): p. 13099-13130 (2016).

17. Bünzli, J.-C.G., Benefiting from the Unique Properties of Lanthanide Ions. *Accounts of Chemical Research*. **39**(1): p. 53-61 (2006).

18. Suyver, J.F., Aebischer, A., Biner, D., Gerner, P., Grimm, J., Heer, S., Krämer, K.W., Reinhard, C., and Güdel, H.U., Novel materials doped with trivalent lanthanides and transition metal ions showing near-

infrared to visible photon upconversion. *Optical Materials*. **27**(6): p. 1111-1130 (2005).

19. Binnemans, K., Lanthanide-Based Luminescent Hybrid Materials. *Chemical Reviews*. **109**(9): p. 4283-4374 (2009).

20. Carnall, W.T., Fields, P.R., and Rajnak, K., Electronic Energy Levels in the Trivalent Lanthanide Aquo Ions. I. Pr^{3+}, Nd^{3+}, Pm^{3+}, Sm^{3+}, Dy^{3+}, Ho^{3+}, Er^{3+}, and Tm^{3+}. *The Journal of Chemical Physics*. **49**(10): p. 4424-4442 (1968).

21. Pollnau, M., Gamelin, D.R., Lüthi, S.R., Güdel, H.U., and Hehlen, M.P., Power dependence of upconversion luminescence in lanthanide and transition-metal-ion systems. *Physical Review B*. **61**(5): p. 3337-3346 (2000).

22. Suyver, J.F., Aebischer, A., García-Revilla, S., Gerner, P., and Güdel, H.U., Anomalous power dependence of sensitized upconversion luminescence. *Physical Review B*. **71**(12): p. 125123 (2005).

23. Chivian, J.S., Case, W.E., and Eden, D.D., The photon avalanche: A new phenomenon in Pr^{3+}-based infrared quantum counters. *Applied Physics Letters*. **35**(2): p. 124-125 (1979).

24. Deng, H., Yang, S., Xiao, S., Gong, H.-M., and Wang, Q.-Q., Controlled Synthesis and Upconverted Avalanche Luminescence of Cerium(III) and Neodymium(III) Orthovanadate Nanocrystals with High Uniformity of Size and Shape. *Journal of the American Chemical Society*. **130**(6): p. 2032-2040 (2008).

25. Joubert, M.-F., Photon avalanche upconversion in rare earth laser materials. *Optical Materials*. **11**(2): p. 181-203 (1999).

26. Zheng, W., Huang, P., Tu, D., Ma, E., Zhu, H., and Chen, X., Lanthanide-doped upconversion nano-bioprobes: electronic structures, optical properties, and biodetection. *Chemical Society Reviews*. **44**(6): p. 1379-1415 (2015).

27. Prorok, K., Gnach, A., Bednarkiewicz, A., and Stręk, W., Energy up-conversion in Tb^{3+}/Yb^{3+} co-doped colloidal α-NaYF$_4$ nanocrystals. *Journal of Luminescence*. **140**: p. 103-109 (2013).

28. Debasu, M.L., Ananias, D., Pinho, S.L.C., Geraldes, C.F.G.C., Carlos, L.D., and Rocha, J., (Gd,Yb,Tb)PO$_4$ up-conversion nanocrystals for bimodal luminescence–MR imaging. *Nanoscale*. **4**(16): p. 5154-5162 (2012).

29. Wang, F., Deng, R., Wang, J., Wang, Q., Han, Y., Zhu, H., Chen, X., and Liu, X., Tuning upconversion through energy migration in core–shell nanoparticles. *Nature Materials*. **10**: p. 968 (2011).

30. Su, Q., Han, S., Xie, X., Zhu, H., Chen, H., Chen, C.-K., Liu, R.-S., Chen, X., Wang, F., and Liu, X., The Effect of Surface Coating on Energy Migration-Mediated Upconversion. *Journal of the American Chemical Society*. **134**(51): p. 20849-20857 (2012).

31. Dong, H., Sun, L.-D., and Yan, C.-H., Energy transfer in lanthanide upconversion studies for extended optical applications. *Chemical Society Reviews*. **44**(6): p. 1608-1634 (2015).

32. Xie, X., Gao, N., Deng, R., Sun, Q., Xu, Q.-H., and Liu, X., Mechanistic Investigation of Photon Upconversion in Nd^{3+}-Sensitized Core–Shell Nanoparticles. *Journal of the American Chemical Society*. **135**(34): p. 12608-12611 (2013).

33. Shen, J., Chen, G., Vu, A.-M., Fan, W., Bilsel, O.S., Chang, C.-C., and Han, G., Engineering the Upconversion Nanoparticle Excitation Wavelength: Cascade Sensitization of Tri-doped Upconversion Colloidal Nanoparticles at 800 nm. *Advanced Optical Materials*. **1**(9): p. 644-650 (2013).

34. Zhong, Y., Rostami, I., Wang, Z., Dai, H., and Hu, Z., Energy Migration Engineering of Bright Rare-Earth Upconversion Nanoparticles for Excitation by Light-Emitting Diodes. *Advanced Materials*. **27**(41): p. 6418-6422 (2015).

35. Liang, L., Xie, X., Loong, D.T.B., All, A.H., Huang, L., and Liu, X., Designing Upconversion Nanocrystals Capable of 745 nm Sensitization and 803 nm Emission for Deep-Tissue Imaging. *Chemistry – A European Journal*. **22**(31): p. 10801-10807 (2016).

36. Cheng, X., Pan, Y., Yuan, Z., Wang, X., Su, W., Yin, L., Xie, X., and Huang, L., Er^{3+} Sensitized Photon Upconversion Nanocrystals. *Advanced Functional Materials*. **28**(22): p. 1800208 (2018).

37. Yan, L., Zhou, B., Song, N., Liu, X., Huang, J., Wang, T., Tao, L., and Zhang, Q., Self-sensitization induced upconversion of Er^{3+} in core–shell nanoparticles. *Nanoscale*. **10**(37): p. 17949-17957 (2018).

38. Cheng, X., Ge, H., Wei, Y., Zhang, K., Su, W., Zhou, J., Yin, L., Zhan, Q., Jing, S., and Huang, L., Design for Brighter Photon Upconversion Emissions via Energy Level Overlap of Lanthanide Ions. *ACS Nano*. **12**(11): p. 10992-10999 (2018).

39. Wu, X., Zhang, Y., Takle, K., Bilsel, O., Li, Z., Lee, H., Zhang, Z., Li, D., Fan, W., Duan, C., Chan, E.M., Lois, C., Xiang, Y., and Han, G., Dye-Sensitized Core/Active Shell Upconversion Nanoparticles for Optogenetics and Bioimaging Applications. *ACS Nano*. **10**(1): p. 1060-1066 (2016).

40. Chen, G., Damasco, J., Qiu, H., Shao, W., Ohulchanskyy, T.Y., Valiev, R.R., Wu, X., Han, G., Wang, Y., Yang, C., Ågren, H., and Prasad, P.N., Energy-Cascaded Upconversion in an Organic Dye-Sensitized Core/Shell Fluoride Nanocrystal. *Nano Letters*. **15**(11): p. 7400-7407 (2015).

41. Saleh, M.I., Panas, I.D., Frenzel, F., Würth, C., Rühle, B., Slominskii, Y.L., Demchenko, A., and Resch-Genger, U., Sensitization of upconverting nanoparticles with a NIR-emissive cyanine dye using a micellar encapsulation approach. *Methods and Applications in Fluorescence*. **7**(1): p. 014003 (2019).

42. Zou, W., Visser, C., Maduro, J.A., Pshenichnikov, M.S., and Hummelen, J.C., Broadband dye-sensitized upconversion of near-infrared light. *Nature Photonics*. **6**: p. 560 (2012).

43. Hyppänen, I., Lahtinen, S., Ääritalo, T., Mäkelä, J., Kankare, J., and Soukka, T., Photon Upconversion in a Molecular Lanthanide Complex in Anhydrous Solution at Room Temperature. *ACS Photonics*. **1**(5): p. 394-397 (2014).

44. Dong, H., Sun, L.-D., and Yan, C.-H., Basic understanding of the lanthanide related upconversion emissions. *Nanoscale*. **5**(13): p. 5703-5714 (2013).

45. Wang, F. and Liu, X., Recent advances in the chemistry of lanthanide-doped upconversion nanocrystals. *Chemical Society Reviews*. **38**(4): p. 976-989 (2009).

46. Vuojola, J., Riuttamäki, T., Kulta, E., Arppe, R., and Soukka, T., Fluorescence-quenching-based homogeneous caspase-3 activity assay using photon upconversion. *Analytica Chimica Acta*. **725**: p. 67-73 (2012).

47. Kale, V., Lastusaari, M., Hölsä, J., and Soukka, T., Intense UV upconversion through highly sensitized $NaRF_4$:Tm (R:Y,Yb) crystals. *RSC Advances*. **5**(45): p. 35858-35865 (2015).

48. Diamente, P.R., Raudsepp, M., and van Veggel, F.C.J.M., Dispersible Tm^{3+}-Doped Nanoparticles that Exhibit Strong 1.47 μm Photoluminescence. *Advanced Functional Materials*. **17**(3): p. 363-368 (2007).

49. Suyver, J.F., Grimm, J., van Veen, M.K., Biner, D., Krämer, K.W., and Güdel, H.U., Upconversion spectroscopy and properties of $NaYF_4$ doped with Er^{3+}, Tm^{3+} and/or Yb^{3+}. *Journal of Luminescence*. **117**(1): p. 1-12 (2006).

50. Krämer, K.W., Biner, D., Frei, G., Güdel, H.U., Hehlen, M.P., and Lüthi, S.R., Hexagonal Sodium Yttrium Fluoride Based Green and Blue Emitting Upconversion Phosphors. *Chemistry of Materials*. **16**(7): p. 1244-1251 (2004).

51. Menyuk N., D.K., and Pierce J.W., $NaYF_4$: Yb,Er—an efficient upconversion phosphor. *Applied Physics Letters*. **21**(4): p. 159-161 (1972).

52. Aebischer, A., Hostettler, M., Hauser, J., Krämer, K., Weber, T., Güdel, H.U., and Bürgi, H.-B., Structural and Spectroscopic Characterization of Active Sites in a Family of Light-Emitting Sodium Lanthanide Tetrafluorides. *Angewandte Chemie International Edition*. **45**(17): p. 2802-2806 (2006).

53. Suyver, J.F., Grimm, J., Krämer, K.W., and Güdel, H.U., Highly efficient near-infrared to visible up-conversion process in $NaYF_4$:Er^{3+},Yb^{3+}. *Journal of Luminescence*. **114**(1): p. 53-59 (2005).

54. Johnson, N.J.J., He, S., Diao, S., Chan, E.M., Dai, H., and Almutairi, A., Direct Evidence for Coupled Surface and Concentration Quenching Dynamics in Lanthanide-Doped Nanocrystals. *Journal of the American Chemical Society*. **139**(8): p. 3275-3282 (2017).

55. Cao, B.S., He, Y.Y., Zhang, L., and Dong, B., Upconversion properties of Er^{3+}– Yb^{3+}:$NaYF_4$ phosphors with a wide range of Yb^{3+} concentration. *Journal of Luminescence*. **135**: p. 128-132 (2013).

56. Yin, A., Zhang, Y., Sun, L., and Yan, C., Colloidal synthesis and blue based multicolor upconversion emissions of size and composition controlled monodisperse hexagonal $NaYF_4$: Yb,Tm nanocrystals. *Nanoscale*. **2**(6): p. 953-959 (2010).

57. Liang, L., Wu, H., Hu, H., Wu, M., and Su, Q., Enhanced blue and green upconversion in hydrothermally synthesized hexagonal $NaY_{1-x}Yb_xF_4$:Ln^{3+} (Ln^{3+} = Er^{3+} or Tm^{3+}). *Journal of Alloys and Compounds*. **368**(1): p. 94-100 (2004).

58. Chen, X.P., Zhang, Q.Y., Yang, C.H., Chen, D.D., and Zhao, C., Comparative investigation on structure and luminescence properties of fluoride phosphors codoped with Er^{3+}/Yb^{3+}. *Spectrochimica Acta Part A: Molecular and Biomolecular Spectroscopy*. **74**(2): p. 441-445 (2009).

59. Zhao, J., Jin, D., Schartner, E.P., Lu, Y., Liu, Y., Zvyagin, A.V., Zhang, L., Dawes, J.M., Xi, P., Piper, J.A., Goldys, E.M., and Monro, T.M., Single-nanocrystal sensitivity achieved by enhanced upconversion luminescence. *Nature Nanotechnology*. **8**: p. 729 (2013).

60. Drees, C., Raj, A.N., Kurre, R., Busch, K.B., Haase, M., and Piehler, J., Engineered Upconversion Nanoparticles for Resolving Protein Interactions inside Living Cells. *Angewandte Chemie International Edition*. **55**(38): p. 11668-11672 (2016).

61. Zhan, Q., Qian, J., Liang, H., Somesfalean, G., Wang, D., He, S., Zhang, Z., and Andersson-Engels, S., Using 915 nm Laser Excited Tm^{3+}/Er^{3+}/Ho^{3+}-Doped $NaYbF_4$ Upconversion Nanoparticles for in Vitro and Deeper in Vivo Bioimaging without Overheating Irradiation. *ACS Nano*. **5**(5): p. 3744-3757 (2011).

62. Wang, Y.-F., Liu, G.-Y., Sun, L.-D., Xiao, J.-W., Zhou, J.-C., and Yan, C.-H., Nd^{3+}-Sensitized Upconversion Nanophosphors: Efficient In Vivo Bioimaging Probes with Minimized Heating Effect. *ACS Nano*. **7**(8): p. 7200-7206 (2013).

63. Tian, B., Fernandez-Bravo, A., Najafiaghdam, H., Torquato, N.A., Altoe, M.V.P., Teitelboim, A., Tajon, C.A., Tian, Y., Borys, N.J., Barnard, E.S., Anwar, M., Chan, E.M., Schuck, P.J., and Cohen, B.E., Low irradiance multiphoton imaging with alloyed lanthanide nanocrystals. *Nature Communications*. **9**(1): p. 3082 (2018).

64. Vetrone, F.B., John-Christopher; and Capobianco, John A., Significance of Yb^{3+} concentration on the upconversion mechanisms in codoped Y_2O_3:Er^{3+}, Yb^{3+} nanocrystals. *Journal of Applied Physics*. **96**(1): p. 661-667 (2004).

65. Zhao, J., Sun, Y., Kong, X., Tian, L., Wang, Y., Tu, L., Zhao, J., and Zhang, H., Controlled Synthesis, Formation Mechanism, and Great Enhancement of Red Upconversion Luminescence of $NaYF_4$:Yb^{3+}, Er^{3+} Nanocrystals/Submicroplates at Low Doping Level. *The Journal of Physical Chemistry B*. **112**(49): p. 15666-15672 (2008).

66. Tian, Y., Tian, Y., Huang, P., Wang, L., Shi, Q., and Cui, C.e., Effect of Yb^{3+} concentration on upconversion luminescence and temperature sensing behavior in Yb^{3+}/Er^{3+} co-doped $YNbO_4$ nanoparticles prepared via molten salt route. *Chemical Engineering Journal*. **297**: p. 26-34 (2016).

67. Ye, X., Luo, Y., Liu, S., Hou, D., and You, W., Intense and color-tunable upconversion luminescence of Er^{3+} doped and Er^{3+}/Yb^{3+} co-doped $Ba_3Lu_4O_9$ phosphors. *Journal of Alloys and Compounds*. **701**: p. 806-815 (2017).

68. Wang, F. and Liu, X., Upconversion Multicolor Fine-Tuning: Visible to Near-Infrared Emission from Lanthanide-Doped NaYF$_4$ Nanoparticles. *Journal of the American Chemical Society*. **130**(17): p. 5642-5643 (2008).

69. Wei, W., Zhang, Y., Chen, R., Goggi, J., Ren, N., Huang, L., Bhakoo, K.K., Sun, H., and Tan, T.T.Y., Cross Relaxation Induced Pure Red Upconversion in Activator- and Sensitizer-Rich Lanthanide Nanoparticles. *Chemistry of Materials*. **26**(18): p. 5183-5186 (2014).

70. Shen, J., Chen, G., Ohulchanskyy, T.Y., Kesseli, S.J., Buchholz, S., Li, Z., Prasad, P.N., and Han, G., Upconversion: Tunable Near Infrared to Ultraviolet Upconversion Luminescence Enhancement in (α-NaYF$_4$:Yb,Tm)/CaF$_2$ Core/Shell Nanoparticles for In situ Real-time Recorded Biocompatible Photoactivation. *Small*. **9**(19): p. 3212-3212 (2013).

71. Wu, H., Hao, Z., Zhang, L., Zhang, X., Xiao, Y., Pan, G.-H., Wu, H., Luo, Y., Zhao, H., and Zhang, J., Phonon Energy Dependent Energy Transfer Upconversion for the Red Emission in the Er^{3+}/Yb^{3+} System. *The Journal of Physical Chemistry C*. **122**(17): p. 9611-9618 (2018).

72. Dong, H., Sun, L.-D., Wang, Y.-F., Ke, J., Si, R., Xiao, J.-W., Lyu, G.-M., Shi, S., and Yan, C.-H., Efficient Tailoring of Upconversion Selectivity by Engineering Local Structure of Lanthanides in Na$_x$REF$_{3+x}$ Nanocrystals. *Journal of the American Chemical Society*. **137**(20): p. 6569-6576 (2015).

73. Tian, D., Gao, D., Chong, B., and Liu, X., Upconversion improvement by the reduction of Na+-vacancies in Mn^{2+} doped hexagonal NaYbF$_4$:Er^{3+} nanoparticles. *Dalton Transactions*. **44**(9): p. 4133-4140 (2015).

74. Zeng, S., Yi, Z., Lu, W., Qian, C., Wang, H., Rao, L., Zeng, T., Liu, H., Liu, H., Fei, B., and Hao, J., Simultaneous Realization of Phase/Size Manipulation, Upconversion Luminescence Enhancement, and Blood Vessel Imaging in Multifunctional Nanoprobes Through Transition Metal Mn^{2+} Doping. *Advanced Functional Materials*. **24**(26): p. 4051-4059 (2014).

75. Tian, G., Gu, Z., Zhou, L., Yin, W., Liu, X., Yan, L., Jin, S., Ren, W., Xing, G., Li, S., and Zhao, Y., Mn^{2+} Dopant-Controlled Synthesis of NaYF$_4$:Yb/Er Upconversion Nanoparticles for in vivo Imaging and Drug Delivery. *Advanced Materials*. **24**(9): p. 1226-1231 (2012).

76. Gainer, C.F. and Romanowski, M., A review of synthetic methods for the production of upconverting lanthanide nanoparticles. *Journal of Innovative Optical Health Sciences*. **07**(02): p. 1330007 (2014).

77. DaCosta, M.V., Doughan, S., Han, Y., and Krull, U.J., Lanthanide upconversion nanoparticles and applications in bioassays and bioimaging: A review. *Analytica Chimica Acta*. **832**: p. 1-33 (2014).

78. Suter, J.D., Pekas, N.J., Berry, M.T., and May, P.S., Real-Time-Monitoring of the Synthesis of β-NaYF$_4$:17% Yb,3% Er Nanocrystals Using NIR-to-Visible Upconversion Luminescence. *The Journal of Physical Chemistry C*. **118**(24): p. 13238-13247 (2014).

79. May, P.B., Suter, J.D., May, P.S., and Berry, M.T., The Dynamics of Nanoparticle Growth and Phase Change During Synthesis of β-NaYF$_4$. *The Journal of Physical Chemistry C*. **120**(17): p. 9482-9489 (2016).

80. Voss, B. and Haase, M., Intrinsic Focusing of the Particle Size Distribution in Colloids Containing Nanocrystals of Two Different Crystal Phases. *ACS Nano*. **7**(12): p. 11242-11254 (2013).

81. Komban, R., Klare, J.P., Voss, B., Nordmann, J., Steinhoff, H.-J., and Haase, M., An Electron Paramagnetic Resonance Spectroscopic Investigation on the Growth Mechanism of NaYF$_4$:Gd Nanocrystals. *Angewandte Chemie International Edition*. **51**(26): p. 6506-6510 (2012).

82. Rinkel, T., Nordmann, J., Raj, A.N., and Haase, M., Ostwald-ripening and particle size focussing of sub-10 nm NaYF$_4$ upconversion nanocrystals. *Nanoscale*. **6**(23): p. 14523-14530 (2014).

83. Ayyub, P., Palkar, V.R., Chattopadhyay, S., and Multani, M., Effect of crystal size reduction on lattice symmetry and

cooperative properties. *Physical Review B*. **51**(9): p. 6135-6138 (1995).

84. Yi, G.S. and Chow, G.M., Synthesis of Hexagonal-Phase NaYF₄:Yb,Er and NaYF₄:Yb,Tm Nanocrystals with Efficient Up-Conversion Fluorescence. *Advanced Functional Materials*. **16**(18): p. 2324-2329 (2006).

85. Ostrowski, A.D., Chan, E.M., Gargas, D.J., Katz, E.M., Han, G., Schuck, P.J., Milliron, D.J., and Cohen, B.E., Controlled Synthesis and Single-Particle Imaging of Bright, Sub-10 nm Lanthanide-Doped Upconverting Nanocrystals. *ACS Nano*. **6**(3): p. 2686-2692 (2012).

86. Ma, C., Xu, X., Wang, F., Zhou, Z., Wen, S., Liu, D., Fang, J., Lang, C.I., and Jin, D., Probing the Interior Crystal Quality in the Development of More Efficient and Smaller Upconversion Nanoparticles. *The Journal of Physical Chemistry Letters*. **7**(16): p. 3252-3258 (2016).

87. Wang, F., Han, Y., Lim, C.S., Lu, Y., Wang, J., Xu, J., Chen, H., Zhang, C., Hong, M., and Liu, X., Simultaneous phase and size control of upconversion nanocrystals through lanthanide doping. *Nature*. **463**: p. 1061 (2010).

88. Noculak, A., Podhorodecki, A., Pawlik, G., Banski, M., and Misiewicz, J., Ion–ion interactions in β-NaGdF₄:Yb³⁺,Er³⁺ nanocrystals – the effect of ion concentration and their clustering. *Nanoscale*. **7**(32): p. 13784-13792 (2015).

89. Sui, Y., Tao, K., Tian, Q., and Sun, K., Interaction Between Y³⁺ and Oleate Ions for the Cubic-to-Hexagonal Phase Transformation of NaYF₄ Nanocrystals. *The Journal of Physical Chemistry C*. **116**(2): p. 1732-1739 (2012).

90. Jingning, S. and Yiguang, J., A single-step synthesis and the kinetic mechanism for monodisperse and hexagonal-phase NaYF₄:Yb, Er upconversion nanophosphors. *Nanotechnology*. **20**(27): p. 275603 (2009).

91. Chan, E.M., Xu, C., Mao, A.W., Han, G., Owen, J.S., Cohen, B.E., and Milliron, D.J., Reproducible, High-Throughput Synthesis of Colloidal Nanocrystals for Optimization in Multidimensional Parameter Space. *Nano Letters*. **10**(5): p. 1874-1885 (2010).

92. Na, H., Woo, K., Lim, K., and Jang, H.S., Rational morphology control of β-NaYF₄: Yb, Er/Tm upconversion nanophosphors using a ligand, an additive, and lanthanide doping. *Nanoscale*. **5**(10): p. 4242-4251 (2013).

93. Li, D., Lai, W.-Y., Shao, Q., and Huang, W., A facile methodology for regulating the size of hexagonal NaYF₄:Yb³⁺,Er³⁺ upconversion nanocrystals. *New Journal of Chemistry*. **41**(20): p. 11521-11524 (2017).

94. Palo, E., Tuomisto, M., Hyppänen, I., Swart, H.C., Hölsä, J., Soukka, T., and Lastusaari, M., Highly uniform up-converting nanoparticles: Why you should control your synthesis even more. *Journal of Luminescence*. **185**: p. 125-131 (2017).

95. Resch-Genger, U. and Gorris, H.H., Perspectives and challenges of photon-upconversion nanoparticles - Part I: routes to brighter particles and quantitative spectroscopic studies. *Analytical and Bioanalytical Chemistry*. **409**(25): p. 5855-5874 (2017).

96. Dong, C., Pichaandi, J., Regier, T., and van Veggel, F.C.J.M., Nonstatistical Dopant Distribution of Ln³⁺-Doped NaGdF₄ Nanoparticles. *The Journal of Physical Chemistry C*. **115**(32): p. 15950-15958 (2011).

97. Xu, X., Clarke, C., Ma, C., Casillas, G., Das, M., Guan, M., Liu, D., Wang, L., Tadich, A., Du, Y., Ton-That, C., and Jin, D., Depth-profiling of Yb³⁺ sensitizer ions in NaYF₄ upconversion nanoparticles. *Nanoscale*. **9**(23): p. 7719-7726 (2017).

98. Li, X., Wang, R., Zhang, F., and Zhao, D., Engineering Homogeneous Doping in Single Nanoparticle To Enhance Upconversion Efficiency. *Nano Letters*. **14**(6): p. 3634-3639 (2014).

99. Prorok, K., Bednarkiewicz, A., Cichy, B., Gnach, A., Misiak, M., Sobczyk, M., and Strek, W., The impact of shell host (NaYF₄/CaF₂) and shell deposition methods on the up-conversion enhancement in Tb³⁺, Yb³⁺ codoped colloidal α-NaYF₄ core–shell

nanoparticles. *Nanoscale*. **6**(3): p. 1855-1864 (2014).

100. Wang, F., Wang, J., and Liu, X., Direct Evidence of a Surface Quenching Effect on Size-Dependent Luminescence of Upconversion Nanoparticles. *Angewandte Chemie International Edition*. **49**(41): p. 7456-7460 (2010).

101. Chen, G., Ågren, H., Ohulchanskyy, T.Y., and Prasad, P.N., Light upconverting core–shell nanostructures: nanophotonic control for emerging applications. *Chemical Society Reviews*. **44**(6): p. 1680-1713 (2015).

102. Boyer, J.-C., Gagnon, J., Cuccia, L.A., and Capobianco, J.A., Synthesis, Characterization, and Spectroscopy of NaGdF$_4$: Ce^{3+}, Tb^{3+}/NaYF$_4$ Core/Shell Nanoparticles. *Chemistry of Materials*. **19**(14): p. 3358-3360 (2007).

103. Johnson, N.J.J., Korinek, A., Dong, C., and van Veggel, F.C.J.M., Self-Focusing by Ostwald Ripening: A Strategy for Layer-by-Layer Epitaxial Growth on Upconverting Nanocrystals. *Journal of the American Chemical Society*. **134**(27): p. 11068-11071 (2012).

104. Dong, C., Korinek, A., Blasiak, B., Tomanek, B., and van Veggel, F.C.J.M., Cation Exchange: A Facile Method To Make NaYF$_4$:Yb,Tm-NaGdF$_4$ Core–Shell Nanoparticles with a Thin, Tunable, and Uniform Shell. *Chemistry of Materials*. **24**(7): p. 1297-1305 (2012).

105. Dong, C. and van Veggel, F.C.J.M., Cation Exchange in Lanthanide Fluoride Nanoparticles. *ACS Nano*. **3**(1): p. 123-130 (2009).

106. Dühnen, S. and Haase, M., Study on the Intermixing of Core and Shell in NaEuF$_4$/NaGdF$_4$ Core/Shell Nanocrystals. *Chemistry of Materials*. **27**(24): p. 8375-8386 (2015).

107. Hudry, D., Busko, D., Popescu, R., Gerthsen, D., Abeykoon, A.M.M., Kübel, C., Bergfeldt, T., and Richards, B.S., Direct Evidence of Significant Cation Intermixing in Upconverting Core@Shell Nanocrystals: Toward a New Crystallochemical Model.

Chemistry of Materials. **29**(21): p. 9238-9246 (2017).

108. Qiu, H., Chen, G., Sun, L., Hao, S., Han, G., and Yang, C., Ethylenediaminetetraacetic acid (EDTA)-controlled synthesis of multicolor lanthanide doped BaYF$_5$ upconversion nanocrystals. *Journal of Materials Chemistry*. **21**(43): p. 17202-17208 (2011).

109. Wang, L., Zhang, Y., and Zhu, Y., One-pot synthesis and strong near-infrared upconversion luminescence of poly(acrylic acid)-functionalized YF$_3$:Yb^{3+}/Er^{3+} nanocrystals. *Nano Research*. **3**(5): p. 317-325 (2010).

110. Feng, W., Dev, K.C., Zhengquan, L., Yong, Z., Xianping, F., and Minquan, W., Synthesis of polyethylenimine/NaYF$_4$ nanoparticles with upconversion fluorescence. *Nanotechnology*. **17**(23): p. 5786 (2006).

111. Sedlmeier, A. and Gorris, H.H., Surface modification and characterization of photon-upconverting nanoparticles for bioanalytical applications. *Chemical Society Reviews*. **44**(6): p. 1526-1560 (2015).

112. Chen, Z., Chen, H., Hu, H., Yu, M., Li, F., Zhang, Q., Zhou, Z., Yi, T., and Huang, C., Versatile Synthesis Strategy for Carboxylic Acid−functionalized Upconverting Nanophosphors as Biological Labels. *Journal of the American Chemical Society*. **130**(10): p. 3023-3029 (2008).

113. Zhou, H.-P., Xu, C.-H., Sun, W., and Yan, C.-H., Clean and Flexible Modification Strategy for Carboxyl/Aldehyde-Functionalized Upconversion Nanoparticles and Their Optical Applications. *Advanced Functional Materials*. **19**(24): p. 3892-3900 (2009).

114. Wang, L., Yan, R., Huo, Z., Wang, L., Zeng, J., Bao, J., Wang, X., Peng, Q., and Li, Y., Fluorescence Resonant Energy Transfer Biosensor Based on Upconversion-Luminescent Nanoparticles. *Angewandte Chemie International Edition*. **44**(37): p. 6054-6057 (2005).

115. Decher, G., Fuzzy Nanoassemblies: Toward Layered Polymeric Multicomposites. *Science*. **277**(5330): p. 1232 (1997).

116. Zhang, Q., Song, K., Zhao, J., Kong, X., Sun, Y., Liu, X., Zhang, Y., Zeng, Q., and Zhang, H., Hexanedioic acid mediated surface–ligand-exchange process for transferring NaYF$_4$:Yb/Er (or Yb/Tm) up-converting nanoparticles from hydrophobic to hydrophilic. *Journal of Colloid and Interface Science*. **336**(1): p. 171-175 (2009).

117. Kong, W., Sun, T., Chen, B., Chen, X., Ai, F., Zhu, X., Li, M., Zhang, W., Zhu, G., and Wang, F., A General Strategy for Ligand Exchange on Upconversion Nanoparticles. *Inorganic Chemistry*. **56**(2): p. 872-877 (2017).

118. Bogdan, N., Vetrone, F., Ozin, G.A., and Capobianco, J.A., Synthesis of Ligand-Free Colloidally Stable Water Dispersible Brightly Luminescent Lanthanide-Doped Upconverting Nanoparticles. *Nano Letters*. **11**(2): p. 835-840 (2011).

119. Dong, A., Ye, X., Chen, J., Kang, Y., Gordon, T., Kikkawa, J.M., and Murray, C.B., A Generalized Ligand-Exchange Strategy Enabling Sequential Surface Functionalization of Colloidal Nanocrystals. *Journal of the American Chemical Society*. **133**(4): p. 998-1006 (2011).

120. Wilhelm, S., Kaiser, M., Würth, C., Heiland, J., Carrillo-Carrion, C., Muhr, V., Wolfbeis, O.S., Parak, W.J., Resch-Genger, U., and Hirsch, T., Water dispersible upconverting nanoparticles: effects of surface modification on their luminescence and colloidal stability. *Nanoscale*. **7**(4): p. 1403-1410 (2015).

121. Jiang, G., Pichaandi, J., Johnson, N.J.J., Burke, R.D., and van Veggel, F.C.J.M., An Effective Polymer Cross-Linking Strategy To Obtain Stable Dispersions of Upconverting NaYF$_4$ Nanoparticles in Buffers and Biological Growth Media for Biolabeling Applications. *Langmuir*. **28**(6): p. 3239-3247 (2012).

122. Pichaandi, J., Boyer, J.-C., Delaney, K.R., and van Veggel, F.C.J.M., Two-Photon Upconversion Laser (Scanning and Wide-Field) Microscopy Using Ln^{3+}-Doped NaYF$_4$ Upconverting Nanocrystals: A Critical Evaluation of their Performance and Potential in Bioimaging. *The Journal of Physical Chemistry C*. **115**(39): p. 19054-19064 (2011).

123. Cheng, L., Yang, K., Zhang, S., Shao, M., Lee, S., and Liu, Z., Highly-sensitive multiplexed in vivo imaging using pegylated upconversion nanoparticles. *Nano Research*. **3**(10): p. 722-732 (2010).

124. Nsubuga, A., Sgarzi, M., Zarschler, K., Kubeil, M., Hübner, R., Steudtner, R., Graham, B., Joshi, T., and Stephan, H., Facile preparation of multifunctionalisable 'stealth' upconverting nanoparticles for biomedical applications. *Dalton Transactions*. **47**(26): p. 8595-8604 (2018).

125. Kuningas, K., Rantanen, T., Karhunen, U., Lövgren, T., and Soukka, T., Simultaneous Use of Time-Resolved Fluorescence and Anti-Stokes Photoluminescence in a Bioaffinity Assay. *Analytical Chemistry*. **77**(9): p. 2826-2834 (2005).

126. Mader, H.S., Link, M., Achatz, D.E., Uhlmann, K., Li, X., and Wolfbeis, O.S., Surface-Modified Upconverting Microparticles and Nanoparticles for Use in Click Chemistries. *Chemistry – A European Journal*. **16**(18): p. 5416-5424 (2010).

127. Zijlmans, H.J.M.A.A., Bonnet, J., Burton, J., Kardos, K., Vail, T., Niedbala, R.S., and Tanke, H.J., Detection of Cell and Tissue Surface Antigens Using Up-Converting Phosphors: A New Reporter Technology. *Analytical Biochemistry*. **267**(1): p. 30-36 (1999).

128. Boyer, J.-C. and van Veggel, F.C.J.M., Absolute quantum yield measurements of colloidal NaYF$_4$: Er^{3+}, Yb^{3+} upconverting nanoparticles. *Nanoscale*. **2**(8): p. 1417-1419 (2010).

129. Xue, X., Uechi, S., Tiwari, R.N., Duan, Z., Liao, M., Yoshimura, M., Suzuki, T., and Ohishi, Y., Size-dependent upconversion luminescence and quenching mechanism of LiYF$_4$: Er^{3+}/Yb^{3+} nanocrystals with oleate ligand adsorbed. *Optical Materials Express*. **3**(7): p. 989-999 (2013).

130. Xu, C.T., Zhan, Q., Liu, H., Somesfalean, G., Qian, J., He, S., and Andersson-Engels, S., Upconverting nanoparticles for pre-clinical diffuse optical imaging, microscopy and

sensing: Current trends and future challenges. *Laser & Photonics Reviews*. **7**(5): p. 663-697 (2013).

131. Kaiser, M., Würth, C., Kraft, M., Hyppänen, I., Soukka, T., and Resch-Genger, U., Power-dependent upconversion quantum yield of $NaYF_4:Yb^{3+},Er^{3+}$ nano- and micrometer-sized particles – measurements and simulations. *Nanoscale*. **9**(28): p. 10051-10058 (2017).

132. Shan, J., Uddi, M., Yao, N., and Ju, Y., Anomalous Raman Scattering of Colloidal Yb^{3+},Er^{3+} Codoped $NaYF_4$ Nanophosphors and Dynamic Probing of the Upconversion Luminescence. *Advanced Functional Materials*. **20**(20): p. 3530-3537 (2010).

133. Zhao, J., Lu, Z., Yin, Y., McRae, C., Piper, J.A., Dawes, J.M., Jin, D., and Goldys, E.M., Upconversion luminescence with tunable lifetime in $NaYF_4:Yb,Er$ nanocrystals: role of nanocrystal size. *Nanoscale*. **5**(3): p. 944-952 (2013).

134. Fischer, S., Johnson, N.J.J., Pichaandi, J., Goldschmidt, J.C., and Veggel, F.C.J.M.v., Upconverting core-shell nanocrystals with high quantum yield under low irradiance: On the role of isotropic and thick shells. *Journal of Applied Physics*. **118**(19): p. 193105 (2015).

135. Gargas, D.J., Chan, E.M., Ostrowski, A.D., Aloni, S., Altoe, M.V.P., Barnard, E.S., Sanii, B., Urban, J.J., Milliron, D.J., Cohen, B.E., and Schuck, P.J., Engineering bright sub-10-nm upconverting nanocrystals for single-molecule imaging. *Nature Nanotechnology*. **9**: p. 300 (2014).

136. Hossan, M.Y., Hor, A., Luu, Q., Smith, S.J., May, P.S., and Berry, M.T., Explaining the Nanoscale Effect in the Upconversion Dynamics of β-$NaYF_4:Yb^{3+}$, Er^{3+} Core and Core–Shell Nanocrystals. *The Journal of Physical Chemistry C*. **121**(30): p. 16592-16606 (2017).

137. Kraft, M., Würth, C., Muhr, V., Hirsch, T., and Resch-Genger, U., Particle-size-dependent upconversion luminescence of $NaYF_4$: Yb, Er nanoparticles in organic solvents and water at different excitation power densities. *Nano Research*, (2018).

138. Cong, T., Ding, Y., Xin, S., Hong, X., Zhang, H., and Liu, Y., Solvent-Induced Luminescence Variation of Upconversion Nanoparticles. *Langmuir*. **32**(49): p. 13200-13206 (2016).

139. Quintanilla, M., Cantarelli, I.X., Pedroni, M., Speghini, A., and Vetrone, F., Intense ultraviolet upconversion in water dispersible $SrF_2:Tm^{3+},Yb^{3+}$ nanoparticles: the effect of the environment on light emissions. *Journal of Materials Chemistry C*. **3**(13): p. 3108-3113 (2015).

140. Boyer, J.-C., Manseau, M.-P., Murray, J.I., and van Veggel, F.C.J.M., Surface Modification of Upconverting $NaYF_4$ Nanoparticles with PEG−Phosphate Ligands for NIR (800 nm) Biolabeling within the Biological Window. *Langmuir*. **26**(2): p. 1157-1164 (2010).

141. Lappi, S.E., Smith, B., and Franzen, S., Infrared spectra of $H_2^{16}O$, $H_2^{18}O$ and D_2O in the liquid phase by single-pass attenuated total internal reflection spectroscopy. *Spectrochimica Acta Part A: Molecular and Biomolecular Spectroscopy*. **60**(11): p. 2611-2619 (2004).

142. Arppe, R., Hyppänen, I., Perälä, N., Peltomaa, R., Kaiser, M., Würth, C., Christ, S., Resch-Genger, U., Schäferling, M., and Soukka, T., Quenching of the upconversion luminescence of $NaYF_4:Yb^{3+},Er^{3+}$ and $NaYF_4:Yb^{3+},Tm^{3+}$ nanophosphors by water: the role of the sensitizer Yb^{3+} in non-radiative relaxation. *Nanoscale*. **7**(27): p. 11746-11757 (2015).

143. Huang, B., Bergstrand, J., Duan, S., Zhan, Q., Widengren, J., Ågren, H., and Liu, H., Overtone Vibrational Transition-Induced Lanthanide Excited-State Quenching in Yb^{3+}/Er^{3+}-Doped Upconversion Nanocrystals. *ACS Nano*. **12**(11): p. 10572-10575 (2018).

144. Rabouw, F.T., Prins, P.T., Villanueva-Delgado, P., Castelijns, M., Geitenbeek, R.G., and Meijerink, A., Quenching Pathways in $NaYF_4:Er^{3+},Yb^{3+}$ Upconversion Nanocrystals. *ACS Nano*. **12**(5): p. 4812-4823 (2018).

145. Rabouw, F.T., Prins, P.T., Villanueva-Delgado, P., Castelijns, M., Geitenbeek, R.G., and Meijerink, A., Reply to "Overtone Vibrational Transition-Induced Lanthanide Excited-State Quenching in Yb^{3+}/Er^{3+}-Doped Upconversion Nanocrystals". *ACS Nano*. **12**(11): p. 10576-10577 (2018).

146. Guo, S., Xie, X., Huang, L., and Huang, W., Sensitive Water Probing through Nonlinear Photon Upconversion of Lanthanide-Doped Nanoparticles. *ACS Applied Materials & Interfaces*. **8**(1): p. 847-853 (2016).

147. Hyppänen, I., Höysniemi, N., Arppe, R., Schäferling, M., and Soukka, T., Environmental Impact on the Excitation Path of the Red Upconversion Emission of Nanocrystalline $NaYF_4:Yb^{3+},Er^{3+}$. *The Journal of Physical Chemistry C*. **121**(12): p. 6924-6929 (2017).

148. Bednarkiewicz, A., Nyk, M., Samoc, M., and Strek, W., Up-conversion FRET from $Er^{3+}/Yb^{3+}:NaYF_4$ Nanophosphor to CdSe Quantum Dots. *The Journal of Physical Chemistry C*. **114**(41): p. 17535-17541 (2010).

149. Jung, T., Jo, H.L., Nam, S.H., Yoo, B., Cho, Y., Kim, J., Kim, H.M., Hyeon, T., Suh, Y.D., Lee, H., and Lee, K.T., The preferred upconversion pathway for the red emission of lanthanide-doped upconverting nanoparticles, $NaYF_4:Yb^{3+},Er^{3+}$. *Physical Chemistry Chemical Physics*. **17**(20): p. 13201-13205 (2015).

150. Shin, K., Jung, T., Lee, E., Lee, G., Goh, Y., Heo, J., Jung, M., Jo, E.-J., Lee, H., Kim, M.-G., and Lee, K.T., Distinct mechanisms for the upconversion of $NaYF_4:Yb^{3+},Er^{3+}$ nanoparticles revealed by stimulated emission depletion. *Physical Chemistry Chemical Physics*. **19**(15): p. 9739-9744 (2017).

151. Anderson, R.B., Smith, S.J., May, P.S., and Berry, M.T., Revisiting the NIR-to-Visible Upconversion Mechanism in β-$NaYF_4:Yb^{3+},Er^{3+}$. *The Journal of Physical Chemistry Letters*. **5**(1): p. 36-42 (2014).

152. Berry, M.T. and May, P.S., Disputed Mechanism for NIR-to-Red Upconversion Luminescence in $NaYF_4:Yb^{3+},Er^{3+}$. *The Journal of Physical Chemistry A*. **119**(38): p. 9805-9811 (2015).

153. Würth, C., Kaiser, M., Wilhelm, S., Grauel, B., Hirsch, T., and Resch-Genger, U., Excitation power dependent population pathways and absolute quantum yields of upconversion nanoparticles in different solvents. *Nanoscale*. **9**(12): p. 4283-4294 (2017).

154. Wang, Y.-F., Sun, L.-D., Xiao, J.-W., Feng, W., Zhou, J.-C., Shen, J., and Yan, C.-H., Rare-Earth Nanoparticles with Enhanced Upconversion Emission and Suppressed Rare-Earth-Ion Leakage. *Chemistry – A European Journal*. **18**(18): p. 5558-5564 (2012).

155. Lisjak, D., Plohl, O., Ponikvar-Svet, M., and Majaron, B., Dissolution of upconverting fluoride nanoparticles in aqueous suspensions. *RSC Advances*. **5**(35): p. 27393-27397 (2015).

156. Plohl, O., Kraft, M., Kovač, J., Belec, B., Ponikvar-Svet, M., Würth, C., Lisjak, D., and Resch-Genger, U., Optically Detected Degradation of $NaYF_4:Yb,Tm$-Based Upconversion Nanoparticles in Phosphate Buffered Saline Solution. *Langmuir*. **33**(2): p. 553-560 (2017).

157. Lisjak, D., Plohl, O., Vidmar, J., Majaron, B., and Ponikvar-Svet, M., Dissolution Mechanism of Upconverting $AYF_4:Yb,Tm$ (A = Na or K) Nanoparticles in Aqueous Media. *Langmuir*. **32**(32): p. 8222-8229 (2016).

158. Li, R., Ji, Z., Dong, J., Chang, C.H., Wang, X., Sun, B., Wang, M., Liao, Y.-P., Zink, J.I., Nel, A.E., and Xia, T., Enhancing the Imaging and Biosafety of Upconversion Nanoparticles through Phosphonate Coating. *ACS Nano*. **9**(3): p. 3293-3306 (2015).

159. Dukhno, O., Przybilla, F., Muhr, V., Buchner, M., Hirsch, T., and Mély, Y., Time-dependent luminescence loss for individual upconversion nanoparticles upon dilution in aqueous solution. *Nanoscale*. **10**(34): p. 15904-15910 (2018).

160. Wang, Y., Tu, L., Zhao, J., Sun, Y., Kong, X., and Zhang, H., Upconversion Luminescence of β-$NaYF_4$: Yb^{3+}, Er^{3+}@β-$NaYF_4$

Core/Shell Nanoparticles: Excitation Power Density and Surface Dependence. *The Journal of Physical Chemistry C*. **113**(17): p. 7164-7169 (2009).

161. Li, D., Liu, X., and Qiu, J., Probing Interaction Distance of Surface Quenchers in Lanthanide-Doped Upconversion Core–Shell Nanoparticles. *The Journal of Physical Chemistry C*. **122**(18): p. 10278-10283 (2018).

162. Würth, C., Fischer, S., Grauel, B., Alivisatos, A.P., and Resch-Genger, U., Quantum Yields, Surface Quenching, and Passivation Efficiency for Ultrasmall Core/Shell Upconverting Nanoparticles. *Journal of the American Chemical Society*. **140**(14): p. 4922-4928 (2018).

163. Homann, C., Krukewitt, L., Frenzel, F., Grauel, B., Würth, C., Resch-Genger, U., and Haase, M., NaYF$_4$:Yb,Er/NaYF$_4$ Core/Shell Nanocrystals with High Upconversion Luminescence Quantum Yield. *Angewandte Chemie International Edition*. **57**(28): p. 8765-8769 (2018).

164. Plohl, O., Kralj, S., Majaron, B., Fröhlich, E., Ponikvar-Svet, M., Makovec, D., and Lisjak, D., Amphiphilic coatings for the protection of upconverting nanoparticles against dissolution in aqueous media. *Dalton Transactions*. **46**(21): p. 6975-6984 (2017).

165. Palo, E., Lahtinen, S., Päkkilä, H., Salomäki, M., Soukka, T., and Lastusaari, M., Effective Shielding of NaYF$_4$:Yb^{3+},Er^{3+} Upconverting Nanoparticles in Aqueous Environments Using Layer-by-Layer Assembly. *Langmuir*. **34**(26): p. 7759-7766 (2018).

166. Palo, E., Salomäki, M., and Lastusaari, M., Restraining fluoride loss from NaYF$_4$:Yb^{3+},Er^{3+} upconverting nanoparticles in aqueous environments using crosslinked poly(acrylic acid)/poly(allylamine hydrochloride) multilayers. *Journal of Colloid and Interface Science*. **538**: p. 320-326 (2019).

167. Estebanez, N., González-Béjar, M., and Pérez-Prieto, J., Polysulfonate Cappings on Upconversion Nanoparticles Prevent Their Disintegration in Water and Provide Superior Stability in a Highly Acidic Medium. *ACS Omega*. **4**(2): p. 3012-3019 (2019).

168. Wang, X., Kong, X., Yu, Y., Sun, Y., and Zhang, H., Effect of Annealing on Upconversion Luminescence of ZnO:Er^{3+} Nanocrystals and High Thermal Sensitivity. *The Journal of Physical Chemistry C*. **111**(41): p. 15119-15124 (2007).

169. Jaque, D., Maestro, L.M., Escudero, E., Rodríguez, E.M., Capobianco, J.A., Vetrone, F., Juarranz de la Fuente, A., Sanz-Rodríguez, F., Iglesias-de la Cruz, M.C., Jacinto, C., Rocha, U., and García Solé, J., Fluorescent nano-particles for multi-photon thermal sensing. *Journal of Luminescence*. **133**: p. 249-253 (2013).

70. Sedlmeier, A., Achatz, D.E., Fischer, L.H., Gorris, H.H., and Wolfbeis, O.S., Photon upconverting nanoparticles for luminescent sensing of temperature. *Nanoscale*. **4**(22): p. 7090-7096 (2012).

171. Vetrone, F., Naccache, R., Zamarrón, A., Juarranz de la Fuente, A., Sanz-Rodríguez, F., Martinez Maestro, L., Martín Rodriguez, E., Jaque, D., García Solé, J., and Capobianco, J.A., Temperature Sensing Using Fluorescent Nanothermometers. *ACS Nano*. **4**(6): p. 3254-3258 (2010).

172. Singh, S.K., Kumar, K., and Rai, S.B., Er^{3+}/Yb^{3+} codoped Gd$_2$O$_3$ nano-phosphor for optical thermometry. *Sensors and Actuators A: Physical*. **149**(1): p. 16-20 (2009).

173. Dong, B., Liu, D.P., Wang, X.J., Yang, T., Miao, S.M., and Li, C.R., Optical thermometry through infrared excited green upconversion emissions in Er^{3+}–Yb^{3+} codoped Al$_2$O$_3$. *Applied Physics Letters*. **90**(18): p. 181117 (2007).

174. Marciniak, L., Prorok, K., Francés-Soriano, L., Pérez-Prieto, J., and Bednarkiewicz, A., A broadening temperature sensitivity range with a core–shell YbEr@YbNd double ratiometric optical nanothermometer. *Nanoscale*. **8**(9): p. 5037-5042 (2016).

175. Singh, A.K., Shahi, P.K., Rai, S.B., and Ullrich, B., Host matrix impact on Er^{3+} upconversion emission and its temperature dependence. *RSC Advances*. **5**(21): p. 16067-16073 (2015).

176. Hyppänen, I., Perälä, N., Arppe, R., Schäferling, M., and Soukka, T., Environmental and Excitation Power Effects on the Ratiometric Upconversion Luminescence Based Temperature Sensing Using Nanocrystalline $NaYF_4:Yb^{3+},Er^{3+}$. *ChemPhysChem*. **18**(6): p. 692-701 (2017).

177. Saleh, S.M., Ali, R., and Wolfbeis, O.S., Quenching of the Luminescence of Upconverting Luminescent Nanoparticles by Heavy Metal Ions. *Chemistry – A European Journal*. **17**(51): p. 14611-14617 (2011).

178. Christ, S. and Schäferling, M., Chemical sensing and imaging based on photon upconverting nano- and microcrystals: a review. *Methods and Applications in Fluorescence*. **3**(3): p. 034004 (2015).

179. Heyduk, T. and Heyduk, E., Luminescence Energy Transfer with Lanthanide Chelates: Interpretation of Sensitized Acceptor Decay Amplitudes. *Analytical Biochemistry*. **289**(1): p. 60-67 (2001).

180. Selvin, P.R., Lanthanide-based resonance energy transfer. *IEEE Journal of Selected Topics in Quantum Electronics*. **2**(4): p. 1077-1087 (1996).

181. Stryer, L., Fluorescence Energy Transfer as a Spectroscopic Ruler. *Annual Review of Biochemistry*. **47**(1): p. 819-846 (1978).

182. Ray, P.C., Fan, Z., Crouch, R.A., Sinha, S.S., and Pramanik, A., Nanoscopic optical rulers beyond the FRET distance limit: fundamentals and applications. *Chemical Society Reviews*. **43**(17): p. 6370-6404 (2014).

183. Bill, A., Blockus, H., Stumpfe, D., Bajorath, J., Schmitz, A., and Famulok, M., A Homogeneous Fluorescence Resonance Energy Transfer System for Monitoring the Activation of a Protein Switch in Real Time. *Journal of the American Chemical Society*. **133**(21): p. 8372-8379 (2011).

184. Ohiro, Y., Ueda, H., Shibata, N., and Nagamune, T., Development of a homogeneous competitive immunoassay for phosphorylated protein antigen based on the enhanced fluorescence resonance energy transfer technology. *Journal of Bioscience and Bioengineering*. **109**(1): p. 15-19 (2010).

185. Vardar-Schara, G., Krab, I.M., Yi, G., and Su, W.W., A homogeneous fluorometric assay platform based on novel synthetic proteins. *Biochemical and Biophysical Research Communications*. **361**(1): p. 103-108 (2007).

186. Sapsford, K.E., Berti, L., and Medintz, I.L., Materials for Fluorescence Resonance Energy Transfer Analysis: Beyond Traditional Donor–Acceptor Combinations. *Angewandte Chemie International Edition*. **45**(28): p. 4562-4589 (2006).

187. Day, R.N. and Davidson, M.W., Fluorescent proteins for FRET microscopy: Monitoring protein interactions in living cells. *BioEssays*. **34**(5): p. 341-350 (2012).

188. Moore, E.G., Xu, J., Jocher, C.J., Corneillie, T.M., and Raymond, K.N., Eu(III) Complexes of Functionalized Octadentate 1-Hydroxypyridin-2-ones: Stability, Bioconjugation, and Luminescence Resonance Energy Transfer Studies. *Inorganic Chemistry*. **49**(21): p. 9928-9939 (2010).

189. Tu, D., Liu, L., Ju, Q., Liu, Y., Zhu, H., Li, R., and Chen, X., Time-Resolved FRET Biosensor Based on Amine-Functionalized Lanthanide-Doped $NaYF_4$ Nanocrystals. *Angewandte Chemie International Edition*. **50**(28): p. 6306-6310 (2011).

190. Kokko, L., Kokko, T., Lövgren, T., and Soukka, T., Particulate and soluble Eu(III)-chelates as donor labels in homogeneous fluorescence resonance energy transfer based immunoassay. *Analytica Chimica Acta*. **606**(1): p. 72-79 (2008).

191. Kuningas, K., Päkkilä, H., Ukonaho, T., Rantanen, T., Lövgren, T., and Soukka, T., Upconversion Fluorescence Enables Homogeneous Immunoassay in Whole Blood. *Clinical Chemistry*. **53**(1): p. 145-146 (2007).

192. Li, Z., Zhang, Y., and Jiang, S., Multicolor Core/Shell-Structured Upconversion Fluorescent Nanoparticles. *Advanced Materials*. **20**(24): p. 4765-4769 (2008).

193. Yan, C., Dadvand, A., Rosei, F., and Perepichka, D.F., Near-IR Photoresponse in New Up-Converting CdSe/NaYF4:Yb,Er Nanoheterostructures. *Journal of the*

American Chemical Society. **132**(26): p. 8868-8869 (2010).

194. Doughan, S., Han, Y., Uddayasankar, U., and Krull, U.J., Solid-Phase Covalent Immobilization of Upconverting Nanoparticles for Biosensing by Luminescence Resonance Energy Transfer. *ACS Applied Materials & Interfaces*. **6**(16): p. 14061-14068 (2014).

195. Cui, S., Xu, S., Song, H., Xu, W., Chen, X., Zhou, D., Yin, Z., and Han, W., Highly sensitive and selective detection of mercury ions based on up-conversion FRET from NaYF$_4$:Yb^{3+}/Er^{3+} nanophosphors to CdTe quantum dots. *RSC Advances*. **5**(120): p. 99099-99106 (2015).

196. Mattsson, L., Wegner, K.D., Hildebrandt, N., and Soukka, T., Upconverting nanoparticle to quantum dot FRET for homogeneous double-nano biosensors. *RSC Advances*. **5**(18): p. 13270-13277 (2015).

197. Doughan, S., Uddayasankar, U., Peri, A., and Krull, U.J., A paper-based multiplexed resonance energy transfer nucleic acid hybridization assay using a single form of upconversion nanoparticle as donor and three quantum dots as acceptors. *Analytica Chimica Acta*. **962**: p. 88-96 (2017).

198. Jesu Raj, J.G., Quintanilla, M., Mahmoud, K.A., Ng, A., Vetrone, F., and Zourob, M., Sensitive Detection of ssDNA Using an LRET-Based Upconverting Nanohybrid Material. *ACS Applied Materials & Interfaces*. **7**(33): p. 18257-18265 (2015).

199. Wu, M., Wang, X., Wang, K., and Guo, Z., An ultrasensitive fluorescent nanosensor for trypsin based on upconversion nanoparticles. *Talanta*. **174**: p. 797-802 (2017).

200. Wang, M., Hou, W., Mi, C.-C., Wang, W.-X., Xu, Z.-R., Teng, H.-H., Mao, C.-B., and Xu, S.-K., Immunoassay of Goat Antihuman Immunoglobulin G Antibody Based on Luminescence Resonance Energy Transfer between Near-Infrared Responsive NaYF$_4$:Yb, Er Upconversion Fluorescent Nanoparticles and Gold Nanoparticles. *Analytical Chemistry*. **81**(21): p. 8783-8789 (2009).

201. Li, X., Wei, L., Pan, L., Yi, Z., Wang, X., Ye, Z., Xiao, L., Li, H.-W., and Wang, J., Homogeneous Immunosorbent Assay Based on Single-Particle Enumeration Using Upconversion Nanoparticles for the Sensitive Detection of Cancer Biomarkers. *Analytical Chemistry*. **90**(7): p. 4807-4814 (2018).

202. Vilela, P., El-Sagheer, A., Millar, T.M., Brown, T., Muskens, O.L., and Kanaras, A.G., Graphene Oxide-Upconversion Nanoparticle Based Optical Sensors for Targeted Detection of mRNA Biomarkers Present in Alzheimer's Disease and Prostate Cancer. *ACS Sensors*. **2**(1): p. 52-56 (2017).

203. Alonso-Cristobal, P., Vilela, P., El-Sagheer, A., Lopez-Cabarcos, E., Brown, T., Muskens, O.L., Rubio-Retama, J., and Kanaras, A.G., Highly Sensitive DNA Sensor Based on Upconversion Nanoparticles and Graphene Oxide. *ACS Applied Materials & Interfaces*. **7**(23): p. 12422-12429 (2015).

204. Liu, C., Wang, Z., Jia, H., and Li, Z., Efficient fluorescence resonance energy transfer between upconversion nanophosphors and graphene oxide: a highly sensitive biosensing platform. *Chemical Communications*. **47**(16): p. 4661-4663 (2011).

205. Wang, Y., Shen, P., Li, C., Wang, Y., and Liu, Z., Upconversion Fluorescence Resonance Energy Transfer Based Biosensor for Ultrasensitive Detection of Matrix Metalloproteinase-2 in Blood. *Analytical Chemistry*. **84**(3): p. 1466-1473 (2012).

206. Wu, Z., Li, H., and Liu, Z., An aptasensor for carcinoembryonic antigen based on upconversion fluorescence resonance energy transfer. *Sensors and Actuators B: Chemical*. **206**: p. 531-537 (2015).

207. Bo, X., Zhou, M., and Guo, L., Electrochemical sensors and biosensors based on less aggregated graphene. *Biosensors and Bioelectronics*. **89**: p. 167-186 (2017).

208. Chen, H., Fang, A., Zhang, Y., and Yao, S., Silver triangular nanoplates as an high efficiently FRET donor-acceptor of upconversion nanoparticles for ultrasensitive "Turn on-off" protamine and trypsin sensor. *Talanta*. **174**: p. 148-155 (2017).

209. Si, B., Wang, Y., Lu, S., Liu, E., Hu, X., and Fan, J., Upconversion luminescence nanoprobe based on luminescence resonance energy transfer from NaYF4:Yb, Tm to Ag nanodisks. *RSC Advances*. **6**(95): p. 92428-92433 (2016).

210. Li, H., Shi, L., Sun, D.-e., Li, P., and Liu, Z., Fluorescence resonance energy transfer biosensor between upconverting nanoparticles and palladium nanoparticles for ultrasensitive CEA detection. *Biosensors and Bioelectronics*. **86**: p. 791-798 (2016).

211. Bhuckory, S., Hemmer, E., Wu, Y.-T., Yahia-Ammar, A., Vetrone, F., and Hildebrandt, N., Core or Shell? Er^{3+} FRET Donors in Upconversion Nanoparticles. *European Journal of Inorganic Chemistry*. **2017**(44): p. 5186-5195 (2017).

212. Melle, S., Calderón, O.G., Laurenti, M., Mendez-Gonzalez, D., Egatz-Gómez, A., López-Cabarcos, E., Cabrera-Granado, E., Díaz, E., and Rubio-Retama, J., Förster Resonance Energy Transfer Distance Dependence from Upconverting Nanoparticles to Quantum Dots. *The Journal of Physical Chemistry C*. **122**(32): p. 18751-18758 (2018).

213. Marin, R., Labrador-Paéz, L., Skripka, A., Haro-González, P., Benayas, A., Canton, P., Jaque, D., and Vetrone, F., Upconverting Nanoparticle to Quantum Dot Förster Resonance Energy Transfer: Increasing the Efficiency through Donor Design. *ACS Photonics*. **5**(6): p. 2261-2270 (2018).

214. Muhr, V., Würth, C., Kraft, M., Buchner, M., Baeumner, A.J., Resch-Genger, U., and Hirsch, T., Particle-Size-Dependent Förster Resonance Energy Transfer from Upconversion Nanoparticles to Organic Dyes. *Analytical Chemistry*. **89**(9): p. 4868-4874 (2017).

215. Dukhno, O., Przybilla, F., Collot, M., Klymchenko, A., Pivovarenko, V., Buchner, M., Muhr, V., Hirsch, T., and Mély, Y., Quantitative assessment of energy transfer in upconverting nanoparticles grafted with organic dyes. *Nanoscale*. **9**(33): p. 11994-12004 (2017).

216. Rantanen, T., Päkkilä, H., Jämsen, L., Kuningas, K., Ukonaho, T., Lövgren, T., and Soukka, T., Tandem Dye Acceptor Used To Enhance Upconversion Fluorescence Resonance Energy Transfer in Homogeneous Assays. *Analytical Chemistry*. **79**(16): p. 6312-6318 (2007).

217. Wang, Y., Liu, K., Liu, X., Dohnalová, K., Gregorkiewicz, T., Kong, X., Aalders, M.C.G., Buma, W.J., and Zhang, H., Critical Shell Thickness of Core/Shell Upconversion Luminescence Nanoplatform for FRET Application. *The Journal of Physical Chemistry Letters*. **2**(17): p. 2083-2088 (2011).

218. Huang, K., Liu, H., Kraft, M., Shikha, S., Zheng, X., Ågren, H., Würth, C., Resch-Genger, U., and Zhang, Y., A protected excitation-energy reservoir for efficient upconversion luminescence. *Nanoscale*. **10**(1): p. 250-259 (2018).

219. Li, Z., Lv, S., Wang, Y., Chen, S., and Liu, Z., Construction of LRET-Based Nanoprobe Using Upconversion Nanoparticles with Confined Emitters and Bared Surface as Luminophore. *Journal of the American Chemical Society*. **137**(9): p. 3421-3427 (2015).

220. Wang, C., Tao, H., Cheng, L., and Liu, Z., Near-infrared light induced in vivo photodynamic therapy of cancer based on upconversion nanoparticles. *Biomaterials*. **32**(26): p. 6145-6154 (2011).

221. Cui, S., Yin, D., Chen, Y., Di, Y., Chen, H., Ma, Y., Achilefu, S., and Gu, Y., In Vivo Targeted Deep-Tissue Photodynamic Therapy Based on Near-Infrared Light Triggered Upconversion Nanoconstruct. *ACS Nano*. **7**(1): p. 676-688 (2013).

222. Riuttamäki, T., Hyppänen, I., Kankare, J., and Soukka, T., Decrease in Luminescence Lifetime Indicating Nonradiative Energy Transfer from Upconverting Phosphors to Fluorescent Acceptors in Aqueous Suspensions. *The Journal of Physical Chemistry C*. **115**(36): p. 17736-17742 (2011).

223. Ding, Y., Wu, F., Zhang, Y., Liu, X., de Jong, E.M.L.D., Gregorkiewicz, T., Hong, X., Liu,

Y., Aalders, M.C.G., Buma, W.J., and Zhang, H., Interplay between Static and Dynamic Energy Transfer in Biofunctional Upconversion Nanoplatforms. *The Journal of Physical Chemistry Letters*. **6**(13): p. 2518-2523 (2015).

224. Alyatkin, S., Asharchuk, I., Khaydukov, K., Nechaev, A., Lebedev, O., Vainer, Y., Semchishen, V., and Khaydukov, E., The influence of energy migration on luminescence kinetics parameters in upconversion nanoparticles. *Nanotechnology*. **28**(3): p. 035401 (2016).

225. Ni, J., Shan, C., Li, B., Zhang, L., Ma, H., Luo, Y., and Song, H., Assembling of a functional cyclodextrin-decorated upconversion luminescence nanoplatform for cysteine-sensing. *Chemical Communications*. **51**(74): p. 14054-14056 (2015).

226. Peng, J., Xu, W., Teoh, C.L., Han, S., Kim, B., Samanta, A., Er, J.C., Wang, L., Yuan, L., Liu, X., and Chang, Y.-T., High-Efficiency in Vitro and in Vivo Detection of Zn^{2+} by Dye-Assembled Upconversion Nanoparticles. *Journal of the American Chemical Society*. **137**(6): p. 2336-2342 (2015).

227. Mendez-Gonzalez, D., Laurenti, M., Latorre, A., Somoza, A., Vazquez, A., Negredo, A.I., López-Cabarcos, E., Calderón, O.G., Melle, S., and Rubio-Retama, J., Oligonucleotide Sensor Based on Selective Capture of Upconversion Nanoparticles Triggered by Target-Induced DNA Interstrand Ligand Reaction. *ACS Applied Materials & Interfaces*. **9**(14): p. 12272-12281 (2017).

228. Farka, Z., Mickert, M.J., Hlaváček, A., Skládal, P., and Gorris, H.H., Single Molecule Upconversion-Linked Immunosorbent Assay with Extended Dynamic Range for the Sensitive Detection of Diagnostic Biomarkers. *Analytical Chemistry*. **89**(21): p. 11825-11830 (2017).

229. Rissin, D.M., Kan, C.W., Campbell, T.G., Howes, S.C., Fournier, D.R., Song, L., Piech, T., Patel, P.P., Chang, L., Rivnak, A.J., Ferrell, E.P., Randall, J.D., Provuncher, G.K., Walt, D.R., and Duffy, D.C., Single-molecule enzyme-linked immunosorbent assay detects serum proteins at subfemtomolar

concentrations. *Nature Biotechnology*. **28**: p. 595 (2010).

230. van de Rijke, F., Zijlmans, H., Li, S., Vail, T., Raap, A.K., Niedbala, R.S., and Tanke, H.J., Up-converting phosphor reporters for nucleic acid microarrays. *Nature Biotechnology*. **19**: p. 273 (2001).

231. Ylihärsilä, M., Valta, T., Karp, M., Hattara, L., Harju, E., Hölsä, J., Saviranta, P., Waris, M., and Soukka, T., Oligonucleotide Array-in-Well Platform for Detection and Genotyping Human Adenoviruses by Utilizing Upconverting Phosphor Label Technology. *Analytical Chemistry*. **83**(4): p. 1456-1461 (2011).

232. Ylihärsilä, M., Alaranta, S., Lahdenperä, S., Lahtinen, S., Arku, B., Hedman, K., Soukka, T., and Waris, M., Array-in-well serodiagnostic assay utilizing upconverting phosphor label technology. *Journal of Virological Methods*. **222**: p. 224-230 (2015).

233. Päkkilä, H., Ylihärsilä, M., Lahtinen, S., Hattara, L., Salminen, N., Arppe, R., Lastusaari, M., Saviranta, P., and Soukka, T., Quantitative Multianalyte Microarray Immunoassay Utilizing Upconverting Phosphor Technology. *Analytical Chemistry*. **84**(20): p. 8628-8634 (2012).

234. Kale, V., Päkkilä, H., Vainio, J., Ahomaa, A., Sirkka, N., Lyytikäinen, A., Talha, S.M., Kutsaya, A., Waris, M., Julkunen, I., and Soukka, T., Spectrally and Spatially Multiplexed Serological Array-in-Well Assay Utilizing Two-Color Upconversion Luminescence Imaging. *Analytical Chemistry*. **88**(8): p. 4470-4477 (2016).

235. Corstjens, P., Zuiderwijk, M., Brink, A., Li, S., Feindt, H., Niedbala, R.S., and Tanke, H., Use of Up-Converting Phosphor Reporters in Lateral-Flow Assays to Detect Specific Nucleic Acid Sequences: A Rapid, Sensitive DNA Test to Identify Human Papillomavirus Type 16 Infection. *Clinical Chemistry*. **47**(10): p. 1885-1893 (2001).

236. Kim, J., Kwon, J.H., Jang, J., Lee, H., Kim, S., Hahn, Y.K., Kim, S.K., Lee, K.H., Lee, S., Pyo, H., Song, C.-S., and Lee, J., Rapid and background-free detection of avian influenza virus in opaque sample using NIR-to-NIR

upconversion nanoparticle-based lateral flow immunoassay platform. *Biosensors and Bioelectronics*. **112**: p. 209-215 (2018).

237. Sedlmeier, A., Hlaváček, A., Birner, L., Mickert, M.J., Muhr, V., Hirsch, T., Corstjens, P.L.A.M., Tanke, H.J., Soukka, T., and Gorris, H.H., Highly Sensitive Laser Scanning of Photon-Upconverting Nanoparticles on a Macroscopic Scale. *Analytical Chemistry*. **88**(3): p. 1835-1841 (2016).

238. Corstjens, P.L.A.M., de Dood, C.J., Priest, J.W., Tanke, H.J., Handali, S., and and the Cysticercosis Working Group in, P., Feasibility of a Lateral Flow Test for Neurocysticercosis Using Novel Up-Converting Nanomaterials and a Lightweight Strip Analyzer. *PLOS Neglected Tropical Diseases*. **8**(7): p. e2944 (2014).

239. You, M., Lin, M., Gong, Y., Wang, S., Li, A., Ji, L., Zhao, H., Ling, K., Wen, T., Huang, Y., Gao, D., Ma, Q., Wang, T., Ma, A., Li, X., and Xu, F., Household Fluorescent Lateral Flow Strip Platform for Sensitive and Quantitative Prognosis of Heart Failure Using Dual-Color Upconversion Nanoparticles. *ACS Nano*. **11**(6): p. 6261-6270 (2017).

240. He, H., Liu, B., Wen, S., Liao, J., Lin, G., Zhou, J., and Jin, D., Quantitative Lateral Flow Strip Sensor Using Highly Doped Upconversion Nanoparticles. *Analytical Chemistry*. **90**(21): p. 12356-12360 (2018).

241. Juntunen, E., Arppe, R., Kalliomäki, L., Salminen, T., Talha, S.M., Myyryläinen, T., Soukka, T., and Pettersson, K., Effects of blood sample anticoagulants on lateral flow assays using luminescent photon-upconverting and Eu(III) nanoparticle reporters. *Analytical Biochemistry*. **492**: p. 13-20 (2016).

242. Choi, D.H., Lee, S.K., Oh, Y.K., Bae, B.W., Lee, S.D., Kim, S., Shin, Y.-B., and Kim, M.-G., A dual gold nanoparticle conjugate-based lateral flow assay (LFA) method for the analysis of troponin I. *Biosensors and Bioelectronics*. **25**(8): p. 1999-2002 (2010).

243. Jin, B., Yang, Y., He, R., Park, Y.I., Lee, A., Bai, D., Li, F., Lu, T.J., Xu, F., and Lin, M., Lateral flow aptamer assay integrated

smartphone-based portable device for simultaneous detection of multiple targets using upconversion nanoparticles. *Sensors and Actuators B: Chemical*. **276**: p. 48-56 (2018).

244. Mendez-Gonzalez, D., Lopez-Cabarcos, E., Rubio-Retama, J., and Laurenti, M., Sensors and bioassays powered by upconverting materials. *Advances in Colloid and Interface Science*. **249**: p. 66-87 (2017).

245. Himmelstoß, S.F. and Hirsch, T., A critical comparison of lanthanide based upconversion nanoparticles to fluorescent proteins, semiconductor quantum dots, and carbon dots for use in optical sensing and imaging. *Methods and Applications in Fluorescence*. **7**(2): p. 022002 (2019).

246. Gorris, H.H. and Resch-Genger, U., Perspectives and challenges of photon-upconversion nanoparticles - Part II: bioanalytical applications. *Analytical and Bioanalytical Chemistry*. **409**(25): p. 5875-5890 (2017).

247. Shan, J., Budijono, S.J., Hu, G., Yao, N., Kang, Y., Ju, Y., and Prud'homme, R.K., Pegylated Composite Nanoparticles Containing Upconverting Phosphors and meso-Tetraphenyl porphine (TPP) for Photodynamic Therapy. *Advanced Functional Materials*. **21**(13): p. 2488-2495 (2011).

248. Liang, S., Zhang, X., Wu, Z., Liu, Y., Zhang, H., Sun, H., Sun, H., and Yang, B., Decoration of up-converting NaYF₄:Yb,Er(Tm) nanoparticles with surfactant bilayer. A versatile strategy to perform oil-to-water phase transfer and subsequently surface silication. *CrystEngComm*. **14**(10): p. 3484-3489 (2012).

249. Muhr, V., Wilhelm, S., Hirsch, T., and Wolfbeis, O.S., Upconversion Nanoparticles: From Hydrophobic to Hydrophilic Surfaces. *Accounts of Chemical Research*. **47**(12): p. 3481-3493 (2014).

250. Li, Z. and Zhang, Y., Monodisperse Silica-Coated Polyvinylpyrrolidone/NaYF₄ Nanocrystals with Multicolor Upconversion Fluorescence Emission. *Angewandte Chemie*

International Edition. **45**(46): p. 7732-7735 (2006).

251. Lei, Z., Pang, X., Li, N., Lin, L., and Li, Y., A novel two-step modifying process for preparation of chitosan-coated Fe_3O_4/SiO_2 microspheres. *Journal of Materials Processing Technology*. **209**(7): p. 3218-3225 (2009).

252. Darbandi, M. and Nann, T., One-pot synthesis of YF_3@silica core/shell nanoparticles. *Chemical Communications*, (7): p. 776-778 (2006).

253. Budijono, S.J., Shan, J., Yao, N., Miura, Y., Hoye, T., Austin, R.H., Ju, Y., and Prud'homme, R.K., Synthesis of stable block-copolymer-protected $NaYF_4$: Yb^{3+}, Er^{3+} up-converting phosphor nanoparticles. *Chemistry of Materials*. **22**(2): p. 311-318 (2009).

254. Hlaváček, A., Mickert, M.J., Soukka, T., Lahtinen, S., Tallgren, T., Pizúrová, N., Król, A., and Gorris, H.H., Large-Scale Purification of Photon-Upconversion Nanoparticles by Gel Electrophoresis for Analogue and Digital Bioassays. *Analytical Chemistry*. **91**(2): p. 1241-1246 (2019).

255. Yi, G.-S. and Chow, G.-M., Water-Soluble $NaYF_4$:Yb,Er(Tm)/$NaYF_4$/Polymer Core/Shell/Shell Nanoparticles with Significant Enhancement of Upconversion Fluorescence. *Chemistry of Materials*. **19**(3): p. 341-343 (2007).

256. Naccache, R., Vetrone, F., Mahalingam, V., Cuccia, L.A., and Capobianco, J.A., Controlled Synthesis and Water Dispersibility of Hexagonal Phase $NaGdF_4$:Ho^{3+}/Yb^{3+} Nanoparticles. *Chemistry of Materials*. **21**(4): p. 717-723 (2009).

257. Duong, H.T.T., Chen, Y., Tawfik, S.A., Wen, S., Parviz, M., Shimoni, O., and Jin, D., Systematic investigation of functional ligands for colloidal stable upconversion nanoparticles. *RSC Advances*. **8**(9): p. 4842-4849 (2018).

258. Chen, G., Qiu, H., Prasad, P.N., and Chen, X., Upconversion Nanoparticles: Design, Nanochemistry, and Applications in Theranostics. *Chemical Reviews*. **114**(10): p. 5161-5214 (2014).

259. Jana, N.R., Earhart, C., and Ying, J.Y., Synthesis of water-soluble and functionalized nanoparticles by silica coating. *Chemistry of Materials*. **19**(21): p. 5074-5082 (2007).

260. Kobayashi, M., Juillerat, F., Galletto, P., Bowen, P., and Borkovec, M., Aggregation and Charging of Colloidal Silica Particles: Effect of Particle Size. *Langmuir*. **21**(13): p. 5761-5769 (2005).

261. Johnson, N.J.J., Sangeetha, N.M., Boyer, J.-C., and van Veggel, F.C.J.M., Facile ligand-exchange with polyvinylpyrrolidone and subsequent silica coating of hydrophobic upconverting β-$NaYF_4$:Yb^{3+}/Er^{3+} nanoparticles. *Nanoscale*. **2**(5): p. 771-777 (2010).

262. Johnson, N.J., Sangeetha, N.M., Boyer, J.-C., and van Veggel, F.C., Facile ligand-exchange with polyvinylpyrrolidone and subsequent silica coating of hydrophobic upconverting β-$NaYF_4$: Yb^{3+}/Er^{3+} nanoparticles. *Nanoscale*. **2**(5): p. 771-777 (2010).

263. Monopoli, M.P., Åberg, C., Salvati, A., and Dawson, K.A., Biomolecular coronas provide the biological identity of nanosized materials. *Nature Nanotechnology*. **7**: p. 779 (2012).

264. Bagwe, R.P., Hilliard, L.R., and Tan, W., Surface Modification of Silica Nanoparticles to Reduce Aggregation and Nonspecific Binding. *Langmuir*. **22**(9): p. 4357-4362 (2006).

265. Hilderbrand, S.A., Shao, F., Salthouse, C., Mahmood, U., and Weissleder, R., Upconverting luminescent nanomaterials: application to in vivo bioimaging. *Chemical Communications*, (28): p. 4188-4190 (2009).

266. Kamimura, M., Miyamoto, D., Saito, Y., Soga, K., and Nagasaki, Y., Design of Poly(ethylene glycol)/Streptavidin Coimmobilized Upconversion Nanophosphors and Their Application to Fluorescence Biolabeling. *Langmuir*. **24**(16): p. 8864-8870 (2008).

267. Nsubuga, A., Zarschler, K., Sgarzi, M., Graham, B., Stephan, H., and Joshi, T., Towards Utilising Photocrosslinking of Polydiacetylenes for the Preparation of "Stealth" Upconverting Nanoparticles.

Angewandte Chemie International Edition. **57**(49): p. 16036-16040 (2018).

268. Wang, F., Han, Y., Lim, C.S., Lu, Y., Wang, J., Xu, J., Chen, H., Zhang, C., Hong, M., and Liu, X., Simultaneous phase and size control of upconversion nanocrystals through lanthanide doping. *nature.* **463**(7284): p. 1061 (2010).

269. Kale, V., Soukka, T., Hölsä, J., and Lastusaari, M., Enhancement of blue upconversion luminescence in hexagonal NaYF4:Yb,Tm by using K and Sc ions. *Journal of Nanoparticle Research.* **15**(8): p. 1850 (2013).

270. Zhang, M., Cushing, B.L., and O'Connor, C.J., Synthesis and characterization of monodisperse ultra-thin silica-coated magnetic nanoparticles. *Nanotechnology.* **19**(8): p. 085601 (2008).

271. Wilhelm, S., Hirsch, T., Patterson, W.M., Scheucher, E., Mayr, T., and Wolfbeis, O.S., Multicolor upconversion nanoparticles for protein conjugation. *Theranostics.* **3**(4): p. 239 (2013).

272. Rantanen, T., Järvenpää, M.-L., Vuojola, J., Arppe, R., Kuningas, K., and Soukka, T., Upconverting phosphors in a dual-parameter LRET-based hybridization assay. *Analyst.* **134**(8): p. 1713-1716 (2009).

273. Liao, Z., Hooley, E.N., Chen, L., Stappert, S., Müllen, K., and Vosch, T., Green emitting photoproducts from terrylene diimide after red illumination. *Journal of the American Chemical Society.* **135**(51): p. 19180-19185 (2013).

274. Välimaa, L., Pettersson, K., Vehniäinen, M., Karp, M., and Lövgren, T., A high-capacity streptavidin-coated microtitration plate. *Bioconjugate chemistry.* **14**(1): p. 103-111 (2003).

275. Graf, C., Vossen, D.L., Imhof, A., and van Blaaderen, A., A general method to coat colloidal particles with silica. *Langmuir.* **19**(17): p. 6693-6700 (2003).

276. Rao, K.S., El-Hami, K., Kodaki, T., Matsushige, K., and Makino, K., A novel method for synthesis of silica nanoparticles.

Journal of colloid and interface science. **289**(1): p. 125-131 (2005).

277. Liu, C., Wang, H., Li, X., and Chen, D., Monodisperse, size-tunable and highly efficient β-NaYF4: Yb, Er (Tm) up-conversion luminescent nanospheres: controllable synthesis and their surface modifications. *Journal of Materials Chemistry.* **19**(21): p. 3546-3553 (2009).

278. Xiong, L., Yang, T., Yang, Y., Xu, C., and Li, F., Long-term in vivo biodistribution imaging and toxicity of polyacrylic acid-coated upconversion nanophosphors. *Biomaterials.* **31**(27): p. 7078-7085 (2010).

279. Lin, C.-L., Lee, C.-F., and Chiu, W.-Y., Preparation and properties of poly (acrylic acid) oligomer stabilized superparamagnetic ferrofluid. *Journal of Colloid and Interface Science.* **291**(2): p. 411-420 (2005).

280. Liufu, S., Xiao, H., and Li, Y., Adsorption of poly(acrylic acid) onto the surface of titanium dioxide and the colloidal stability of aqueous suspension. *Journal of Colloid and Interface Science.* **281**(1): p. 155-163 (2005).

281. Marin, R., Halimi, I., Errulat, D., Mazouzi, Y., Lucchini, G., Speghini, A., Murugesu, M., and Hemmer, E., Harnessing the Synergy between Upconverting Nanoparticles and Lanthanide Complexes in a Multiwavelength-Responsive Hybrid System. *ACS Photonics.* **6**(2): p. 436-445 (2019).

282. Lee, E., Jung, M., Han, Y., Lee, G., Shin, K., Lee, H., and Lee, K.T., Stochastic Photon Emission from Nonblinking Upconversion Nanoparticles. *The Journal of Physical Chemistry C.* **121**(38): p. 21073-21079 (2017).

283. Bergstrand, J., Liu, Q., Huang, B., Peng, X., Würth, C., Resch-Genger, U., Zhan, Q., Widengren, J., Ågren, H., and Liu, H., On the decay time of upconversion luminescence. *Nanoscale.* **11**(11): p. 4959-4969 (2019).

284. Wen, S., Zhou, J., Zheng, K., Bednarkiewicz, A., Liu, X., and Jin, D., Advances in highly doped upconversion nanoparticles. *Nature Communications.* **9**(1): p. 2415 (2018).

285. Demers, L.M. and Spencer, C.A., Laboratory medicine practice guidelines: laboratory support for the diagnosis and monitoring of thyroid disease. *Clinical endocrinology.* **58**(2): p. 138-140 (2003).

286. Zhou, Y., Xia, X., Xu, Y., Ke, W., Yang, W., and Li, Q., Application of europium(III) chelates-bonded silica nanoparticle in time-resolved immunofluorometric detection assay for human thyroid stimulating hormone. *Analytica Chimica Acta.* **722**: p. 95-99 (2012).

287. Näreoja, T., Rosenholm, J.M., Lamminmäki, U., and Hänninen, P.E., Super-sensitive time-resolved fluoroimmunoassay for thyroid-stimulating hormone utilizing europium(III) nanoparticle labels achieved by protein corona stabilization, short binding time, and serum preprocessing. *Analytical and Bioanalytical Chemistry.* **409**(13): p. 3407-3416 (2017).

288. Miller, A.E., Hollars, C.W., Lane, S.M., and Laurence, T.A., Fluorescence Cross-Correlation Spectroscopy as a Universal Method for Protein Detection with Low False Positives. *Analytical Chemistry.* **81**(14): p. 5614-5622 (2009).

289. Wang, J., Huang, X., Liu, H., Dong, C., and Ren, J., Fluorescence and Scattering Light Cross Correlation Spectroscopy and Its Applications in Homogeneous Immunoassay. *Analytical Chemistry.* **89**(10): p. 5230-5237 (2017).

**UNIVERSITY
OF TURKU**